

Time Averaged Density Matrix as an Optimization Problem

V. Nebendahl

*Institut für Theoretische Physik, Universität Innsbruck,
Technikerstr. 25, A-6020 Innsbruck, Austria**

Abstract

A new method is presented which allows time averaged density matrices of closed quantum systems to be computed via a constraint overlap maximization. Due to its simplicity, this method can be combined with algorithms based on tensor networks, as, e.g., matrix product operators (MPO). An algorithm is explained and several results for non-integrable Ising chains are given. Among them are scaling examples, time averaged expectation values, their variances and operator space entanglement entropies.

PACS numbers: 05.10.-a, 05.30.-d, 03.67.Ac

I. INTRODUCTION

An isolated classical system approaches its thermal equilibrium by maximizing its entropy. A closed quantum system on the other hand can not thermalize in this way, since it is subjected to a unitary time evolution, which does not change the entropy. So, by which mechanism do closed quantum systems equilibrate, if they equilibrate at all? This question was already investigated 1929 by John von Neumann in the early days of quantum mechanics [1], see also the comments in Ref. [2]. While at that time, the thermalization of a pure quantum state might have seem solely as an academic question, the interest in this subject has recently rekindled with the advent of new experimental techniques which allow to study almost undisturbed long-time evolution of ultracold atoms and trapped ions [3, 4].

To start with, we like to remark that even in classical physics, the definition of thermal equilibrium is far from trivial if we look at the deterministic evolution of a specific microstate. Therefore, one resorts to macrostates, which implies an averaging over a vast number of microstates. In statistical mechanics, an isolated system with known total energy is described by the a microcanonical ensemble, which assigns to each microstate with suitable energy the same probability. For ergodic systems, the microcanonical ensemble coincides with the long-time average of the system. These two definitions can also be used for closed quantum systems. But here, the density matrices obtained from the microcanonical ensemble $\varrho_{\text{m.c.}}$ and the long-time average

$$\bar{\varrho} = \lim_{T \rightarrow \infty} \left(\frac{1}{T} \int_0^T \varrho(t) dt \right) \quad (1)$$

do generally not coincide [1]. Both density matrices $\varrho_{\text{m.c.}}$ and $\bar{\varrho}$ are diagonal in the energy eigenstates basis. Yet, the diagonal elements of $\varrho_{\text{m.c.}}$ consist only of zeros and ones (disregarding normalization), while the diagonal el-

ements of $\bar{\varrho}$ depend on the initial state (see also Eq. (5), below).

Instead of considering the entire system, one can also focus on a small subsystem. Then, the (much larger) rest of the system can be seen as thermal bath of the subsystem. Interestingly, in this case thermalization might even be obtained without any ensemble or time averaging. Due to entanglement, the reduced density matrix of a pure state is a mixed state and therefore it is possible that after sufficiently long time, the reduced density matrix of a subsystem describes a thermal state. Various publications have shown that this is indeed the case for many systems, see e.g. Ref. [5–12], but also Ref. [13, 14] as counter examples.

One of the leading theories to explain thermalization is the so called eigenstate thermalization hypothesis (ETH) [5, 6]. Here, it is assumed that for energy eigenstates, the reduced density matrices of local subsystems are thermal. That is, an initially out of equilibrium state relaxes due to a dephasing of the different energy eigenstates such that the coherences average out. More background information can also be found in the reviews [15–17].

In the context of thermalization, it is important to distinguish between integrable and non-integrable systems. While for non-integrable systems it is widely assumed that their reduced density matrices relax to a standard Gibbs ensemble, this is generally not possible for integrable systems, where an extensive number of local integrals of motions \mathcal{I}_j conserves a memory of the initial state. In such a case, the system can still equilibrate to a generalized Gibbs ensemble [7].

However, integrable systems have the undoubted advantage that closed analytical solution might be found [18, 19], while the numerically accessible timespan of non-integral systems might not suffice to observe equilibration [12, 20]. The situation might even be worse, if the system is non-integrable but has quasi-conserved local integrals of motions, which can result in very long relaxation times [21].

In any case, if a closed quantum system respectively its subsystems equilibrate, the equilibrium states must coincide with the time averages of these states and hence, can all be obtained from the time averaged density ma-

*Electronic address: Volckmar.Nebendahl@uibk.ac.at

trix (TADM) $\bar{\varrho}$ defined in Eq. (1). In order to actually compute the TADM $\bar{\varrho}$, two methods come immediately into mind: One can take Eq. (1) literally and calculate various time evolved states $\Psi(t)$ and sum up their $\varrho(t)$. Alternatively, one can recall that the TADM $\bar{\varrho}$ consists of the diagonal elements of the initial density matrix ϱ_0 expressed in energy eigenstates $|E_j\rangle$. Hence, one can use diagonalization techniques to find the relevant eigenstates of the Hamiltonian to reconstruct $\bar{\varrho}$. Unfortunately, for many systems of interest, both methods are of very limited applicability.

Here, we introduce an alternative strategy based on a simple constraint overlap optimization procedure. Due to its simple structure, the optimization can be easily carried out with matrix product operators (MPO) or other tensor network operators [22–25]. This is demonstrated by various applications in Sec. III, where among others expectation values, variances and operator space entanglement entropies for non-integrable Ising spin chains are presented. Further, we compare spin chains of different lengths and also study the influence of the so-called bond dimension of the MPO on the obtainable results.

The key idea of tensor networks as matrix product states (MPS) and MPO is to express high-dimensional quantum states and operators as products of low-dimensional matrices respectively tensors. Such an ansatz works fine as long as the system’s entanglement is limited. Unfortunately, this is not a situation we can expect to find in a generic TADM $\bar{\varrho}$. Hence, in many cases of interest, a tensor network can only represent an approximation of the TADM which is more or less rough. However, since our approach is based on an optimization principle, we can at least hope to get the best out of our limited resources within the chosen ansatz class.

The quality of the solution also depends on the chosen type of tensor network. In this paper, we will mainly deal with MPO. That is, we aim directly for the density *operator*, while e.g. the methods based on time evolution or diagonalization primarily calculate the *states* $|\Psi(t)\rangle$ or $|E_j\rangle$. In appendix M, we will also give brief account how the algorithm can be used with MPS.

Not surprisingly, the decision to calculate states or to aim directly for the operator entails certain advantages and disadvantages. For example, if the TADM is mainly described by one dominant energy eigenstate $\bar{\varrho} \approx |E\rangle\langle E|$, it is generally easier to compute this state $|E\rangle$ instead of the operator $|E\rangle\langle E|$. Here, the entropy of $\bar{\varrho} \approx |E\rangle\langle E|$ is close to zero. Then again, if the entropy of the TADM is high, i.e., if it is composed of many similarly weighted energy eigenstates $\bar{\varrho} = \sum_j p_{jj} |E_j\rangle\langle E_j|$, targeting the operator directly seems favorable, since a MPO can handle arbitrary amounts of entropy. For the same reason, MPO are better suited for the time average of a (local) measurement operator $\bar{O} = \sum_j o_{jj} |E_j\rangle\langle E_j|$.

A. Structure of this paper

In writing this paper, we had two different types of readers in mind. On the one hand, the reader who likes to understand the basic ideas, but has no need for all algorithmic detail. On the other hand, the reader who likes to reproduce our algorithm and hence, needs all the details (s)he can get. The main paper should fit the first type of readers, while readers of the second type find all the information they need in a vast appendix, where various special topics are treated.

The key insight of our method is that the search for the TADM can be phrased as simple optimization problem. This is explained in Sec. II, while a detailed presentation of an algorithm solving the optimization problem is outsourced into the appendix: In appendix E, a general strategy for solving the optimization problem is explained, yet without any references to tensor networks. The modifications needed to incorporate tensor networks are discussed in appendix F. Further improvements are presented in the appendices H, I, and J.

For readers who do not intent to study the appendix, Sec. IID provides a quick overview of the crucial ideas used for the numerical solution, but here, explanations are sparse. In Sec. III, we present our numerical results. Finally, the main paper is concluded with a discussion and outlook in Sec. IV.

II. FORMAL SOLUTIONS FOR THE TIME AVERAGED DENSITY MATRIX

In this section, we look at the general structure of the time averaged density matrix (TADM) $\bar{\varrho}$ and show in the following subsections how the calculation of $\bar{\varrho}$ can be cast into the alternative form of a simple optimization problem.

For the theoretical considerations, we always choose the energy eigenstates as preferred basis. In this basis, we express the initial density matrix ϱ_0 at time $t = 0$ as

$$\varrho_0 = \sum_{j,k} p_{jk} |E_j\rangle\langle E_k| \quad \text{with} \quad p_{jk} = \langle E_j | \varrho_0 | E_k \rangle, \quad (2)$$

while at any other time t , the time evolved density matrix $\varrho(t)$ is given as

$$\varrho(t) = \sum_{j,k} \exp\left(-\frac{i}{\hbar}(E_j - E_k)t\right) p_{jk} |E_j\rangle\langle E_k|. \quad (3)$$

Inserting this notation into the definition of the TADM $\bar{\varrho}$

$$\bar{\varrho} := \lim_{T \rightarrow \infty} \left(\frac{1}{T} \int_0^T \varrho(t) dt \right), \quad (4)$$

we obtain

$$\begin{aligned}\bar{\varrho} &= \sum_{j,k} \bar{p}_{jk} |E_j\rangle\langle E_k|, \\ &= \sum_{j,k} \delta_{E_j, E_k} p_{jk} |E_j\rangle\langle E_k|,\end{aligned}\quad (5)$$

where we used the symbol δ_{E_j, E_k} as abbreviation for

$$\begin{aligned}\delta_{E_j, E_k} &= \lim_{T \rightarrow \infty} \left(\frac{1}{T} \int_0^T \exp\left(-\frac{i}{\hbar}(E_j - E_k)t\right) dt \right) \\ &= \begin{cases} 1 & \text{for } E_j = E_k \\ 0 & \text{for } E_j \neq E_k \end{cases}.\end{aligned}\quad (6)$$

For a non-degenerate energy spectrum, the TADM $\bar{\varrho}$ consists of the diagonal elements of ϱ_0 . In case of a degenerate energy spectrum, $\bar{\varrho}$ is made up of the corresponding block diagonal elements of ϱ_0 . To keep the notation simple, we will still refer to these elements as ϱ_{diag} , i.e.

$$\begin{aligned}\varrho_{\text{diag}} = \bar{\varrho} &= \sum_{j,k} \delta_{E_j, E_k} p_{jk} |E_j\rangle\langle E_k| \\ &= \sum_{E_j = E_k} p_{jk} |E_j\rangle\langle E_k|.\end{aligned}\quad (7)$$

Correspondingly, we define $\varrho_{\text{off-diag}}$ as

$$\begin{aligned}\varrho_{\text{off-diag}} &= \sum_{j,k} (1 - \delta_{E_j, E_k}) p_{jk} |E_j\rangle\langle E_k| \\ &= \sum_{E_j \neq E_k} p_{jk} |E_j\rangle\langle E_k|.\end{aligned}\quad (8)$$

A. Structure of the solution

The idea we pursue to obtain the time averaged density matrix (TADM) $\bar{\varrho}$ is to calculate (respectively approximate) $\varrho_{\text{off-diag}}$ (8) and subtract it from ϱ_0

$$\bar{\varrho} \stackrel{(7)}{=} \varrho_{\text{diag}} = \varrho_0 - \varrho_{\text{off-diag}}.\quad (9)$$

To this end, we express $\varrho_{\text{off-diag}}$ as commutator of the Hamiltonian and an unknown matrix M , which still has to be determined, i.e.

$$\varrho_{\text{off-diag}} = [H, M].\quad (10)$$

The purpose of the commutator will become clear in the following. In a first step, we write the matrix $M = \sum_{j,k} m_{jk} |E_j\rangle\langle E_k|$ as

$$M = \underbrace{\sum_{E_j = E_k} m_{jk} |E_j\rangle\langle E_k|}_{=M_{\text{diag}}} + \underbrace{\sum_{E_j \neq E_k} m_{jk} |E_j\rangle\langle E_k|}_{=M_{\text{off-diag}}}.\quad (11)$$

With that, we obtain for the commutator of *any* matrix M with the Hamiltonian H

$$[H, M] = \underbrace{[H, M_{\text{diag}}]}_{=0} + [H, M_{\text{off-diag}}],\quad (12)$$

where

$$[H, M_{\text{off-diag}}] = \sum_{E_j \neq E_k} (E_j - E_k) m_{jk} |E_j\rangle\langle E_k| \quad (13)$$

$$[H, M_{\text{diag}}] = 0.\quad (14)$$

Obviously, $[H, M] = [H, M_{\text{off-diag}}]$ is always an off-diagonal matrix for any matrix M . Further, Eq. (13) can be inverted to solve $\varrho_{\text{off-diag}} = [H, M]$ (10), since the term $E_j - E_k$ never becomes zero for $E_j \neq E_k$. That is,

$$\forall \varrho_{\text{off-diag}}, \exists M \quad \text{with} \quad \varrho_{\text{off-diag}} = [H, M].\quad (15)$$

In this equation, only the off-diagonal part $M_{\text{off-diag}}$ of the matrix M is unique, while the diagonal part M_{diag} is arbitrary due to $[H, M_{\text{diag}}] = 0$ (14). Inserting Eq. (15) into Eq. (9), we find

$$\forall \varrho_0, \exists M \quad \text{with} \quad \bar{\varrho} = \varrho_0 - [H, M].\quad (16)$$

B. Commutator operator \mathfrak{C}

Before we explain the advantage of expressing the TADM as $\bar{\varrho} = \varrho_0 - [H, M]$ (16), it will be convenient to introduce the superoperator $\mathfrak{C} = [H, \dots]$ which acts on a matrix A as

$$\mathfrak{C}A := [H, A].\quad (17)$$

Formally, \mathfrak{C} can be seen as a tensor of fourth order ($[H, A]^{lm} = \mathfrak{C}_{jk}^{lm} \cdot A^{jk}$). In other contexts, the superoperator \mathfrak{C} is often called Liouvillian. Unfortunately, the term Liouvillian is not unique and also understood in other ways. Therefore, we will simply refer to \mathfrak{C} as ‘‘commutator operator’’, which should be free of any ambiguity.

In the following, we will not distinguish between operator and superoperator and also vectorize matrices as M writing $|M\rangle$. Here, we take advantage of the Choi-Jamiolkowski isomorphism $M_{jk} \cdot |j\rangle\langle k| \Leftrightarrow M_{jk} \cdot |j\rangle \otimes |k\rangle$.

For the Hilbert-Schmidt inner product (which we use throughout this paper) of matrices A, B , we find that the commutator operator \mathfrak{C} behaves self-adjoint $\langle \mathfrak{C}A | B \rangle = \langle A | \mathfrak{C}B \rangle$, despite the anti-hermiticity $(\mathfrak{C}A)^\dagger = -\mathfrak{C}A$ for Hermitian matrices $A^\dagger = A$. Hence, we can use notations like e.g. $\|[H, M]\|^2 = \langle M | \mathfrak{C}^2 | M \rangle$. Since we will need this property quite often, we derive it explicitly

$$\begin{aligned}\langle \mathfrak{C}A | B \rangle &:= \text{tr}\left(\left((HA - AH)^\dagger B\right)\right) \\ &= \text{tr}\left(A^\dagger HB - HA^\dagger B\right) \\ &= \text{tr}\left(A^\dagger HB - A^\dagger BH\right) \\ &= \text{tr}\left(A^\dagger [H, B]\right) \\ &= \langle A | \mathfrak{C}B \rangle.\end{aligned}\quad (18)$$

C. Optimization problem

In this subsection, we show how the TADM $\bar{\varrho}$ can be solved as optimization problem. We start with Eq. (10), which expresses the off-diagonal elements of ϱ_0 as commutator

$$\varrho_{\text{off-diag}} \stackrel{(10)}{=} [H, M] \stackrel{(17)}{=} \mathfrak{C}M, \quad (19)$$

with a yet unknown matrix M . Formally, this can be solved as

$$M = \mathfrak{C}^{-1} \varrho_{\text{off-diag}}. \quad (20)$$

In appendix A, we have a closer look at this strategy and also comment on problems arising due to quasi-degenerate eigenstates, but we will not use these findings in the rest of the paper. Here, we follow a different approach.

In a first step, we note that the TADM $\bar{\varrho} = \varrho_{\text{diag}}$ has a vanishing overlap with the commutator $\mathfrak{C}M$ for *any* matrix M with finite norm, since \mathfrak{C} is a purely off-diagonal matrix (in energy eigenstates)

$$\langle \varrho_{\text{diag}} | \mathfrak{C}M \rangle \stackrel{(18)}{=} \underbrace{\langle \mathfrak{C} \varrho_{\text{diag}} | M \rangle}_{=0 \text{ (14)}} = 0. \quad (21)$$

So far, neither ϱ_{diag} nor $\varrho_{\text{off-diag}}$ nor M are known objects. What we know is ϱ_0 . Hence, let us look at the overlap of ϱ_0 with the commutator $\mathfrak{C}M$

$$\begin{aligned} \langle \varrho_0 | \mathfrak{C}M \rangle &= \langle \varrho_{\text{diag}} + \varrho_{\text{off-diag}} | \mathfrak{C}M \rangle \\ &= \underbrace{\langle \varrho_{\text{diag}} | \mathfrak{C}M \rangle}_{=0 \text{ (21)}} + \langle \varrho_{\text{off-diag}} | \mathfrak{C}M \rangle \\ &= \langle \varrho_{\text{off-diag}} | \mathfrak{C}M \rangle. \end{aligned} \quad (22)$$

This simple result is one of the cornerstones for the time averaged density matrix algorithms we are going to derive in this paper: For any matrix M , the inner product of the commutator $\mathfrak{C}M$ with the unknown matrix $\varrho_{\text{off-diag}}$ equals the inner product with the known matrix ϱ_0 .

With the identity $\langle \varrho_0 | \mathfrak{C}M \rangle = \langle \varrho_{\text{off-diag}} | \mathfrak{C}M \rangle$ (22), we also find that the matrices M which maximize the two inner products are the same

$$\arg \max_{\|\mathfrak{C}M\|^2=1} \left(\langle \varrho_0 | \mathfrak{C}M \rangle \right) = \arg \max_{\|\mathfrak{C}M\|^2=1} \left(\langle \varrho_{\text{off-diag}} | \mathfrak{C}M \rangle \right), \quad (23)$$

where we use

$$\|\mathfrak{C}M\|^2 = \langle \mathfrak{C}M | \mathfrak{C}M \rangle = 1 \quad (24)$$

as normalization condition and not $\langle M | M \rangle = 1$. Eq. (23) is maximized for

$$\mathfrak{C}M = \frac{1}{c} \varrho_{\text{off-diag}}, \quad (25)$$

with $c = \|\varrho_{\text{off-diag}}\| = \langle \mathfrak{C}M | \varrho_{\text{off-diag}} \rangle = \langle \mathfrak{C}M | \varrho_0 \rangle$. Actually, we also have to ensure the existence of matrices M which satisfy Eq. (25). But this we have already done in Eq. (15).

Putting all together, we find that any matrix M which maximizes the inner product $\langle \varrho_0 | \mathfrak{C}M \rangle$ under the condition $\|\mathfrak{C}M\|^2 = 1$

$$M = \arg \max_{\|\mathfrak{C}M'\|^2=1} \left(\langle \varrho_0 | \mathfrak{C}M' \rangle \right) \quad (26)$$

also satisfies

$$\begin{aligned} \bar{\varrho} &\stackrel{(9)}{=} \varrho_0 - \varrho_{\text{off-diag}} \\ &\stackrel{(25)}{=} \varrho_0 - \langle \mathfrak{C}M | \varrho_0 \rangle \mathfrak{C}M \\ &= \varrho_0 - \mathfrak{C}\bar{M}, \end{aligned} \quad (27)$$

with $\bar{M} = \langle \mathfrak{C}M | \varrho_0 \rangle M$. That is, the TADM $\bar{\varrho}$ can be solved as an optimization problem, which only involves basic matrix operations as addition, multiplication and inner product.

1. Alternative optimization ansatz

It is relative straight forward to see that the conditioned maximization of Eq. (26) is equivalent to the unconditioned minimization of

$$\begin{aligned} M &= \arg \min \left(\|\varrho_0 - \mathfrak{C}M'\|^2 \right) \\ &= \arg \min \left(\underbrace{\langle \varrho_0 | \varrho_0 \rangle}_{=\text{const.}} - 2\text{Re}(\langle \varrho_0 | \mathfrak{C}M' \rangle) + \langle M' | \mathfrak{C}^2 | M' \rangle \right). \end{aligned} \quad (28)$$

While Eq. (26) and Eq. (28) are equivalent, one might also find alternative approaches for M which would yield the same $\bar{\varrho}$ for optimal M , but result in qualitatively different approximations $\bar{\varrho}_{\text{approx}}$ for imperfect M . In appendix B, we discuss such an approach given by

$$M = \arg \min \left(\|\mathfrak{C}(\varrho_0 - \mathfrak{C}M')\|^2 \right). \quad (29)$$

This method minimizes the residual time dependence of $\bar{\varrho}_{\text{approx}}$, while for most other physical properties, the standard method described by Eqs. (26) and (28) seems more promising; see appendix B 1.

2. General eigenvector problem

Instead of maximizing $\langle \varrho_0 | \mathfrak{C}M \rangle$ as in Eq. (26), one can also maximize $\langle \mathfrak{C}M | \varrho_0 \rangle \langle \varrho_0 | \mathfrak{C}M \rangle$. The advantage of this bilinear form is that the search for an optimal M can now be phrased as

$$M = \arg \max \left(\frac{\langle \mathfrak{C}M' | \varrho_0 \rangle \langle \varrho_0 | \mathfrak{C}M' \rangle}{\langle \mathfrak{C}M' | \mathfrak{C}M' \rangle} \right), \quad (30)$$

which can be solved as a general eigenvector problem for the maximal eigenvalue λ

$$(\mathfrak{C}|\varrho_0\rangle\langle\varrho_0|\mathfrak{C})|M\rangle = \lambda \cdot \mathfrak{C}\mathfrak{C}|M\rangle \quad (31)$$

Unfortunately, both sides of the eigenvector equation can become zero at the same time for $\|M\| > 0$, which is a notorious source of trouble for the numerical treatment of generalized eigenvector problems. Therefore, we do not consider this approach as ideal and present an alternative strategy in the appendices E and F. Still, the reader who has already a good and stable software solution for this problem at his or her disposal might give it a try, anyway.

D. Solving the optimization problem

In the following, we just give a short (an hence incomplete) overview of the method used for solving the optimization problem. Further information and omitted explanations can be found in the appendices E, F, and beyond, where an in-detail description is provided.

We need to find a matrix M (27), with $\varrho_{\text{off-diag}} = \mathfrak{C}M$ (19). To this end, the matrix M is expressed as a linear combination

$$M = \sum_j \alpha_j \mathcal{M}_j, \quad (32)$$

i.e., $\varrho_{\text{off-diag}} = \sum_j \alpha_j \mathfrak{C}\mathcal{M}_j$. For the matrices \mathcal{M} , we demand $\langle \mathfrak{C}\mathcal{M}_j | \mathfrak{C}\mathcal{M}_k \rangle = \delta_{jk}$, which allows us to obtain the optimal coefficients α_j as

$$\alpha_j = \langle \mathfrak{C}\mathcal{M}_j | \varrho_{\text{off-diag}} \rangle \stackrel{(22)}{=} \langle \mathfrak{C}\mathcal{M}_j | \varrho_0 \rangle. \quad (33)$$

We like to find matrices \mathcal{M}_j with high α_j , respectively with high overlap $\langle \mathfrak{C}\mathcal{M}_j | \varrho_0 \rangle$. A suitable way is to generate the matrices \mathcal{M}_j iteratively as elements of a Krylov subspace \mathcal{K}

$$\mathcal{K} = \text{span} \{ \mathfrak{C}\varrho_0, \mathfrak{C}^3\varrho_0, \mathfrak{C}^5\varrho_0, \dots, \mathfrak{C}^{2j-1}\varrho_0 \}. \quad (34)$$

But in this Krylov subspace approach, we still ignore the fact that the matrices \mathcal{M}_j exhibit the same exponential scaling with the system size as ϱ_0 itself, which generally foils an explicit calculation of these matrices.

To master this exponential scaling, we resort to a tensor network representation [22–25], i.e., we use MPO (appendix F 1) and double MPS, a tensor network explained in appendix M. The basic idea of a tensor network is to express (or approximate) a high-dimensional object M as a product of low-dimensional tensors $M_{[k]}$

$$M = \prod_k M_{[k]}. \quad (35)$$

This is a short hand notation, where we omitted the indices used for the multiplications of the tensors $M_{[k]}$; see also appendix F 1. The dimension of these indices

is commonly referred to as bond dimension and has to be limited for a successful numerical handling. This also imposes limitations on the maximal amount of entanglement which can be represented faithfully.

In case of a tensor network, we need an optimization procedure for the network tensors $M_{[k]}$ (35). Here, we can use the same idea as before and express each $M_{[k]}$ as a linear combination of iteratively generated tensors $M_{[k]}^{(j)}$

$$M_{[k]} = \sum \alpha'_j M_{[k]}^{(j)}. \quad (36)$$

But in contrast to Eq. (34), it is no longer advisable to generate the tensors $M_{[k]}^{(j)}$ as elements of a simple Krylov subspace. Here, a more elaborated iteration rule is needed (I1), which also takes information from previous optimizations into account. This is explained in appendix F 3 and further improved in appendix I.

III. RESULTS

In this paper, we have presented a new numerical method, which naturally raises lots of questions concerning its performance. In case of highly entangled time averaged density matrices or operators, the probably most urgent question is how much insight we can really gain if the chosen tensor network ansatz only supports a limited amount of entanglement. We strongly focus on this question comparing results for different bond dimensions $D = 2^n$ ranging from $D = 4$ to $D = 512$. Hereby, D always refers to the bond dimension used for the ansatz M in $\bar{\varrho} = \varrho_0 - \mathfrak{C}M$ (27). Other interesting aspects as convergence properties and the achievable precision are addressed in appendix N.

As already mentioned in the introduction (Sec. I), integrable and non integrable systems are expected to thermalize differently. Further, for integrable systems, the tensor network based simulation of time evolution can often be done with less computational resources, i.e., with lower bond dimensions [26]. As an example for an integrable system, we look at the Ising Hamiltonian H of a spin chain of length L

$$H = - \sum_{j=1}^{L-1} \sigma_z^{(j)} \sigma_z^{(j+1)} - \sum_{j=1}^L \sigma_x^{(j)}, \quad (37)$$

where $\sigma_x^{(j)}$ and $\sigma_z^{(j)}$ denote the Pauli matrices applied to the j th spin. This Hamiltonian can be mapped onto a system of free fermions by a Jordan-Wigner transformation. Also numerically, one quickly finds that the time average of a single $\sigma_x^{(k)}$ operator (Heisenberg picture, see appendix C) can be described by a MPO with bond dimension $D \leq L + 2$ and for the time average of the operator $S_x = \sum_{j=1}^L \sigma_x^{(j)}$, even $D = 4$ is sufficient. For non-integrable Ising models on the other hand, such simplifications cannot be found.

For the rest of this paper, we consider the non-integrable Ising Hamiltonian H

$$H = - \sum_{j=1}^{L-1} \sigma_z^{(j)} \sigma_z^{(j+1)} - \sum_{j=1}^L \frac{\sigma_x^{(j)} + \sigma_z^{(j)}}{\sqrt{2}}, \quad (38)$$

for which we compare spin chains of different length, $L = 13, 25, 51$. As examples for time averaged operators, we look at the polarization of the central spin $\sigma_{\text{field}}^{\text{central}}$ and the average polarization S_{field} in direction of the applied field

$$\sigma_{\text{field}}^{\text{central}} = \frac{\sigma_x^{(c)} + \sigma_z^{(c)}}{\sqrt{2}}, \quad \text{with } c = \lceil \frac{L}{2} \rceil \quad (39)$$

$$S_{\text{field}} = \sum_{j=1}^L \frac{\sigma_x^{(j)} + \sigma_z^{(j)}}{\sqrt{2} \cdot L}. \quad (40)$$

As states, we consider the two initial state

$$|\Psi_+\rangle = |+\rangle^{\otimes L} = 2^{-\frac{L}{2}} \begin{pmatrix} 1 \\ 1 \end{pmatrix}^{\otimes L} \quad (41)$$

$$|\Psi_\uparrow\rangle = |0\rangle^{\otimes L} = \begin{pmatrix} 1 \\ 0 \end{pmatrix}^{\otimes L}. \quad (42)$$

Further, we look at the ground state $|E_0\rangle$ of the Hamiltonian (38) where either the central spin is flipped or the left and right outer spins together

$$|\Psi_{\text{central flip}}\rangle = \sigma_x^{(c)} |E_0\rangle, \quad \text{with } c = \lceil \frac{L}{2} \rceil \quad (43)$$

$$|\Psi_{\text{outer flip}}\rangle = \sigma_x^{(1)} \otimes \sigma_x^{(L)} |E_0\rangle. \quad (44)$$

In the ground state, the spins are mostly in the ‘‘up’’ position $\begin{pmatrix} 1 \\ 0 \end{pmatrix}$ such that we can e.g. expect much higher precisions for $|\Psi_\uparrow\rangle$ (42) than for $|\Psi_+\rangle$ (41). For $|\Psi_{\text{outer flip}}\rangle$, the precisions is even high enough to calculate reliable results for the variances of $\langle \sigma_z^{(j)} \rangle$ with the help of the method explained in appendix D.

A. Performance of the different methods

We start by comparing the performance of four different ways to calculate the TADM of the initial states $|\Psi_\uparrow\rangle$ (42) and $|\Psi_+\rangle$ (41).

1. q value

To estimate the quality of the approximated TADM $\bar{\rho}_{\text{approx}}$ without knowledge of the exact TADM $\bar{\rho}$, we look at the residual time dependence of $\bar{\rho}_{\text{approx}}$ and set it in relation to the time dependence of the initial state ϱ_0

$$q = \frac{\| [H, \varrho_0] \|}{\| [H, \bar{\rho}_{\text{approx}}] \|} = \frac{\| \dot{\varrho}_0 \|}{\| \dot{\bar{\rho}}_{\text{approx}} \|}. \quad (45)$$

That is, q is the factor by which the time dependence of $\bar{\rho}_{\text{approx}}$ was reduced compared to ϱ_0 . In Sec. II C 1,

we mentioned an alternative optimization ansatz which minimizes the time derivative $\| \dot{\bar{\rho}}_{\text{approx}} \|$ (29) (and with that maximizes q), while the standard method used in the rest of the paper minimizes $\| \bar{\rho}_{\text{approx}} \|$ (28) without time derivative. This alternative optimization ansatz is discussed in more detail in appendix B. To distinguish these two methods, we denote them by $T+$ and $T-$

$$\begin{aligned} T+ & \quad \text{method which minimizes } \| \dot{\bar{\rho}}_{\text{approx}} \| \\ T- & \quad \text{standard method, which minimizes } \| \bar{\rho}_{\text{approx}} \|. \end{aligned} \quad (46)$$

These two optimization methods are used in combination with two different tensor network ansätze: 1) MPO and 2) double MPS. A double MPS is a MPS of twice the size of a regular MPS and acts as an operator, as is discussed in appendix M. The double MPS was chosen because only marginal adaptations are necessary to run the MPO algorithm with a double MPS.

Fig. 1 shows a log-log plot of q (45) in dependence of the bond dimension D for the initial states $|\Psi_\uparrow\rangle = |0\rangle^{\otimes 25}$ and $|\Psi_+\rangle = |+\rangle^{\otimes 25}$. As can be seen, the double MPS allows to obtain better results than the MPO for these states. Not surprisingly, we also find that the $T+$ method performs better than the standard $T-$ method, since the $T+$ method was designed to generate the highest possible q values.

2. Fidelity

Nonetheless, theoretical considerations in appendix B suggest that the $T-$ method should be better suited to compute physical quantities than the $T+$ method. To verify this thesis, we studied a small and hence exactly solvable spin chain of length $L = 13$, which allows us to calculate the fidelity F

$$F = \text{Tr} \sqrt{\sqrt{\bar{\rho}} \bar{\rho}_{\text{approx}} \sqrt{\bar{\rho}}}. \quad (47)$$

We remark that F is normally used in the context of positive matrices only, while the numerically approximated TADM $\bar{\rho}_{\text{approx}}$ might have a few small negative eigenvalues. Still, this has no essential influence on our line of argumentation.

In Fig. 2, the results for $1 - F$ are shown in a log-log plot in dependence of the bond dimension D for the initial states $|\Psi_\uparrow\rangle = |0\rangle^{\otimes 13}$ and $|\Psi_+\rangle = |+\rangle^{\otimes 13}$. We still find that the double MPS performs better than the MPO and as expected, the standard $T-$ method generates better results than the $T+$ method.

As a consequence of these findings, we use the standard $T-$ method to compute the physical properties of a TADM $\bar{\rho}$, while we employ the MPO based $T+$ method to compare the q values of different spin chains, as we do next.

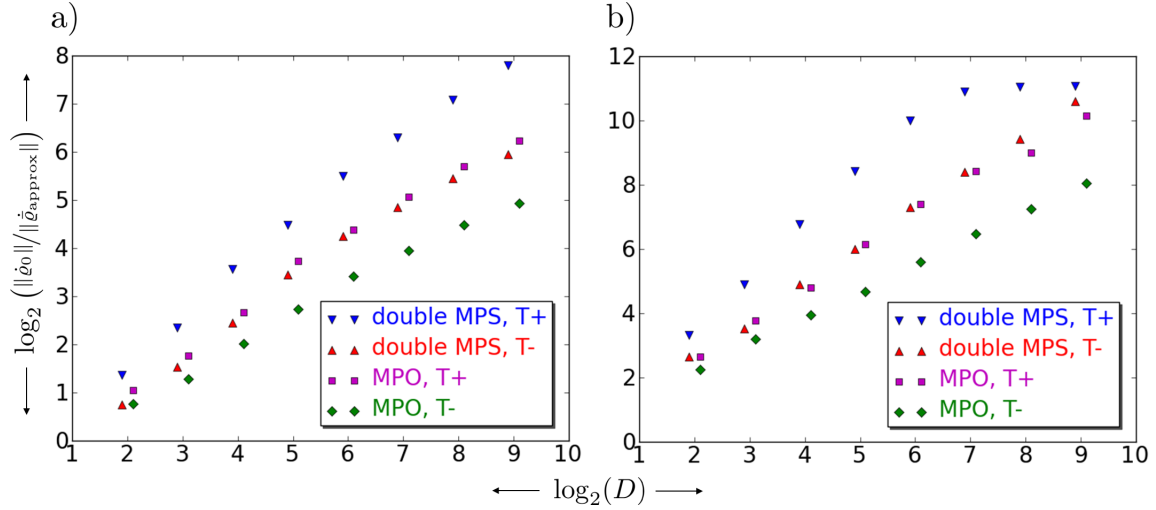


Figure 1: Comparison of the q value (45) for different methods. The logarithm of the q value is plotted over the logarithm of the bond dimension D , for a) $|\Psi_+\rangle$ (41) and b) $|\Psi_+\rangle$ (42). In both cases, the system size is $L = 25$. The different methods are explained in the main text (Sec. III A). For better visibility, the data points are slightly shifted – $\log_2(D)$ is always an integer.

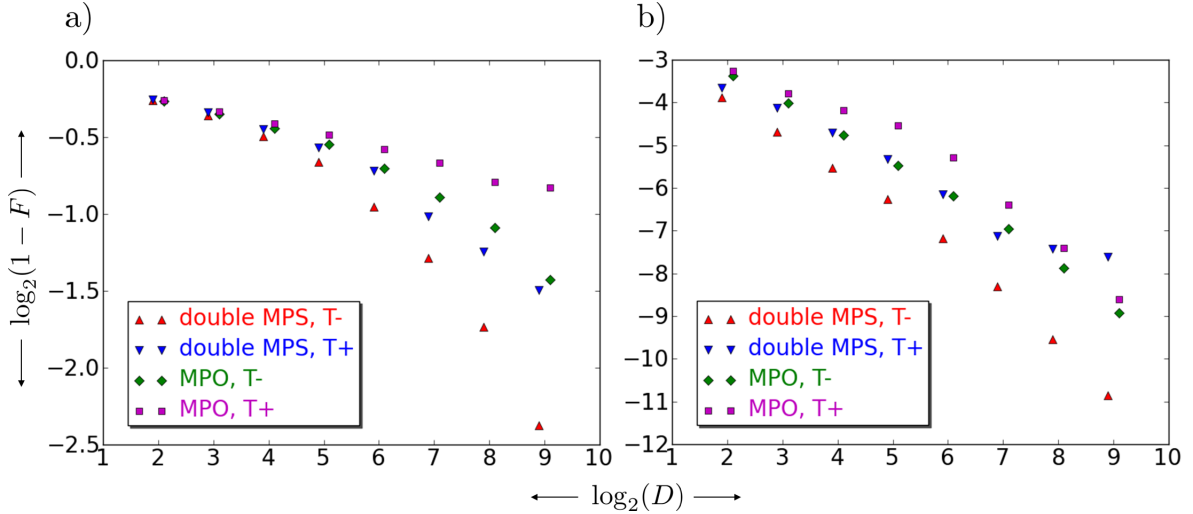


Figure 2: Comparison of the fidelity F (47) for different methods. The logarithm of $1 - F$ is plotted over the logarithm of the bond dimension D , for a) $|\Psi_+\rangle$ (41) and b) $|\Psi_+\rangle$ (42). In both cases, the system size is $L = 13$. The different methods are explained in the main text (Sec. III A). For better visibility, the data points are slightly shifted – $\log_2(D)$ is always an integer.

B. Spin chains of different length

In Fig. 3, the q values (45) of the initial operators $\sigma_{\text{field}}^{\text{central}}$ (39), S_{field} (40) and the initial states $|\Psi_+\rangle$ (41), $|\Psi_+\rangle$ (42) are shown for spin chains of length $L = 13, 25, 51$. Especially for the time average of the operator $\sigma_{\text{field}}^{\text{central}}$ (Fig. 3 a), the q value is mostly independent of the length of the spin chain. For S_{field} and $|\Psi_+\rangle$, this is roughly true, as well, while for $|\Psi_+\rangle$, we see a pronounced difference. At least for $\sigma_{\text{field}}^{\text{central}}$, this weak dependence on the length of the spin chain can be understood when we look at the operator space entanglement entropy of the time averages, what we do next.

C. Entanglement entropy

In the following five figures, we study the operator space entanglement entropy (OSEE) [27] in dependence of the position where the spin chain is split into two parts. Each plot consists of a family of curves, where each curve depicts the results obtained for one specific bond dimension $D = 2^n$ between $D = 4$ and $D = 512$. To emphasize the symmetry of the plots, the center of the spin chain is denoted as zero and the spin positions left from the center are addressed with negative numbers.

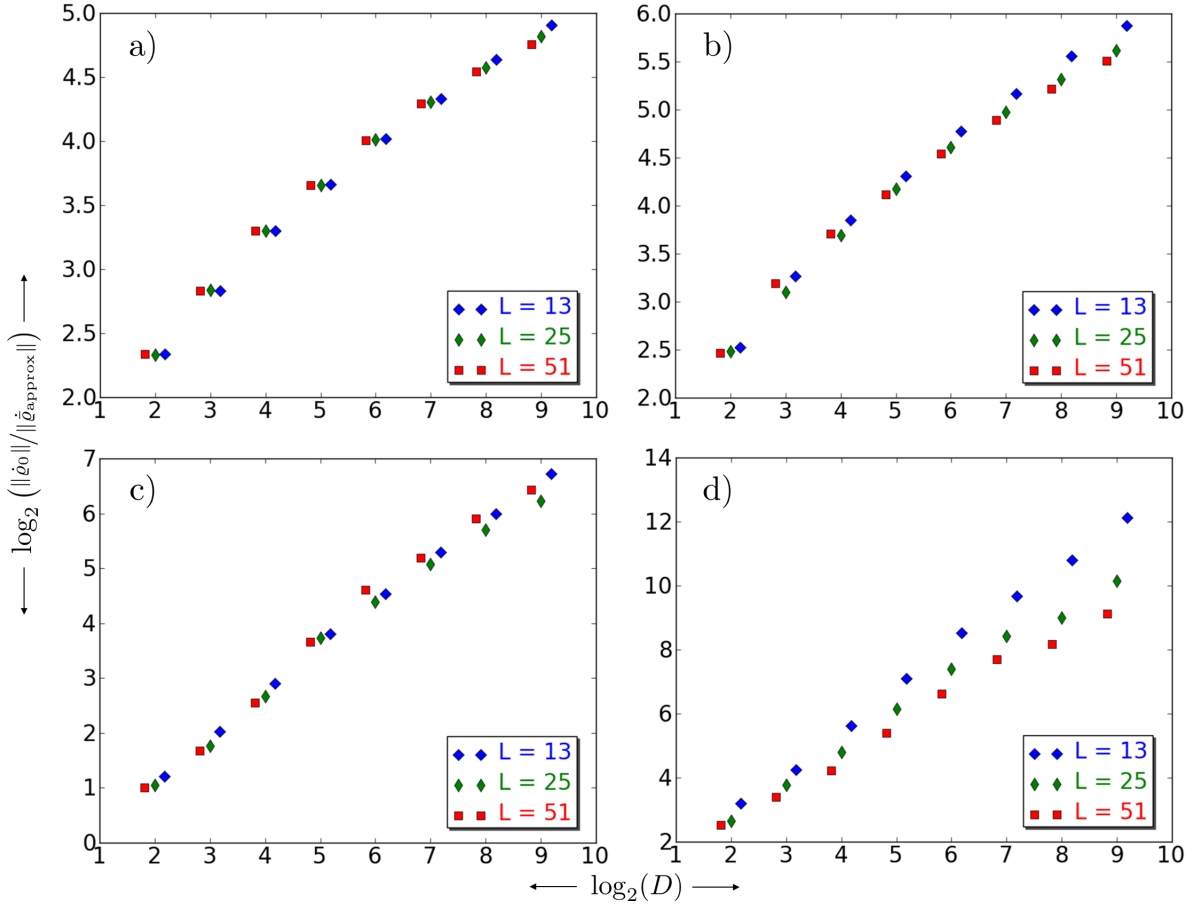


Figure 3: Comparison of the q values (45) for different system lengths $L = 13, 25, 51$. The logarithm of the q value is plotted over the logarithm of the bond dimension D , for a) $\sigma_{\text{field}}^{\text{central}}$ (39), b) S_{field} (40), c) $|\Psi_+\rangle$ (41) and d) $|\Psi_\uparrow\rangle$ (42). In all four cases, the $T+$ method (46) was used combined with a MPO ansatz. For better visibility, the data points are slightly shifted $-\log_2(D)$ is always an integer.

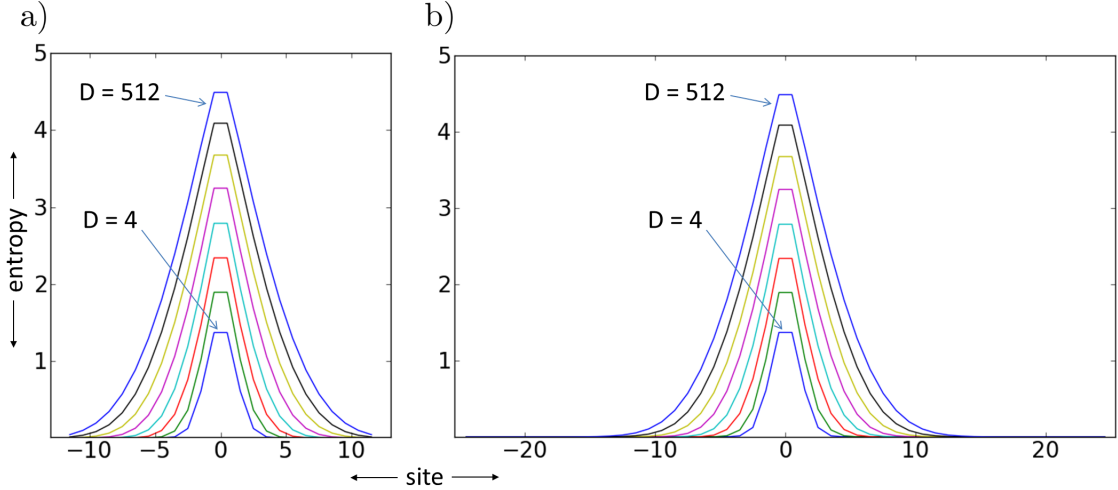


Figure 4: For the time averaged operator $\bar{\sigma}_{\text{field}}^{\text{central}}$ (39) and system sizes a) $L = 25$ and b) $L = 51$, the operator space entanglement entropy (OSEE) is plotted over the position of the bipartition. The OSEE is plotted for all bond dimensions $D = 2^k$ with $k = 2, 3, \dots, 9$, whereby the OSEE is monotone increasing with D . To emphasize the symmetry, the center spin is denoted as position zero.

1. $\bar{\sigma}_{\text{field}}^{\text{central}}$

Fig. 4 shows the OSEE of $\bar{\sigma}_{\text{field}}^{\text{central}}$ (the time average of the operator $\sigma_{\text{field}}^{\text{central}}$ (39)) for two spin chains of length $L = 25$ and $L = 51$. Next to the nearly equidistant scaling of the entropy curves with the bond dimension, we notice a striking resemblance between the plots for $L = 25$ and $L = 51$. The $L = 51$ appears like the trivial continuation of the $L = 25$ plot, where the OSEE is zero for all bipartitions sufficiently far from the center.

A closer inspection shows that the approximated $\bar{\sigma}_{\text{field}}^{\text{central}}$ acts as an identity operator on spins in the area of vanishing OSEE. This explains the findings in Fig. 3 a) that the q value (45) is nearly independent of the system's length.

In the context of MPS approximations, it is quite common that the limitation of the bond dimension induces exponentially decaying correlations. Usually, this can be understood by the mere observation that the amount of information a MPS can transmit is limited, while the amount of transmittable information increases exponentially and hence, has to be damped. In contrast, for the approximated $\bar{\sigma}_{\text{field}}^{\text{central}}$, most of the MPO's capacity to transmit information appears widely unused.

2. S_{field}

Fig. 5 shows the OSEE of the approximated time averaged operator \bar{S}_{field} (40) for two spin chains of length $L = 25$ and $L = 51$. As for $\bar{\sigma}_{\text{field}}^{\text{central}}$ (Fig. 4), a nearly equidistant scaling of the entropy curves with the bond dimension can be observed, but with a much smaller spacing and a distinct offset. Further, the entropy for $L = 51$ is lower than for $L = 25$. Interestingly, if one uses the equidistant scaling for a bold extrapolation to the maximally needed bond dimensions $D = 2^{24}$ respectively $D = 2^{50}$, one finds that the maximal value of the OSEE S is around $S \approx 2$ for both system lengths, $L = 25$ as well as $L = 51$.

3. $|\Psi_+\rangle$ and $|\Psi_\uparrow\rangle$

The OSEE of $\bar{\rho}_{\text{approx}}$ for the initial states $|\Psi_+\rangle$ (41) and $|\Psi_\uparrow\rangle$ (42) is shown in Fig. 6 ($L = 51$). The arguably more interesting plot is the one for $|\Psi_\uparrow\rangle$ (Fig. 6 b). Here, the entropy *decreases* with increasing bond dimension. This anomalous behavior might be a consequence of the unorthodox optimization ansatz $\bar{\rho} = \rho_0 - \mathcal{E}M$ (27).

Besides the anomalous decrease of the OSEE with increasing bond dimension, we also notice a convergence of the OSEE. This convergence is even more distinct for smaller spin chains (not shown here), which is in accordance with the stronger dependence of the q value on the system size for $|\Psi_\uparrow\rangle$ (Fig. 3 d). Although the convergence of the OSEE does not necessarily imply the convergence

of the TADM $\bar{\rho}_{\text{approx}} \rightarrow \bar{\rho}_{\text{exact}}$, it is still a good indicator.

4. $|\Psi_{\text{outer flip}}\rangle$ and $|\Psi_{\text{central flip}}\rangle$

The convergence of the OSEE is even more pronounced for the initial states $|\Psi_{\text{central flip}}\rangle$ (43) and $|\Psi_{\text{outer flip}}\rangle$ (44), as shown in Fig. 7. For $|\Psi_{\text{outer flip}}\rangle$ (Fig. 7 a), the OSEE for the bond dimensions 128, 256 and 512 appear as one line and cannot be distinguished.

Due to the excellent convergence of $\bar{\rho}_{\text{approx}}$ for $|\Psi_{\text{outer flip}}\rangle$, we also calculated the time average of the doubled system \mathcal{P}

$$\mathcal{P} := |\Psi_{\text{outer flip}}\rangle\langle\Psi_{\text{outer flip}}| \otimes |\Psi_{\text{outer flip}}\rangle\langle\Psi_{\text{outer flip}}|, \quad (48)$$

whose TADM $\bar{\mathcal{P}}$ allows to compute variances σ^2 (D2) for the time averaged expectation values of $|\Psi_{\text{outer flip}}(t)\rangle$, as is explained in appendix D. The OSEE of the time averaged $\bar{\mathcal{P}}$ is shown in Fig. 8 and indicates a very good convergence, as well.

D. Expectation values

While the OSEE of $\bar{\rho}_{\text{approx}}$ indicates an excellent convergence for the initial state $|\Psi_{\text{outer flip}}\rangle$, the convergence for $|\Psi_\uparrow\rangle$ is less clear and for $|\Psi_+\rangle$, we see no convergence at all. Since this might be the more common situation, we look at the time averaged expectation values of $|\Psi_+\rangle$ and $|\Psi_\uparrow\rangle$ first. As operator, we choose S_{field} (40), for which we have calculated the time average, as well.

Since we have chosen a non-integrable Hamiltonian (38), we do not know the correct results for large systems. The only indicators we can provide are the common convergence of three different methods (MPO and double MPS ansatz for $\bar{\rho}$ and the MPO ansatz for the time averaged operator \bar{S}_{field}) and a comparison with a small, exactly solvable system of 13 sites. The results are shown in Fig. 9. Here, the worst result is arguably the one for the 51 sites long $|\Psi_+\rangle$ state (Fig. 9 b). But taking the difficulty of the task into account, one might still find the results encouraging.

1. Variances

Finally, we come to the most precise results: The TADM for the initial state $|\Psi_{\text{outer flip}}\rangle$ (44), which we employ to determine the time averaged expectation values of the local Pauli matrices $\sigma_z^{(j)}$. As already announced, we can take advantage of the techniques described in appendix D and use the time average $\bar{\mathcal{P}}$ of the doubled system to compute the variances

$$\begin{aligned} \text{Var}\left(\langle\sigma_z^{(j)}\rangle\right) &= \frac{\langle\Psi_{\text{outer flip}}|\sigma_z^{(j)}|\Psi_{\text{outer flip}}\rangle^2}{\langle\Psi_{\text{outer flip}}|\sigma_z^{(j)}|\Psi_{\text{outer flip}}\rangle} \\ &- \frac{\langle\Psi_{\text{outer flip}}|\sigma_z^{(j)}|\Psi_{\text{outer flip}}\rangle^2}{\langle\Psi_{\text{outer flip}}|\sigma_z^{(j)}|\Psi_{\text{outer flip}}\rangle}. \quad (49) \end{aligned}$$

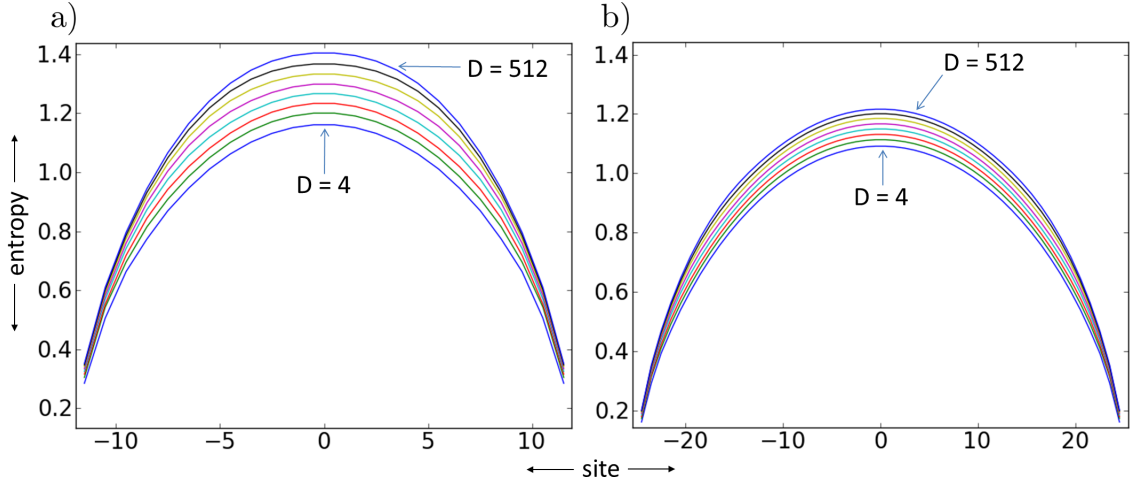


Figure 5: For the time averaged operator \bar{S}_{field} (39) and system sizes a) $L = 25$ and b) $L = 51$, the operator space entanglement entropy (OSEE) is plotted over the position of the bipartition. The different curves belong to different bond dimensions $D = 2^k$ with $k = 2, 3, \dots, 9$, whereby the OSEE is monotone increasing with D . To emphasize the symmetry, the center spin is denoted as position zero.

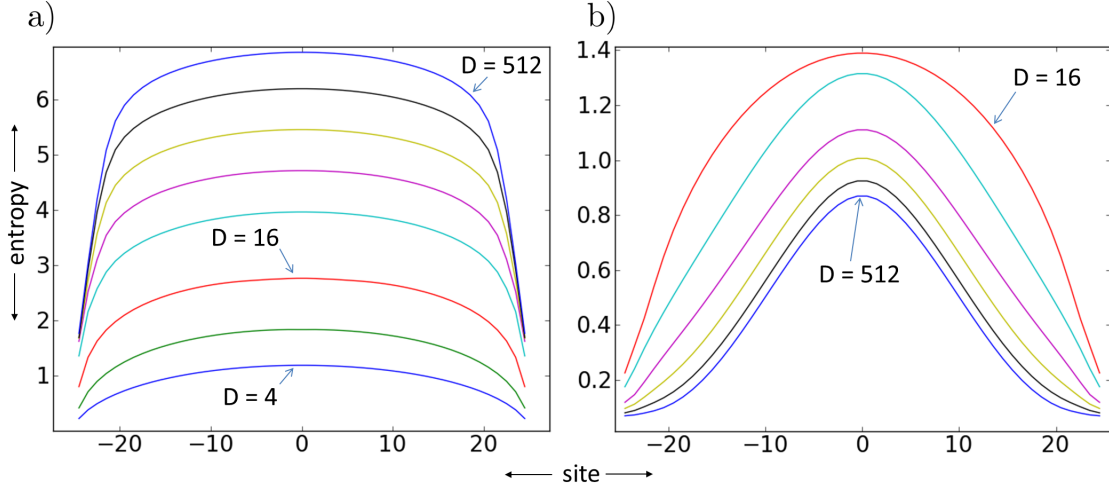


Figure 6: For the initial states a) $|\Psi_+\rangle$ (41) and b) $|\Psi_\uparrow\rangle$ (42) and a system size $L = 51$, the operator space entanglement entropy (OSEE) of the TADM $\bar{\rho}$ is plotted over the position of the bipartition. The different curves belong to different bond dimensions $D = 2^k$, where for a) $k = 2, 3, \dots, 9$ and b) $k = 4, 5, \dots, 9$. For $|\Psi_+\rangle$, the OSEE is monotone increasing with D , while for $|\Psi_\uparrow\rangle$, the OSEE is monotone decreasing with D . To have an unambiguously decreasing plot for $|\Psi_\uparrow\rangle$, the bond dimensions $D = 4, 8$ were omitted, since for for them, the OSEE is smaller than for $D = 16$. To emphasize the symmetry, the center spin is denoted as position zero.

We determined the time averaged expectation values $\overline{\langle \sigma_z^{(j)} \rangle}$ and the associated variances for spin systems of lengths $L = 13, 25, 51$, see Fig. 10. Here, we find virtually identical results for the MPO and the double MPS ansatz.

For $L = 13$, the time averaged expectation values $\overline{\langle \sigma_z^{(j)} \rangle}$ and their variances can also be calculated exactly (D8). The results of our algorithm display a slight overestimation of the variances compared to the exact results. To put this finding into the right perspective, we also determined the variances by sampling over $1.5 \cdot 10^5$ different

$|\Psi_{\text{outer flip}}(t)\rangle$ for times $t = 0 \dots 10^5$ and $3 \cdot 10^5$ samples for $t = 0 \dots 10^{10}$. Hereby, we observed a greater difference between the variances belonging to the time interval $t = 0 \dots 10^5$ and the exact result than for the result of the time interval $t = 0 \dots 10^5$ and the outcome of our algorithm. For smaller time intervals, this effect is even more pronounced. But even for $t = 0 \dots 10^{10}$, we still notice a difference between the sampled variance and the exact result. This indicates changes on timescales which are extremely long compared to the timespans which are usually accessible for numerical simulations. Independent of

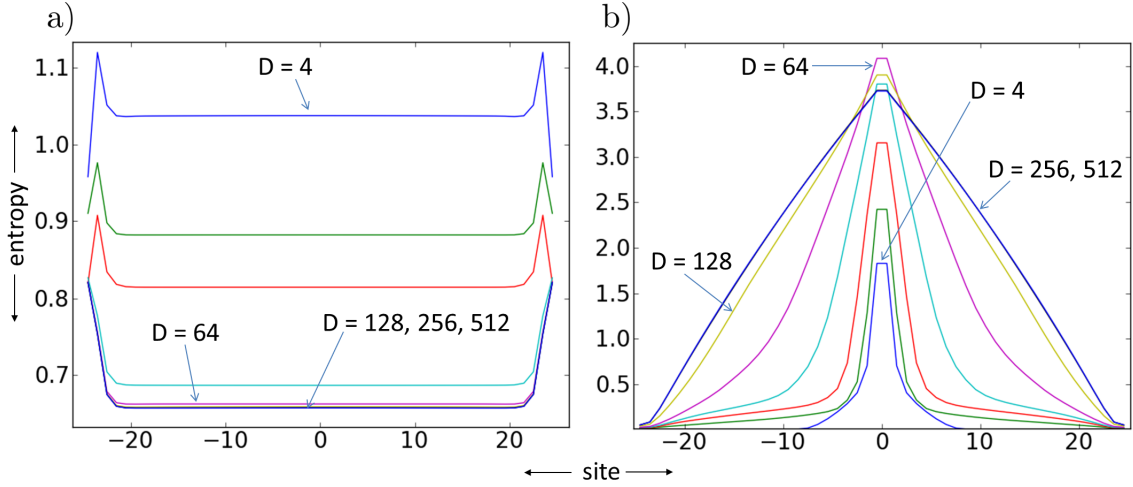


Figure 7: For the initial states a) $|\Psi_{\text{outer flip}}\rangle$ (44) and b) $|\Psi_{\text{central flip}}\rangle$ (43) and a system size $L = 51$, the operator space entanglement entropy (OSEE) of the TADM $\bar{\rho}$ is plotted over the position of the bipartition. The different curves belong to different bond dimensions $D = 2^k$, with $k = 2, 3, \dots, 9$. For $|\Psi_{\text{outer flip}}\rangle$, the OSEE is monotone decreasing with D , while for $|\Psi_{\text{central flip}}\rangle$, the curves broaden with increasing D . To emphasize the symmetry, the center spin is denoted as position zero.

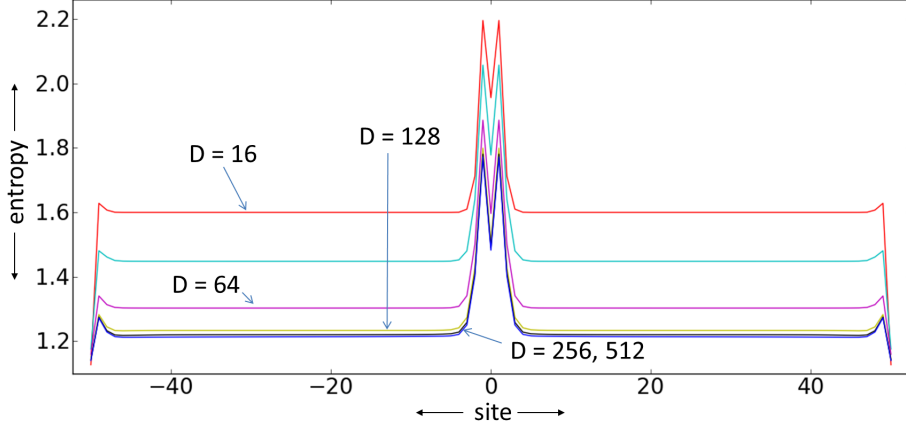


Figure 8: For the initial state \mathcal{P} (48), the operator space entanglement entropy (OSEE) of the TADM $\bar{\rho}$ is plotted over the position of the bipartition. The different curves belong to different bond dimensions $D = 2^k$, with $k = 4, 5, \dots, 9$. The OSEE is monotone decreasing with D . To have an unambiguously decreasing plot, the bond dimensions $D = 4, 8$ were omitted, since for them, the OSEE is smaller than for $D = 16$. The state \mathcal{P} is an artificial double state, consisting of two systems in a row, each of length $L = 51$ in the $|\Psi_{\text{outer flip}}\rangle$ state. The zero position denotes the bipartition which separates these two systems. For the OSEE at this position and the consequences for the variances σ^2 , see also appendix D 1.

these differences, our findings clearly indicate that also for larger systems, the three outer spins do not equilibrate within a predictable timeframe.

Finally, to underpin the reliability (and also the limitations) of our results, in Fig. 11, we show the q values (45) for $\bar{\rho}_{\text{approx}} = |\Psi_{\text{outer flip}}\rangle\langle\Psi_{\text{outer flip}}|$ and $\bar{\mathcal{P}}_{\text{approx}}$ (48). We emphasize that these are not the values obtained from the $T+$ method as in Fig. 3, but the results of the $T-$ method (46), which were also used for the computation of the variances.

IV. DISCUSSION AND OUTLOOK

We have presented a new method to compute time averages of density matrices and operators based on a constraint overlap maximization. A big advantage of this method is that it can be easily combined with a tensor network ansatz, as we demonstrated for matrix product operators (MPO) and double MPS (appendix M). As a new method, it should be compared with already existing ones. Of all possible alternative methods, here, we consider exact diagonalization.

Despite its name, the term *exact* diagonalization is commonly used for a numerical method. Often, the term

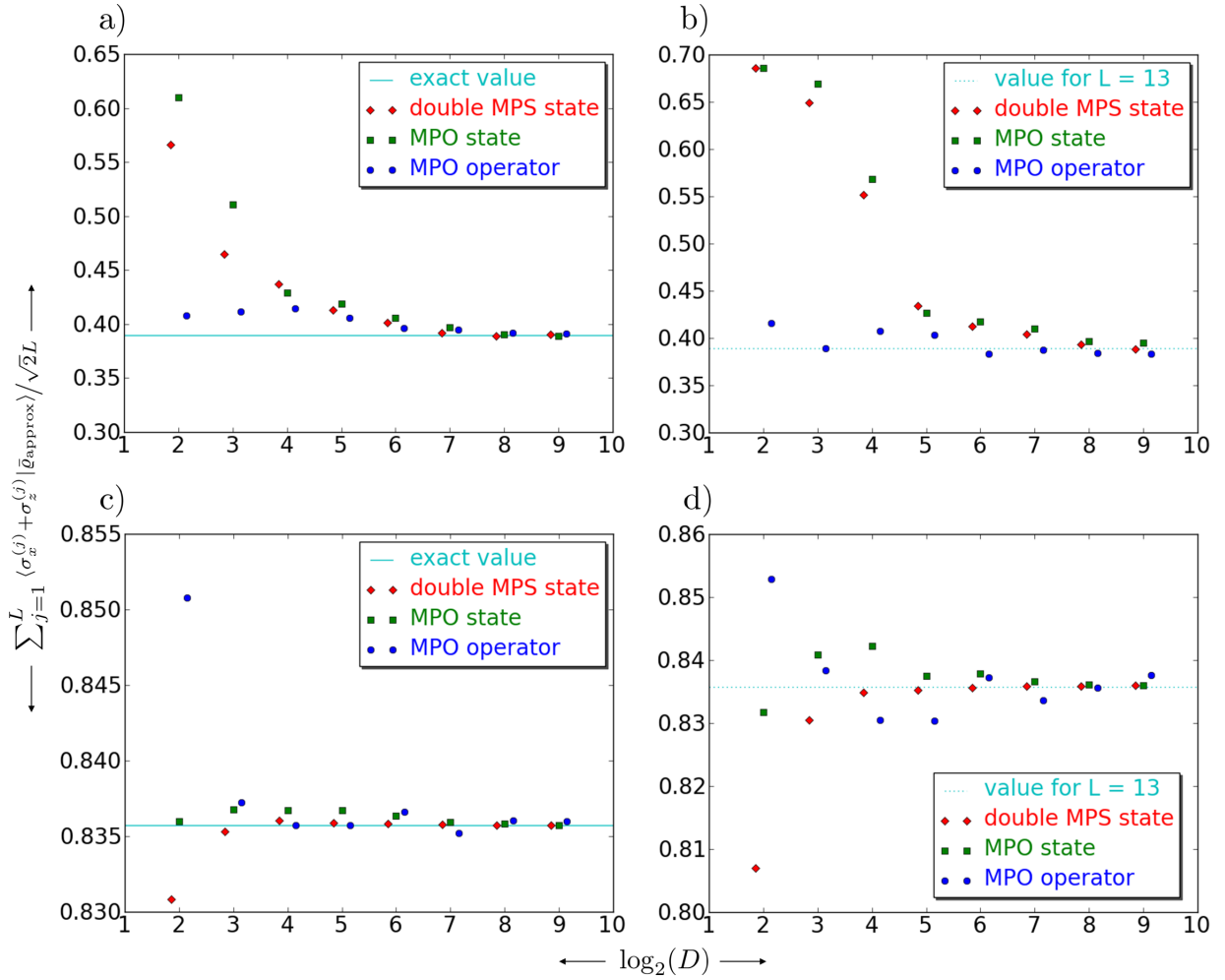


Figure 9: The approximation of the time averaged expectation value $\overline{\langle S_{\text{field}} \rangle}$ (40) is plotted over the logarithm of the bond dimension D . The initial states are a) $|\Psi_+\rangle$ with a system length $L = 13$, b) $|\Psi_+\rangle$ with $L = 51$, c) $|\Psi_\uparrow\rangle$ with $L = 13$ and d) $|\Psi_\uparrow\rangle$ with $L = 51$. To determine the time averaged expectation values, the time average $\overline{S_{\text{field}}}$ of the operator was calculated, as well as the time averaged density matrices $\bar{\rho}$. For $\bar{\rho}$, a MPO and a double MPS (appendix M) ansatz were used. For better visibility, the data points are slightly shifted – $\log_2(D)$ is always an integer.

exact diagonalization is also used for solutions obtained by, e.g., the Lanczos algorithm [28] or related iterative methods [29]. These methods allow to obtain faithful results for some eigenvectors of the outer energy spectrum (especially the ground state) but the results for other eigenvectors in the middle of the spectrum are usually poor for systems of none-trivial sizes.

Here, we only consider system sizes which do not allow a *complete* diagonalization into all eigenvectors. If such a complete diagonalization is possible, this should be the method of choice. Also the iterative diagonalization algorithms can only handle systems up to a certain size. Beyond this limit, one might still combine these algorithms with a tensor network ansatz. This entails new complication, which will not be listed here, but see e.g. Ref. [30] for a detailed treatment.

In case of an exact diagonalization of the outer spectrum only, the decisive question is whether these outer

eigenvectors suffice, e.g., to reconstruct the initial state Ψ_0 . If this is possible, the time averaged density matrix $\bar{\rho}$ can be immediately constructed from these eigenvectors (although for many tasks, the explicit construction is not necessary). Therefore, various initial states Ψ_0 might be categorized by terms like “easy”, “difficult” or “impossible”, depending on their overlap with the eigenvectors of the outer energy spectrum. For the Hamiltonian described by Eq. (38), initial states like $|\Psi_+\rangle$ should qualify for “difficult” up to “impossible” (we did not check this explicitly). Further, determining the time average of an operator $\hat{O}(t)$ with exact diagonalization should be impossible for nearly all commonly used operators.

These tasks, which are difficult up to impossible for exact diagonalization, are also difficult for our algorithm, in the sense that an exact solutions requires huge bond dimensions which exceed our resources. Still, since having a weak approximation is still better than having no

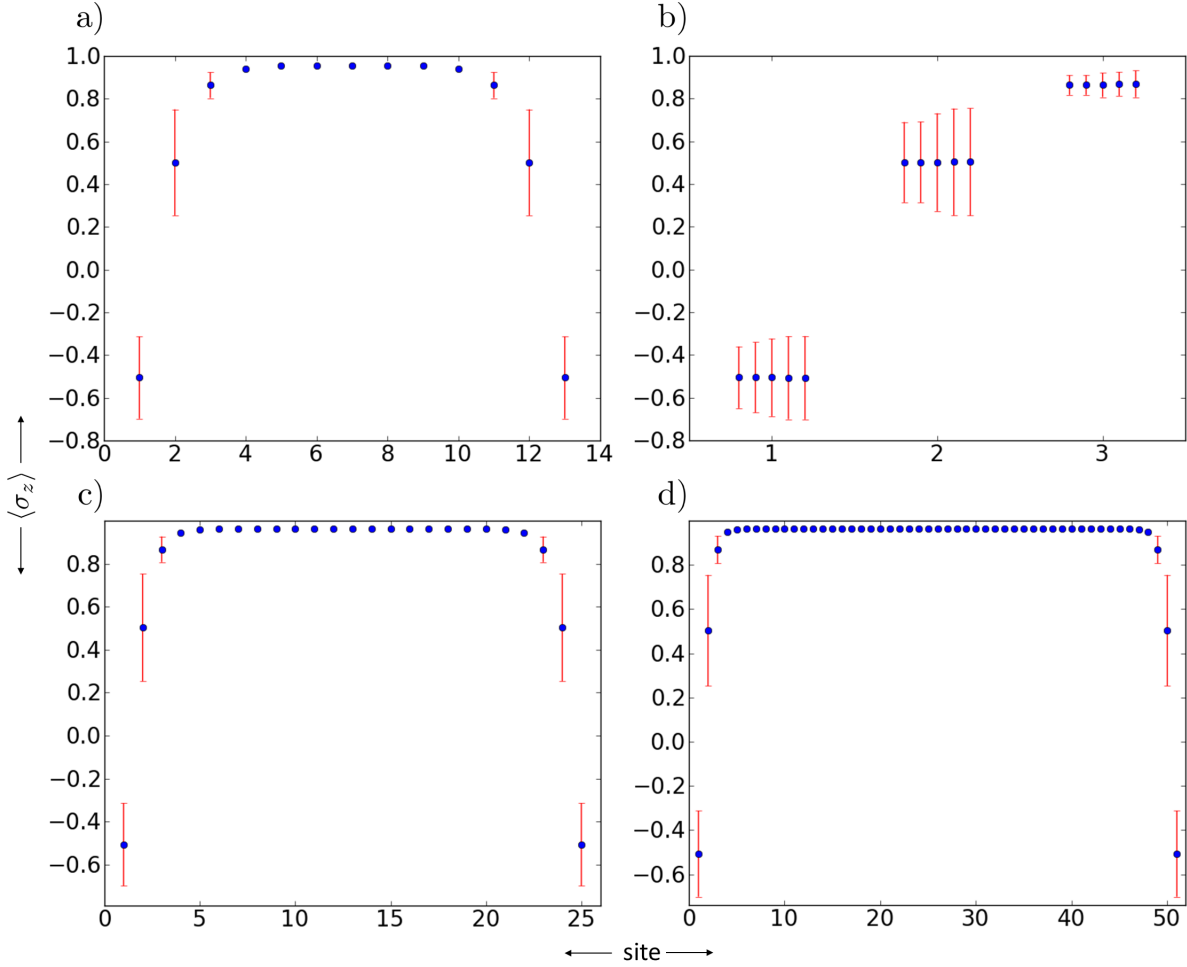


Figure 10: For the initial state $|\Psi_{\text{outer flip}}\rangle$ (44), the time averaged expectation values $\overline{\langle \sigma_z^{(j)} \rangle}$ and their variances are plotted over the site index j , for system lengths a) $L = 13$, c) $L = 25$ and d) $L = 51$. Figure b) shows a comparison of the variances of the three outer sites for $L = 13$, calculated with five different methods (the data points are slightly shifted for better visibility). The methods used for the calculation of these three variances are (from left to right): 1/ exact result according to Eq. (D8); 2/ sampling of $|\Psi_{\text{outer flip}}(t)\rangle$ with $t = 0 \dots 10^{10}$; 3/ sampling of $|\Psi_{\text{outer flip}}(t)\rangle$ with $t = 0 \dots 10^5$; 4/ algorithm with double MPS ansatz (appendix M) and 5/ algorithm with MPO ansatz. For other sites beyond the outer three ones, the variances become so small to separate them reliably from numerical imprecision. The bond dimension is always $D = 512$.

solution at all, this is probably the realm where our algorithm has its strongest superiority compared to exact diagonalization.

For the “easy” states, future investigations have to show which approach is the most promising. Here, exact diagonalization algorithms have a certain advantage, since they only deal with states and not with density matrices, as our algorithm does. But one also has to consider the task at hand. For expectation values, working with a collection of eigenstates is numerically favorable, while for the operator space entanglement entropy (OSEE) calculated in Sec. III C, one needs the explicit form of $\bar{\rho}$. Here, even for many easy initial states, our algorithm should be favorable.

We also determined the variances (Sec. III D 1) associated with the initial state $|\Psi_{\text{outer flip}}\rangle$ (44) and unveiled that the outer spins do not equilibrate. Although

$|\Psi_{\text{outer flip}}\rangle$ should qualify as “easy” state, we are not aware of any previous tensor network based approaches which did a similar calculation.

For future applications, it might be interesting to combine the TADM algorithm with other types of tensor networks, which allow the handling of greater amounts of entanglement and/or higher dimensions than the one-dimensional case treated here. Several alternative tensor network structures are known [31–34] with different advantages and drawbacks. It remains to be seen which of them can be integrated well in the algorithm presented here.

At the end, we like to add the speculation that there is a certain chance that even flawed $\bar{\rho}_{\text{approx}}$ of difficult states might give rise to suitable results for expectation values, if the erroneous contributions average out. For a better understanding, we start with the widely ac-

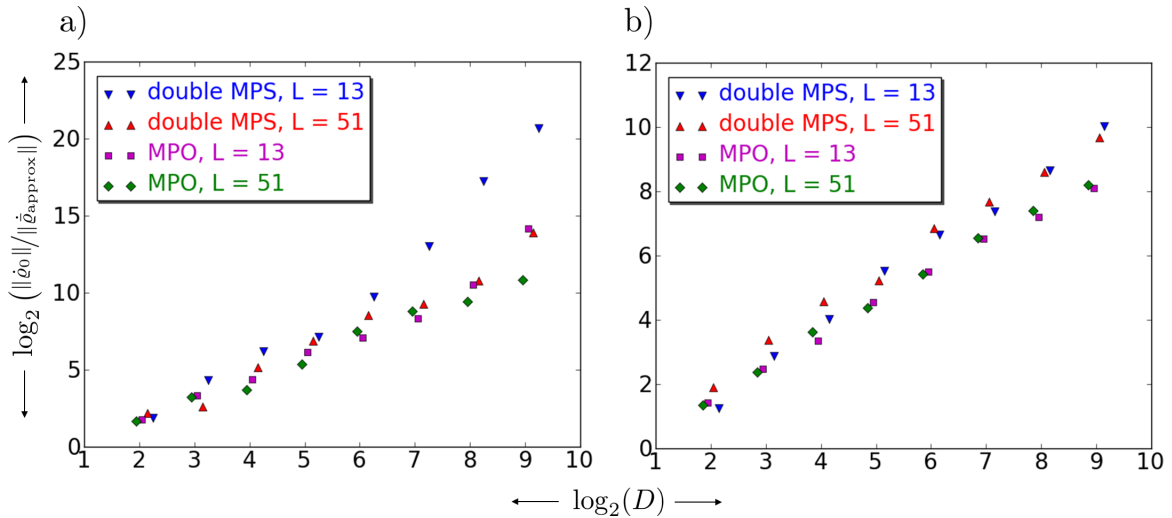


Figure 11: Comparison of the q value (45) for different system lengths $L = 13, 51$ combined with either a MPO or a double MPS ansatz (appendix M). The logarithm of the q value is plotted over the logarithm of the bond dimension D , for a) $|\Psi_{\text{outer flip}}\rangle$ (44) and b) \mathcal{P} (48). In both cases, the T -method (46) was used. For better visibility, the data points are slightly shifted – $\log_2(D)$ is always an integer.

cepted assumption that for most closed quantum states $\varrho(t)$, local expectation values reach an equilibrium value, which they adopt most of the time. If such equilibrium value exists, it has to be the same for $\varrho(t)$ as for the TADM $\bar{\varrho}$. Looking at the off-diagonal elements of such $\varrho(t) = p_{jk}(t)|E_j\rangle\langle E_k|$, we find that $|p_{jk}(t)| = \text{const.}$ That is, contrary to the TADM $\bar{\varrho}$, the off-diagonal elements do not vanish. Still, both density matrices $\varrho(t)$ and $\bar{\varrho}$ have the same expectation values. Here, the general assumption is that the initially aligned $p_{jk}(t = 0)$ dephase and as a consequence, average out.

Now, this dephasing is also an interesting aspect in the context of flawed $\bar{\varrho}_{\text{approx}}$. For difficult states, the algorithm might fail to remove all off-diagonal elements in $\bar{\varrho}_{\text{approx}}$, but if the residual off-diagonal elements are sufficiently randomized, their influence on expectation values might simply average out, as well. At this point, further investigations are needed to decide, whether or not the algorithm really randomizes the residual off-diagonal elements. In any case, we remind the reader that our

algorithm does not introduce errors by altering the diagonal elements of the TADM $\bar{\varrho}$, which is e.g. not true for a flawed diagonalization algorithm.

Acknowledgments

This research was funded by the Austrian Science Fund (FWF): P24273-N16 and by the Austrian Ministry of Science BMWF as part of the UniInfrastrukturprogramm of the Focal Point Scientific Computing at the University of Innsbruck. I like to thank Lars Bonnes and Andreas Läuchli for bringing the TADM problem to my attention. Further, I like to thank them, Jens Eisert and Tomotoshi Nishino for animating discussions, as well as Wolfgang Dür and Jens Eisert for reading the manuscript and providing me with valuable advise.

I'm currently looking for a PostDoc position.

-
- [1] J. Neumann, *Zeitschrift für Physik* **57**, 30 (1929).
 - [2] S. Goldstein, J. L. Lebowitz, R. Tumulka, and N. Zanghi, *European Phys. J. H* **35**, 173 (2010).
 - [3] T. Kinoshita, T. Wenger, and D. Weiss, *Nature* **440**, 900 (2006).
 - [4] V. Yukalov, *Laser Phys. Lett.* **8**, 485 (2011).
 - [5] J. Deutsch, *Phys. Rev. A* **43**, 4 (1991).
 - [6] M. Srednicki, *Phys. Rev. E* **50**, 2 (1994).
 - [7] M. Rigol, V. Dunjko, V. Yurovsky, and M. Olshanii, *Phys. Rev. Lett.* **98**, 050405 (2007).
 - [8] P. Reimann, *Phys. Rev. Lett.* **101**, 190403 (2008).
 - [9] M. Rigol, V. Dunjko, and M. Olshanii, *Nature* **452**, 854 (2008).
 - [10] M. Cramer, C. M. Dawson, J. Eisert, and T. J. Osborne, *Phys. Rev. Lett.* **100**, 030602 (2008).
 - [11] N. Linden, S. Popescu, A. J. Short, and A. Winter, *Phys. Rev. E* **79**, 061103 (2009).
 - [12] M. C. Bañuls, J. I. Cirac, and M. B. Hastings, *Phys. Rev. Lett.* **106**, 050405 (2011).
 - [13] M. Rigol, *Phys. Rev. Lett.* **103**, 100403 (2009).
 - [14] C. Gogolin, M. P. Müller, and J. Eisert, *Phys. Rev. Lett.* **106**, 040401 (2011).
 - [15] M. A. Cazalilla and M. Rigol, *New J. of Phys.* **12**, 055006 (2010).

- [16] A. Polkovnikov, K. Sengupta, and A. S. ans M. Vengalattore, *Rev. Mod. Phys.* **83**, 863 (2011).
- [17] J. Eisert, M. Friesdorf, and C. Gogolin, *Nature Physics* **11** (2015).
- [18] P. Calabrese, F. H. L. Essler, and M. Fagotti, *Phys. Rev. Lett.* **106**, 227203 (2011).
- [19] M. Kormos, M. Collura, and P. Calabrese, *Phys. Rev. A* **89**, 013609 (2014).
- [20] N. Schuch, M. M. Wolf, K. G. H. Vollbrecht, and J. I. Cirac, *New J. Phys.* **10**, 033032 (2008).
- [21] H. Kim, M. C. Bañuls, J. I. Cirac, M. B. Hastings, and D. A. Huse, *Slowest local operators in quantum spin chains*, E-print: arXiv:1410.4186v1 (2014).
- [22] F. Verstraete, J. I. Cirac, and V. Murg, *Adv. Phys.* **57**, 143 (2008).
- [23] U. Schollwöck, *Annals of Physics* **326**, 96 (2011).
- [24] J. Eisert, *Modeling and Simulation* **3**, 520 (2013).
- [25] R. Orus, *Annals of Physics* **349**, 117 (2014).
- [26] T. Prosen and M. Znidaric, *Phys.Rev.E* **75**, 015202 (2007).
- [27] T. Prosen and I. Pizorn, *Phys. Rev. A* **76**, 032316 (2007).
- [28] C. Lanczos, *Journal of research of the National Bureau of Standards* **45**, 255 (1951).
- [29] Y. Saad, *Iterative methods for sparse linear systems (2nd ed.)* (SIAM. ISBN 0898715342, 2003).
- [30] P. E. Dargel, A. Wöllert, A. Honecker, I. P. McCulloch, U. Schollwöck, and T. Pruschke, *Phys. Rev. B* **85** (2012).
- [31] F. Verstraete and J. I. Cirac, *Renormalization algorithms for quantum-many body systems in two and higher dimensions*, E-print: arXiv: cond-mat/0407066 (2004).
- [32] G. Vidal, *Phys. Rev. Lett.* **99**, 220405 (2007).
- [33] R. Hübener, C. Kruszynska, L. Hartmann, W. Dür, F. Verstraete, J. Eisert, and M. Plenio, *Phys. Rev. A* **79**, 022317 (2009).
- [34] R. Hübener, V. Nebendahl, and W. Dür, *New J. Phys.* **12**, 025004 (2010).
- [35] W. Arnoldi, *Quarterly of Applied Mathematics* **9**, 17 (1951).
- [36] G. M. Crosswhite and D. Bacon, *Phys. Rev. A* **78**, 012356 (2008).
- [37] F. Fröwis, V. Nebendahl, and W. Dür, *Phys. Rev. A* **81**, 062337 (2010).

Appendix A: Inverse problem

Here, we study the possibility to solve the time averaged density matrix (TADM) $\bar{\varrho}$ as inverse problem. We start with Eq. (10), which expresses the off-diagonal elements $\varrho_{\text{off-diag}}$ of ϱ_0 as commutator

$$\varrho_{\text{off-diag}} = [H, M] \stackrel{(17)}{=} \mathfrak{C}M. \quad (\text{A1})$$

Our task is to find a suitable matrix M . Formally, this is solved by

$$M = \mathfrak{C}^{-1}\varrho_{\text{off-diag}}. \quad (\text{A2})$$

We do not know the inverse operator \mathfrak{C}^{-1} and generally, it is much more demanding to construct \mathfrak{C}^{-1} than to find a suitable M . Still, it seems beneficial to have a short

look at the formal structure of the inverse problem, since with Eq. (A2), we have establish a link to a well known class of problems. As a bonus, the algorithms derived for the calculation of the matrix M might also be used for other inverse problems, arising from completely different tasks.

In our particular problem, we have to keep in mind that \mathfrak{C} has a non-vanishing kernel $\mathfrak{C}M_{\text{diag}} = 0$ (14). Hence, \mathfrak{C}^{-1} should be a well defined Pseudo-Inverse. That is, while $\mathfrak{C}\cdot\mathfrak{C}^{-1}\varrho_{\text{off-diag}} = \varrho_{\text{off-diag}}$, we also have to demand that

$$\mathfrak{C}\cdot\mathfrak{C}^{-1}\varrho_{\text{diag}} = 0. \quad (\text{A3})$$

As a consequence, we find

$$\begin{aligned} \mathfrak{C}\cdot\mathfrak{C}^{-1}\varrho_0 &= \underbrace{\mathfrak{C}\cdot\mathfrak{C}^{-1}\varrho_{\text{diag}}}_0 + \underbrace{\mathfrak{C}\cdot\mathfrak{C}^{-1}\varrho_{\text{off-diag}}}_{\varrho_{\text{off-diag}}} \\ &= \varrho_{\text{off-diag}}. \end{aligned} \quad (\text{A4})$$

With that, the ansatz described by Eq. (9) reads

$$\bar{\varrho} = \varrho_0 - \mathfrak{C}\cdot\mathfrak{C}^{-1}\varrho_0, \quad (\text{A5})$$

which evidently would not work if \mathfrak{C}^{-1} were a regular inverse.

1. Quasi-degenerate eigenstates

A key aspect of our algorithm is the distinction between diagonal and off-diagonal elements, respectively the difference between the two cases $E_j = E_k$ and $E_j \neq E_k$. Numerically, this distinction becomes blurred for quasi-degenerate energy eigenvalues E_q , E_r with $E_q - E_r = \varepsilon$, where $0 < \varepsilon \ll E_r \lesssim E_q$. As a consequence, if the energy difference ε becomes too small, the calculated time averaged density matrix $\bar{\varrho}$ might contain non-zero matrix elements $\bar{p}_{qr} \neq 0$, which should actually be zero.

To be fair, one has to mention that quasi-degenerate energy eigenvalues pose a general problem, which is not restricted to the method presented here. To illustrate this, let us replace the idealized limit $T \rightarrow \infty$ in the definition (4) of the time averaged density matrix $\bar{\varrho} = \lim_{T \rightarrow \infty} \left(\frac{1}{T} \cdot \int_0^T \varrho(t) \cdot dt \right)$ by a more realistic finite value of T . As long as for this T the condition

$$(E_q - E_r)T \gg \hbar \quad (\text{A6})$$

holds, Eq. (6) is still a good approximation

$$\int_0^T \exp\left(-\frac{i}{\hbar}(E_q - E_r)t\right) dt \approx 0. \quad (\text{A7})$$

But for quasi-degenerate energy eigenvalues, the condition $(E_q - E_r)T \gg \hbar$ might no longer hold and the density matrix $\bar{\varrho}_T$ averaged over the finite timespan T might contain off-diagonal matrix elements \bar{p}_{qr} which deviate substantially from zero.

Appendix B: Alternative optimization ansatz

Throughout this paper, we follow the strategy to express the TADM as $\bar{\varrho} = \varrho_0 - \mathfrak{C}M$ (27). In a realistic setting, the optimal M will be a highly structured object, which is often far to complex to be represented faithfully on a classical computer. Therefore, we have to settle for good approximations of M . This raises the question, how the optimal approximation of M respectively $\bar{\varrho}$ should look like. The answer to this question is not unique and closely related to the question how we actually measure the quality of a given $\bar{\varrho}_{\text{approx}}$.

In general, we need a quality measure which is numerically calculable with the limited computational resources at hand and which does not require knowledge of the exact TADM $\bar{\varrho}$. Under these conditions, the arguably best choice is the residual time dependence of $\bar{\varrho}_{\text{approx}}$, respectively

$$\|\dot{\bar{\varrho}}_{\text{approx}}\| = \|\mathfrak{C}\bar{\varrho}_{\text{approx}}\| \geq 0, \quad (\text{B1})$$

which vanishes for a perfect approximation. Normally, in case of $\|\mathfrak{C}\bar{\varrho}_{\text{approx}}\| = 0$, the diagonal elements of $\bar{\varrho}_{\text{approx}}$ (expressed in energy eigenstates) could still be erroneous. But for our method, which is based on the ansatz $\bar{\varrho}_{\text{approx}} = \varrho_0 - \mathfrak{C}M$ (27), the diagonal elements are guaranteed to be flawless, since $\mathfrak{C}M$ is a purely off-diagonal matrix. Hence, $\|\mathfrak{C}\bar{\varrho}_{\text{approx}}\| = 0$ if and only if the approximation is perfect.

Now, let us try to find the matrices M which minimize $\|\mathfrak{C}\bar{\varrho}_{\text{approx}}\| = \|\mathfrak{C}(\varrho_0 - \mathfrak{C}M)\|$

$$\begin{aligned} M &= \arg \min \left(\|\mathfrak{C}(\varrho_0 - \mathfrak{C}M')\|^2 \right) \\ &= \arg \min \left(\underbrace{\langle \varrho_0 | \mathfrak{C}^2 | \varrho_0 \rangle}_{=\text{const.}} - 2\text{Re}(\langle \varrho_0 | \mathfrak{C}^3 | M' \rangle) \right. \\ &\quad \left. + \langle M' | \mathfrak{C}^4 | M' \rangle \right). \end{aligned} \quad (\text{B2})$$

This minimization can be done in two steps. First, we determine the optimal M_{normed} under the condition that $\langle M | \mathfrak{C}^4 | M \rangle = 1$, i.e.

$$M_{\text{normed}} = \arg \max_{\langle M' | \mathfrak{C}^4 | M' \rangle = 1} \left(\langle \varrho_0 | \mathfrak{C}^3 | M' \rangle \right). \quad (\text{B3})$$

Once this M_{normed} is found, we can rescale it similar to Eq. (27). Hence, Eq. (B2) becomes minimal for

$$M = \langle \mathfrak{C}^3 M_{\text{normed}} | \varrho_0 \rangle \cdot M_{\text{normed}}. \quad (\text{B4})$$

1. Which method is better?

The minimization of Eq. (B2) results in a $\bar{\varrho}_{\text{approx}}$ with the smallest possible time dependence. But how about other physical properties as expectation values? Here, the standard method which minimizes $\|\bar{\varrho}_{\text{approx}}\|$ (28) should still be the better choice, as we discuss in the following.

The error in any expectation value made by using $\bar{\varrho}_{\text{approx}}$ instead of the exact $\bar{\varrho}$ stems entirely from residual off-diagonal elements $\bar{p}_{jk} |E_j\rangle \langle E_k|$ in $\bar{\varrho}_{\text{approx}}$ with $\bar{p}_{jk} \neq 0$. Both methods try to remove these off-diagonal elements, but for the minimization of $\|\mathfrak{C}\bar{\varrho}_{\text{approx}}\|$, elements with small energy differences $|E_j - E_k|$ have lower priority than elements with high energy differences. Generally, there is no reason why elements with high energy differences should have a stronger impact on the error than elements with low energy differences. It is even more likely to assume that for a local operator O_{local} , the unwanted contribution $\langle E_k | O_{\text{local}} | E_j \rangle$ is close to zero if the energy difference $|E_j - E_k|$ is high.

For the remainder of the paper, only the minimization of $\|\bar{\varrho}_{\text{approx}}\|$ respectively Eq. (26) are explained. However, the adaptations to be made to handle Eq. (B3) and with that the minimization of $\|\mathfrak{C}\bar{\varrho}_{\text{approx}}\|$ should be quite obvious, once the principles of the algorithm are understood.

Appendix C: Time averaged operator and error reduction

The TADM $\bar{\varrho}$ is an object which is associated with the Schrödinger picture, where states are time dependent and operators are time independent. In the Heisenberg picture, where states are time independent and the operators are time dependent, the analog to the TADM is a time averaged operator \bar{O}

$$\bar{O} = \lim_{T \rightarrow \infty} \left(\frac{1}{T} \int_0^T O(t) dt \right). \quad (\text{C1})$$

As done for ϱ_0 , the initial operator O_0 at time $t = 0$ can be written as

$$O_0 = \sum_{j,k} o_{jk} |E_j\rangle \langle E_k|. \quad (\text{C2})$$

Analog to Eq. (9), the time averaged operator \bar{O} consists of (block-)diagonal elements only and can be expressed as

$$\bar{O} = O_{\text{diag}} = O_0 - O_{\text{off-diag}}. \quad (\text{C3})$$

Following the same line of argumentation that led to Eq. (27) for the TADM $\bar{\varrho}$, we find that \bar{O} can be obtained as

$$\bar{O} = O_0 - \langle \mathfrak{C}\tilde{M} | O_0 \rangle \cdot \mathfrak{C}\tilde{M}, \quad (\text{C4})$$

where \tilde{M} has to be chosen such that the inner product $\langle O_0 | \mathfrak{C}\tilde{M} \rangle$ is maximized and $\|\mathfrak{C}\tilde{M}\|^2 = 1$.

Using the decomposition into diagonal and off-diagonal elements $\bar{\varrho} = \varrho_{\text{diag}}$ and $O_0 = O_{\text{diag}} + O_{\text{off-diag}}$, we find for

time averaged expectations values $\langle \bar{O} \rangle$

$$\begin{aligned}
\langle \bar{O} \rangle &:= \langle \bar{\varrho} | O_0 \rangle \\
&= \langle \varrho_{\text{diag}} | O_{\text{diag}} + O_{\text{off-diag}} \rangle \\
&= \langle \varrho_{\text{diag}} | O_{\text{diag}} \rangle + \underbrace{\langle \varrho_{\text{diag}} | O_{\text{off-diag}} \rangle}_{=0} \\
&= \langle \bar{\varrho} | \bar{O} \rangle,
\end{aligned} \tag{C5}$$

where we used that $\langle A_{\text{diag}} | B_{\text{off-diag}} \rangle \equiv 0$ for any matrices A, B due to structure of the inner product $\langle A | B \rangle = \sum_{j,k} a_{jk}^* b_{jk}$. Similarly, we find

$$\langle \bar{\varrho} | O_0 \rangle = \langle \bar{\varrho} | \bar{O} \rangle = \langle \varrho_0 | \bar{O} \rangle. \tag{C6}$$

The possibility to use both time averaged matrices $\bar{\varrho}$ and \bar{O} to calculate the time averaged expectation value $\langle \bar{O} \rangle = \langle \bar{\varrho} | \bar{O} \rangle$ offers a potential way to reduce numerical errors, as we show next.

1. Error reduction

For most non-trivial cases, any numerical optimization routine will only be able to find approximated matrices M (27) and \bar{M} (C4), which deviate from the optimal ones. In this case, the off-diagonal elements of the obtained $\bar{\varrho}_{\text{approx}}$ and \bar{O}_{approx} do not vanish completely, as they should. That is

$$\begin{aligned}
\bar{\varrho}_{\text{approx}} &= \varrho_{\text{diag}} + \mathcal{E}_{\text{off-diag}}^{[\bar{\varrho}]} \\
\bar{O}_{\text{approx}} &= O_{\text{diag}} + \mathcal{E}_{\text{off-diag}}^{[\bar{O}]},
\end{aligned} \tag{C7}$$

where, $\mathcal{E}_{\text{off-diag}}^{[\bar{\varrho}]}$ and $\mathcal{E}_{\text{off-diag}}^{[\bar{O}]}$ represent the erroneous off-diagonal elements. In any case, the diagonal elements are always correct for the approach presented here. With this, we find for the time averaged expectation value $\langle \bar{O} \rangle_{\text{approx}}$

$$\begin{aligned}
\langle \bar{O}_{\text{approx}} \rangle &\stackrel{(48)}{=} \langle \bar{\varrho}_{\text{approx}} | \bar{O}_{\text{approx}} \rangle \\
&\stackrel{(C7)}{=} \langle \varrho_{\text{diag}} + \mathcal{E}_{\text{off-diag}}^{[\bar{\varrho}]} | O_{\text{diag}} + \mathcal{E}_{\text{off-diag}}^{[\bar{O}]} \rangle \\
&= \underbrace{\langle \varrho_{\text{diag}} | O_{\text{diag}} \rangle}_{=\langle \bar{O} \rangle} + \langle \mathcal{E}_{\text{off-diag}}^{[\bar{\varrho}]} | \mathcal{E}_{\text{off-diag}}^{[\bar{O}]} \rangle
\end{aligned} \tag{C8}$$

where we used again that $\langle A_{\text{diag}} | B_{\text{off-diag}} \rangle \equiv 0$. Evidently, in case we use both approximated time averages $\bar{\varrho}_{\text{approx}}$ and \bar{O}_{approx} , the error $E^{[\bar{\varrho}, \bar{O}]}$ in the time averaged expectation value $\langle \bar{O}_{\text{approx}} \rangle$ is given as

$$E^{[\bar{\varrho}, \bar{O}]} = \langle \bar{\varrho}_{\text{approx}} | \bar{O}_{\text{approx}} \rangle - \langle \bar{O} \rangle = \langle \mathcal{E}_{\text{off-diag}}^{[\bar{\varrho}]} | \mathcal{E}_{\text{off-diag}}^{[\bar{O}]} \rangle. \tag{C9}$$

If one resorts to $\langle \bar{O} \rangle = \langle \bar{\varrho} | O_0 \rangle$ or $\langle \bar{O} \rangle = \langle \varrho_0 | \bar{O} \rangle$ instead, the expressions for the errors is obtained by the same line

of reasoning are

$$\begin{aligned}
E^{[\bar{\varrho}]} &= \langle \bar{\varrho}_{\text{approx}} | O_0 \rangle - \langle \bar{O} \rangle = \langle \mathcal{E}_{\text{off-diag}}^{[\bar{\varrho}]} | O_{\text{off-diag}} \rangle \\
E^{[\bar{O}]} &= \langle \varrho_0 | \bar{O}_{\text{approx}} \rangle - \langle \bar{O} \rangle = \langle \varrho_{\text{off-diag}} | \mathcal{E}_{\text{off-diag}}^{[\bar{O}]} \rangle.
\end{aligned} \tag{C10}$$

To compare the errors $E^{[\bar{\varrho}, \bar{O}]}$, $E^{[\bar{\varrho}]}$ and $E^{[\bar{O}]}$, we start with a simple error model, which assumes that all off-diagonal elements are roughly damped by the same factor $\varepsilon < 1$, giving us

$$\begin{aligned}
\mathcal{E}_{\text{off-diag}}^{[\bar{\varrho}]} &= \varepsilon \varrho_{\text{off-diag}} \\
\mathcal{E}_{\text{off-diag}}^{[\bar{O}]} &= \varepsilon O_{\text{off-diag}}.
\end{aligned} \tag{C11}$$

In this case, $E^{[\bar{\varrho}, \bar{O}]} = \varepsilon^2 \langle \varrho_{\text{off-diag}} | O_{\text{off-diag}} \rangle$ scales with the square of ε , while $E^{[\bar{\varrho}]} = E^{[\bar{O}]} = \varepsilon \langle \varrho_{\text{off-diag}} | O_{\text{off-diag}} \rangle$ are only linear in ε .

Unfortunately, for our MPO based calculations, this error model proved to be insufficient. Instead of using one damping factor ε for all matrix elements, it seems more adequate to use individual damping factors ε_{jk} for each matrix element

$$\begin{aligned}
\mathcal{E}_{\text{off-diag}}^{[\bar{\varrho}]} &= \sum_{E_j \neq E_k} \varepsilon_{jk}^{[\bar{\varrho}]} p_{jk} |E_j\rangle \langle E_k| \\
\mathcal{E}_{\text{off-diag}}^{[\bar{O}]} &= \sum_{E_j \neq E_k} \varepsilon_{jk}^{[\bar{O}]} o_{jk} |E_j\rangle \langle E_k|,
\end{aligned} \tag{C12}$$

where p_{jk} and o_{jk} are the matrix elements of ϱ_0 respectively O_0 . With that, we obtain

$$\begin{aligned}
E^{[\bar{\varrho}, \bar{O}]} &\stackrel{(C9)}{=} \sum_{E_j \neq E_k} \varepsilon_{jk}^{[\bar{\varrho}]*} \varepsilon_{jk}^{[\bar{O}]} p_{jk}^* \cdot o_{jk} \\
E^{[\bar{\varrho}]} &\stackrel{(C10)}{=} \sum_{E_j \neq E_k} \varepsilon_{jk}^{[\bar{\varrho}]*} p_{jk}^* o_{jk} \\
E^{[\bar{O}]} &\stackrel{(C10)}{=} \sum_{E_j \neq E_k} \varepsilon_{jk}^{[\bar{O}]} p_{jk}^* o_{jk}.
\end{aligned} \tag{C13}$$

For statistically distributed $|\varepsilon_{jk}^{[\bar{\varrho}]}| \leq 1 \geq |\varepsilon_{jk}^{[\bar{O}]}|$, the error $E^{[\bar{\varrho}, \bar{O}]}$ will generally be smaller than the errors $E^{[\bar{\varrho}]}$ and $E^{[\bar{O}]}$. But we can also find an error model, where this is not the case. Let us suppose that most matrix elements belonging to the bases $|E_j\rangle \langle E_k|$ are either extremely easy to approximate or extremely difficult. In the first case, we expect $\varepsilon_{jk}^{[\bar{\varrho}]} \approx \varepsilon_{jk}^{[\bar{O}]} \approx 0$, while in the second case, $\varepsilon_{jk}^{[\bar{\varrho}]} \approx \varepsilon_{jk}^{[\bar{O}]} \approx 1$ seems an adequate assumption. Evidently, for this error model $\varepsilon_{jk}^{[\bar{\varrho}]*} \cdot \varepsilon_{jk}^{[\bar{O}]} \approx \varepsilon_{jk}^{[\bar{\varrho}]*} \approx \varepsilon_{jk}^{[\bar{O}]}$ and with that, all three errors $E^{[\bar{\varrho}, \bar{O}]}$, $E^{[\bar{\varrho}]}$ and $E^{[\bar{O}]}$ are roughly the same.

Even for the model, where $\varepsilon_{jk}^{[\bar{\varrho}]}$ and $\varepsilon_{jk}^{[\bar{O}]}$ only adopt the two values zero and one, using both time averages $\bar{\varrho}_{\text{approx}}$ and \bar{O}_{approx} to calculate $\langle \bar{O} \rangle$ offers still an advantage, if the values of $\varepsilon_{jk}^{[\bar{\varrho}]}$ and $\varepsilon_{jk}^{[\bar{O}]}$ are not correlated, i.e., if the combinations $\varepsilon_{jk}^{[\bar{\varrho}]} = 1$, $\varepsilon_{jk}^{[\bar{O}]} = 0$ and $\varepsilon_{jk}^{[\bar{\varrho}]} = 0$, $\varepsilon_{jk}^{[\bar{O}]} = 1$ are

realistic. The likelihood of having uncorrelated $\varepsilon_{jk}^{[\bar{\rho}]}$ and $\varepsilon_{jk}^{[O]}$ might strongly increase, if $\bar{\rho}_{\text{approx}}$ and \bar{O}_{approx} are calculated by two different methods. Unfortunately, the error reduction relies on the property of the commutator based method (27) that the error is entirely restricted to the off-diagonal matrix elements of $\bar{\rho}_{\text{approx}}$ and \bar{O}_{approx} , while the diagonal elements are 100% accurate. For other methods, this is not necessarily the case.

Further, we have to ponder the computational effort to contract $\langle \bar{\rho}_{\text{approx}} | \bar{O}_{\text{approx}} \rangle$. While for two MPO, this effort is acceptable, this is e.g. no longer necessarily true if $\bar{\rho}_{\text{approx}}$ is given as double MPS (appendix M) and \bar{O}_{approx} as MPO. For two double MPS, the effort would be acceptable again, but it seems unlikely that a good operator approximation \bar{O}_{approx} can be obtained with an double MPS ansatz. In our MPO based applications, the error correction only provided a slight improvement.

Appendix D: Variance of expectation values

Here, we study the possibility to compute the variance $\sigma^2 = \text{Var}(\langle \varrho(t) | O \rangle)$ of the expectation value $\langle \varrho(t) | O \rangle$ with respect to time for an arbitrary operator O

$$\sigma^2 = \overline{\langle \varrho(t) | O \rangle^2} - \overline{\langle \varrho(t) | O \rangle}^2, \quad (\text{D1})$$

where the overbar $\overline{\dots}$ indicates time average.

The second term in Eq. (D1) is simply $\overline{\langle \varrho(t) | O \rangle}^2 = \langle \bar{\rho} | O \rangle^2$ (C6), while the first term $\overline{\langle \varrho(t) | O \rangle^2}$ needs a more thorough treatment. In order to find the time average with the means presented in this paper, we write

$$\begin{aligned} \langle \varrho(t) | O \rangle^2 &= \langle \varrho(t) | O \rangle \langle \varrho(t) | O \rangle \\ &= \underbrace{\langle \varrho(t) \otimes \varrho(t) |}_{\mathcal{P}(t)} \underbrace{| O \otimes O \rangle}_{\mathcal{O}} \\ &= \langle \mathcal{P}(t) | \mathcal{O} \rangle. \end{aligned} \quad (\text{D2})$$

That is, by squaring the Hilbert space respectively doubling the quantum system, we formally transformed the quadratic expression $\langle \varrho(t) | O \rangle^2$ into the linear expression $\langle \mathcal{P}(t) | \mathcal{O} \rangle$. This allows us to proceed as follows

$$\begin{aligned} \overline{\langle \varrho(t) | O \rangle^2} &= \lim_{T \rightarrow \infty} \left(\frac{1}{T} \int_0^T \langle \varrho(t) | O \rangle^2 dt \right) \\ &\stackrel{(\text{D2})}{=} \lim_{T \rightarrow \infty} \left(\frac{1}{T} \int_0^T \langle \mathcal{P}(t) | \mathcal{O} \rangle dt \right) \\ &= \left\langle \lim_{T \rightarrow \infty} \left(\frac{1}{T} \int_0^T \mathcal{P}(t) dt \right) \middle| \mathcal{O} \right\rangle \\ &= \langle \bar{\mathcal{P}} | \mathcal{O} \rangle. \end{aligned} \quad (\text{D3})$$

Alternatively, we could also compute the time averaged $\bar{\mathcal{O}}$ instead of $\bar{\mathcal{P}}$, since $\langle \bar{\mathcal{P}} | \mathcal{O} \rangle = \langle \mathcal{P}_0 | \bar{\mathcal{O}} \rangle$ (C6). To calculate $\bar{\mathcal{P}} = \mathcal{P}_{\text{diag}}$, we can use Eq. (27) $\bar{\mathcal{P}} = \mathcal{P}_0 - [\mathcal{H}, \mathcal{M}]$, where \mathcal{M} is a suitable matrix we have to find and $\mathcal{H} = H \otimes$

$\mathbb{1} + \mathbb{1} \otimes H$ is the Hamiltonian of the doubled quantum system. The chosen structure of the Hamiltonian \mathcal{H} is easily understood when we look at the time evolution of $\mathcal{P}(t) = \varrho(t) \otimes \varrho(t)$

$$\begin{aligned} \varrho(t) \otimes \varrho(t) &= (e^{-iHt} \varrho_0 e^{iHt}) \otimes (e^{-iHt} \varrho_0 e^{iHt}) \\ &= e^{-iH \otimes \mathbb{1} t} e^{-i\mathbb{1} \otimes H t} (\varrho_0 \otimes \varrho_0) e^{iH \otimes \mathbb{1} t} e^{i\mathbb{1} \otimes H t} \\ &= e^{-i(H \otimes \mathbb{1} + \mathbb{1} \otimes H)t} (\varrho_0 \otimes \varrho_0) e^{i(H \otimes \mathbb{1} + \mathbb{1} \otimes H)t} \\ &= e^{-i\mathcal{H}t} (\varrho_0 \otimes \varrho_0) e^{i\mathcal{H}t}, \end{aligned} \quad (\text{D4})$$

with $\hbar := 1$.

1. Fully equilibrated systems

Analog to Eq. (D2), we can write $\overline{\langle \varrho(t) | O \rangle^2} = \langle \bar{\rho} | O \rangle^2$ as $\langle \bar{\rho} | O \rangle^2 = \langle \bar{\rho} \otimes \bar{\rho} | O \otimes O \rangle$ and with that

$$\sigma^2 \stackrel{(\text{D1}), (\text{D2})}{=} \langle \bar{\mathcal{P}} | O \otimes O \rangle - \langle \bar{\rho} \otimes \bar{\rho} | O \otimes O \rangle. \quad (\text{D5})$$

If a quantum system can fully equilibrate in the sense that the variances σ^2 vanish for *all* operators O , we must have

$$\forall O : \sigma^2 = 0 \stackrel{(\text{D5})}{\iff} \bar{\mathcal{P}} = \bar{\rho} \otimes \bar{\rho}. \quad (\text{D6})$$

That is, $\bar{\mathcal{P}}$ is a product state consisting of two $\bar{\rho}$. Conversely, the amount of entanglement between the two subsystems in $\bar{\mathcal{P}}$ can be regarded as indirect measure for incomplete equilibration. For most systems, demanding that the variances σ^2 vanish for *all* operators (not just the local ones) should be too strong. On the other hand, we can always restrict the operators to a certain subsystem A by tracing out all parts of \mathcal{P} which do not belong to A and look for the entanglement in the remaining system.

2. Energy eigenstates

The eigenstates $|\mathcal{E}\rangle$ of the Hamiltonian $\mathcal{H} = H \otimes \mathbb{1} + \mathbb{1} \otimes H$ are simply given by $|E_j\rangle \otimes |E_k\rangle$, where $|E_j\rangle$ are the eigenstates of H . Both eigenstates $|E_j\rangle \otimes |E_k\rangle$ and $|E_k\rangle \otimes |E_j\rangle$ have the same eigenvalue $E_j + E_k$. Hence, the spectrum of \mathcal{H} is always degenerate and $\bar{\mathcal{P}}$ is a block-diagonal matrix.

On page 3, we introduced the convention to refer to the block-diagonal elements as “diagonal”, as well (see Eq. (7)). Here, for once, we have to discriminate between diagonal and block-diagonal. Actually, $\bar{\rho} \otimes \bar{\rho}$ and $\bar{\mathcal{P}}$ have the same diagonal elements, but in addition, $\bar{\mathcal{P}}$ has some extra block-diagonal elements due to the afore-mentioned degeneration. Assuming that the spectrum of H itself is non-degenerate and that the spectrum of \mathcal{H} exhibits no further degeneration beyond the one identified above, we

find that

$$\begin{aligned}\bar{\varrho} \otimes \bar{\varrho} &= \sum_{j,k} p_{jj} p_{kk} |E_j\rangle\langle E_j| \otimes |E_k\rangle\langle E_k| \\ \bar{P} &= \bar{\varrho} \otimes \bar{\varrho} + \sum_{j \neq k} p_{jk} p_{kj} |E_j\rangle\langle E_k| \otimes |E_k\rangle\langle E_j|,\end{aligned}\quad (\text{D7})$$

with $p_{jk} = \langle E_j | \varrho_0 | E_k \rangle$. Inserting this result into Eq. (D5), we find for the variance σ^2 of the time averaged expectation value $\langle \bar{O} \rangle$

$$\begin{aligned}\sigma^2 &= \sum_{j \neq k} \|p_{jk} \langle E_k | O | E_j \rangle\|^2 \\ &= \sum_{j \neq k} \|p_{jk} o_{kj}\|^2,\end{aligned}\quad (\text{D8})$$

with $o_{jk} = \langle E_j | O | E_k \rangle$.

Appendix E: Solving the optimization problem – general approach

In Sec. II, we have seen how the calculation of the time averaged density matrix (TADM) $\bar{\varrho}$ can be formulated as a common linear optimization problem with quadratic normalization condition. Here, we study a general approach to solve this problem, whereby, we assume that the needed matrix operations can all be executed. Due to the exponential scaling of the Hilbert space, this assumption is usually only justified for quantum systems consisting of very few particles. Still, other more powerful methods might adopt the ideas of this section, as we will demonstrate for the MPO based approach in appendix F.

We like to construct a matrix M which fulfills Eq. (19)

$$\varrho_{\text{off-diag}} \stackrel{(19)}{=} \mathfrak{C}M \stackrel{(17)}{:=} [H, M] \quad (\text{E1})$$

and hence allows to calculate $\bar{\varrho} = \varrho_0 - \varrho_{\text{off-diag}}$ (9). The strategy we are going to pursue is to approximate M as a sum of iteratively generated matrices \mathcal{M}_j

$$\begin{aligned}M &= \sum_j \alpha_j \mathcal{M}_j \\ \varrho_{\text{off-diag}} &\stackrel{(E1)}{=} \sum_j \alpha_j \mathfrak{C}\mathcal{M}_j,\end{aligned}\quad (\text{E2})$$

with $\alpha_j \in \mathbb{C}$. The matrices \mathcal{M}_j are modified in such a way that the commutators $\mathfrak{C}\mathcal{M}_j$ build an orthonormal system

$$\langle \mathfrak{C}\mathcal{M}_j | \mathfrak{C}\mathcal{M}_k \rangle = \delta_{jk}.\quad (\text{E3})$$

To do so, we can use an iterative method similar to the Gram-Schmidt orthonormalization. Any time we generate a new matrix $\tilde{\mathcal{M}}_n$, it is orthonormalized $\tilde{\mathcal{M}}_n \rightarrow \mathcal{M}_n$

against its precursors $\mathcal{M}_{j < n}$ by the following steps

$$\begin{aligned}\tilde{\mathcal{M}}'_n &= \tilde{\mathcal{M}}_n - \sum_{j=1}^{n-1} \langle \mathfrak{C}\mathcal{M}_j | \mathfrak{C}\tilde{\mathcal{M}}_n \rangle \mathcal{M}_j \\ \mathcal{M}_n &= \|\mathfrak{C}\tilde{\mathcal{M}}'_n\|^{-1} \tilde{\mathcal{M}}'_n.\end{aligned}\quad (\text{E4})$$

The correctness of this procedure is easily seen when we multiply the two equations from the left with \mathfrak{C} , which turns the procedure into the standard Gram-Schmidt orthonormalization for matrices $A_n = \mathfrak{C}\tilde{\mathcal{M}}_n$.

Using Eq. (E2) for $\varrho_{\text{off-diag}}$ and the orthonormalization Eq. (E3), we find

$$\begin{aligned}\langle \mathfrak{C}\mathcal{M}_k | \varrho_{\text{off-diag}} \rangle &\stackrel{(E2)}{=} \sum_j \alpha_j \langle \mathfrak{C}\mathcal{M}_k | \mathfrak{C}\mathcal{M}_j \rangle, \\ &\stackrel{(E3)}{=} \alpha_k.\end{aligned}\quad (\text{E5})$$

According to Eq. (22), the overlap $\langle \mathfrak{C}\mathcal{M}_k | \varrho_{\text{off-diag}} \rangle$ with the unknown $\varrho_{\text{off-diag}}$ is the same as the overlap $\langle \mathfrak{C}\mathcal{M}_k | \varrho_0 \rangle$ with the known ϱ_0 , such that

$$\alpha_k = \langle \mathfrak{C}\mathcal{M}_k | \varrho_0 \rangle \quad (\text{E6})$$

can be calculated for any given \mathcal{M}_k .

In other words, we are able to project the unknown matrix $\varrho_{\text{off-diag}}$ onto a set of orthonormalized commutators $\mathfrak{C}\mathcal{M}_j$. After n iteration steps, the absolute difference between $\varrho_{\text{off-diag}}$ and its approximation $\sum_{j=1}^n \alpha_j \mathfrak{C}\mathcal{M}_j$ is

$$\left\| \varrho_{\text{off-diag}} - \sum_{j=1}^n \alpha_j \mathfrak{C}\mathcal{M}_j \right\| = \left(\|\varrho_{\text{off-diag}}\|^2 - \sum_{j=1}^n |\alpha_j|^2 \right)^{\frac{1}{2}}.\quad (\text{E7})$$

Since we do not know the exact value of $\|\varrho_{\text{off-diag}}\| \leq \|\varrho_0\|$, we have no good estimator for the quality of the approximation. If we had used the numerically more demanding Eq. (B3) instead of Eq. (26) as optimization objective, we would have obtained $\sum_{j=1}^n |\alpha_j|^2 \xrightarrow{n \rightarrow \infty} 1$. But here, we can only state the obvious that the approximation gets better with each new matrix \mathcal{M}_{n+1} with $\alpha_{n+1} \neq 0$. For fast convergence, we like to find new matrices \mathcal{M}_{n+1} with $|\alpha_{n+1}|$ which are preferably as big as possible. This is what we are going to study next.

1. Generating the matrices \mathcal{M}_j

In this subsection, we present a method to generate suitable matrices \mathcal{M}_j for Eq. (E2). To start with the first matrix \mathcal{M}_1 , we like to find a \mathcal{M}_1 with a big absolute value $|\alpha_1|$ (E2), which is according to Eq. (E6)

$$\alpha_1 \stackrel{(E6)}{=} \langle \mathfrak{C}\mathcal{M}_1 | \varrho_0 \rangle \stackrel{(18)}{=} \langle \mathcal{M}_1 | \mathfrak{C}\varrho_0 \rangle.\quad (\text{E8})$$

Therefore, as educated guess, we choose $\tilde{\mathcal{M}}_1 = \mathfrak{C}\varrho_0$. Here, a tilde is used to distinguish the matrices $\tilde{\mathcal{M}}_j$ from

the matrices \mathcal{M}_j which are already correctly orthonormalized according to Eq. (E3). For \mathcal{M}_1 , this simply means $\mathcal{M}_1 = \|\mathfrak{C}\tilde{\mathcal{M}}_1\|^{-1}\tilde{\mathcal{M}}_1$.

Now, what do we choose as second matrix $\tilde{\mathcal{M}}_2$? If we use the same ansatz as for $\tilde{\mathcal{M}}_1$, we have $\alpha_2 = \langle \mathcal{M}_2 | \mathfrak{C} \varrho_0 \rangle$ and hence $\tilde{\mathcal{M}}_2 = \mathfrak{C} \varrho_0$ – but that is the result we already had for $\tilde{\mathcal{M}}_1$, so we cannot use it again. This problem actually occurs for all $\tilde{\mathcal{M}}_{j>1}$. To solve it, we have to go back to the first line of Eq. (E5)

$$\begin{aligned} \langle \mathfrak{C} \mathcal{M}_n | \varrho_{\text{off-diag}} \rangle &\stackrel{\text{(E5)}}{=} \sum_j \alpha_j \langle \mathfrak{C} \mathcal{M}_n | \mathfrak{C} \mathcal{M}_j \rangle \\ &\stackrel{\text{(22)}}{\Leftrightarrow} \langle \mathfrak{C} \mathcal{M}_n | \varrho_0 \rangle = \sum_j \alpha_j \langle \mathfrak{C} \mathcal{M}_n | \mathfrak{C} \mathcal{M}_j \rangle \\ \langle \mathfrak{C} \mathcal{M}_n | \varrho_0 - \sum_{j \neq n} \alpha_j \mathfrak{C} \mathcal{M}_j \rangle &= \alpha_n \langle \mathfrak{C} \mathcal{M}_n | \mathfrak{C} \mathcal{M}_n \rangle \\ \stackrel{\text{(18)}}{\Leftrightarrow} \langle \mathcal{M}_n | \mathfrak{C} \varrho_0 - \sum_{j \neq n} \alpha_j \mathfrak{C}^2 \mathcal{M}_j \rangle &= \alpha_n \langle \mathfrak{C} \mathcal{M}_n | \mathfrak{C} \mathcal{M}_n \rangle. \end{aligned} \quad (\text{E9})$$

Now, we introduce two approximations: First, we ignore the quadratic term $\langle \mathfrak{C} \mathcal{M}_n | \mathfrak{C} \mathcal{M}_n \rangle$ (i.e., treat it as = 1). Second, since we do not know $\mathcal{M}_{j>n}$, we simply ignore them (which is the same as demanding that \mathcal{M}_n will be perfect and no more $\mathcal{M}_{j>n}$ are needed). With that, our educated guess becomes

$$\tilde{\mathcal{M}}_n = \mathfrak{C} \varrho_0 - \sum_{j=1}^{n-1} \alpha_j \mathfrak{C}^2 \mathcal{M}_j. \quad (\text{E10})$$

This can also be written as $\tilde{\mathcal{M}}_n = \tilde{\mathcal{M}}_{n-1} - \alpha_{n-1} \mathfrak{C}^2 \mathcal{M}_{n-1}$. We still have to orthonormalize $\tilde{\mathcal{M}}_n$ (E4). Therefore, we can drop the term $\tilde{\mathcal{M}}_{n-1}$ in $\tilde{\mathcal{M}}_n$, since it can be expressed as linear combination of the previous matrices $\mathcal{M}_{j<n}$

$$\tilde{\mathcal{M}}_n \rightarrow \hat{\mathcal{M}}_n = \mathfrak{C}^2 \mathcal{M}_{n-1}. \quad (\text{E11})$$

Now, \mathcal{M}_n is obtained orthonormalizing $\hat{\mathcal{M}}_n$. From Eq. (E11), we find by induction that the matrices \mathcal{M}_n can be expressed as

$$\mathcal{M}_n = \sum_{j=1}^n \gamma_{nj} \mathfrak{C}^{2j-1} \varrho_0, \quad (\text{E12})$$

with some appropriate coefficients γ_{nj} . Hence, the subspace spanned by the matrices \mathcal{M}_j is

$$\begin{aligned} \text{span} \{ \mathcal{M}_1, \mathcal{M}_2, \dots, \mathcal{M}_n \} &= \text{span} \{ \mathfrak{C} \varrho_0, \mathfrak{C}^3 \varrho_0, \dots \\ &\quad \dots, \mathfrak{C}^{2n-1} \varrho_0 \}, \end{aligned} \quad (\text{E13})$$

which has the structure of a Krylov subspace.

a. Orthogonality

At the end, the matrix \mathcal{M}_n can be obtained orthonormalizing (E4) either $\tilde{\mathcal{M}}_n$ (E10) or $\hat{\mathcal{M}}_n$ (E11) against the previous matrices $\mathcal{M}_{j<n}$. Actually, for $\hat{\mathcal{M}}_n$ it already suffices to orthonormalize it against the last two matrices \mathcal{M}_{n-2} and \mathcal{M}_{n-1} to ensure that it is orthonormal to all matrices $\mathcal{M}_{j<n}$. For $\tilde{\mathcal{M}}_n$, it is even sufficient to orthonormalize it against the last matrix \mathcal{M}_{n-1} only. The proofs are given in appendix G. Still, in practical calculations, such orthogonality results for iteratively generated Krylov subspace basis are often undermined by numerical imprecision and should be handled with care. Therefore, one might still consider to orthonormalize each new matrix against all previous \mathcal{M}_j .

2. Discussion of the general method

To generate suitable \mathcal{M}_j (E2), we have studied a method building up a Krylov subspace, which is a common approach, as, e.g., used by the Lanczos algorithm [28] to find eigenvectors. Therefore, we have a closer look at the inner structure of the solution, which might help to put the method into the right perspective compared to alternative methods. This is a special topic, which might be skipped.

Combing Eq. (E2) and Eq. (E12), we find that after n iterations, $\varrho_{\text{off-diag}}$ is approximated as

$$\begin{aligned} \varrho_{\text{off-diag}} &\stackrel{\text{(E2)}}{\approx} \sum_{j=1}^n \alpha_j \mathfrak{C} \mathcal{M}_j, \\ &\stackrel{\text{(E12)}}{=} \sum_{j=1}^n \alpha_j \mathfrak{C} \sum_{k=1}^j \gamma_{jk} \mathfrak{C}^{2k-1} \varrho_0 \\ &= \sum_{j=1}^n \beta_j \mathfrak{C} \varrho_0, \quad \text{with } \beta_j = \sum_{p=j}^n \alpha_p \gamma_{pj}. \end{aligned} \quad (\text{E14})$$

Evidently, this ansatz uses only even powers of \mathfrak{C} . This corresponds with the general eigenvector problem in Eq. (31). Here, we find the two operators \mathfrak{C}^2 and $\mathfrak{C} | \varrho_0 \rangle \langle \varrho_0 | \mathfrak{C}$, where the latter can be absorbed into the normalization (E3). Solving the general eigenvector problem by a Lanczos algorithm using the same initial vector would result into the same Krylov subspace. Still, one might wonder whether odd powers of \mathfrak{C} could possibly be useful, as well. For the commutator operator (17), the answer is definitely no. For odd powers of the commutator operator, the matrix $\mathfrak{C}^{2j+1} \varrho_0$ has zero overlap with the matrices ϱ_0 and $\varrho_{\text{off-diag}}$, as we prove below (E19).

$$\langle \varrho_{\text{off-diag}} | \mathfrak{C}^{2j+1} \varrho_0 \rangle \stackrel{\text{(22)}}{=} \langle \varrho_0 | \mathfrak{C}^{2j+1} \varrho_0 \rangle \stackrel{\text{(E19)}}{=} 0. \quad (\text{E15})$$

Even with this vanishing overlap, the odd power terms $\mathfrak{C}^{2j+1} \varrho_0$ could still be useful in an indirect way, if they

had an overlap with any of the even power terms $\mathfrak{C}^{2j}\varrho_0$ which have non-vanishing overlaps with ϱ_0 . But this is never the case

$$\langle \mathfrak{C}^{2k}\varrho_0 | \mathfrak{C}^{2j+1}\varrho_0 \rangle \stackrel{(18)}{=} \langle \varrho_0 | \mathfrak{C}^{2(j+k)+1}\varrho_0 \rangle \stackrel{(E19)}{=} 0. \quad (E16)$$

Hence, the terms with odd powers of \mathfrak{C} are of no help to approximate $\varrho_{\text{off-diag}}$.

We still have to prove Eq. (E15) $\langle \varrho_0 | \mathfrak{C}^{2j+1}\varrho_0 \rangle = 0$. To see this, it is useful to expand the commutators \mathfrak{C}^n

$$\langle \varrho_0 | \mathfrak{C}^n \varrho_0 \rangle \stackrel{(17)}{=} \sum_{p=0}^n (-1)^p \binom{n}{p} \langle \varrho_0 | H^{n-p} \varrho_0 H^p \rangle, \quad (E17)$$

with the binomial coefficients $\binom{n}{p}$ as in $(a-b)^n = \sum_{p=0}^n (-1)^p \binom{n}{p} a^{n-p} b^p$. Since ϱ_0 and H are a Hermitian matrices, we can use the cyclic property of the trace to derive

$$\langle \varrho_0 | H^{n-p} \varrho_0 H^p \rangle = \langle \varrho_0 | H^p \varrho_0 H^{n-p} \rangle. \quad (E18)$$

Using this equation together with the identity $\binom{n}{p} = \binom{n}{n-p}$, we can add the terms for p and $n-p$ in Eq. (E17) and use their average to obtain

$$\langle \varrho_0 | \mathfrak{C}^n \varrho_0 \rangle = \sum_{p=0}^n \frac{(-1)^p + (-1)^{n-p}}{2} \binom{n}{p} \langle \varrho_0 | H^{n-p} \varrho_0 H^p \rangle. \quad (E19)$$

Since $(-1)^p + (-1)^{n-p}$ vanishes for all odd numbers n independent of $p \in \mathbb{N}$, the inner product $\langle \varrho_0 | \mathfrak{C}^n \varrho_0 \rangle$ is zero for odd powers $n = 2j + 1$ of \mathfrak{C} , as claimed in Eq. (E15).

The ansatz described by Eq. (E14) does not make use of any terms $H^{n-p}\varrho_0 H^p$ with odd n . It is not that these terms are not useful per se. They are just not generated in a useful combination applying powers of the commutator \mathfrak{C} on ϱ_0 . If we produce these terms by other means, they can be part of the approximation (E2) of $\varrho_{\text{off-diag}}$, as well.

The reason for using the commutator \mathfrak{C} was that it generates matrices which have no overlap with the time averaged density matrix $\bar{\varrho}$. In other words, the components $|E_j\rangle\langle E_k|$ vanish in the matrices generated by the commutator \mathfrak{C} for identical energy eigenvalues $E_j = E_k$. Another way to guaranty the vanishing of these components is resorting to matrices

$$\mathcal{M} = \sum_{p=0}^n a_p H^{n-p} \varrho_0 H^p, \quad \text{with} \quad \sum_{p=0}^n a_p = 0, \quad a_p \in \mathbb{C}. \quad (E20)$$

This can be seen inserting $\varrho_0 = \sum p_{jk} |E_j\rangle\langle E_k|$ in Eq. (E20). Actually, the matrices $\mathfrak{C}^n \varrho_0$ build a subset of the matrices \mathcal{M} (E20). Another example for a subset of the matrices \mathcal{M} are the matrices $\mathfrak{M} = \mathfrak{C}(H^p \varrho_0 H^q)$, with arbitrary $p, q \in \mathbb{N}$.

A special situation arises, when the initial state is pure $\varrho_0 = |\Psi_0\rangle\langle\Psi_0|$. Then, inner products as

$$\langle \varrho_0 | H^p \varrho_0 H^q \rangle = \langle \Psi_0 | H^p | \Psi_0 \rangle \langle \Psi_0 | H^q | \Psi_0 \rangle \quad (E21)$$

are easily calculated if we know all $H^r |\Psi_0\rangle$. In this case, we could also use a diagonalization method based on the Krylov subspace \mathcal{K}_n

$$\mathcal{K}_n = \text{span} \{ |\Psi_0\rangle, H |\Psi_0\rangle, \dots, H^{n-1} |\Psi_0\rangle \}, \quad (E22)$$

as the Lanczos or Arnoldi algorithm [28, 35] to obtain approximated energy eigenstates $|\tilde{E}_j\rangle$. With these, the TADM $\bar{\varrho}$ can be approximated as

$$\bar{\varrho}_{\text{approx}} = \sum_j |\tilde{E}_j\rangle\langle\tilde{E}_j|. \quad (E23)$$

We emphasize that the $\bar{\varrho}_{\text{approx}}$ obtained by this Eq. (E23) is not suitable for the error reduction method introduced in appendix C 1. For this method to work, it is essential that the diagonal elements of the approximated TADM $\bar{\varrho}_{\text{approx}}$ are error-free, i.e.

$$\langle E_j | \bar{\varrho}_{\text{approx}} | E_k \rangle \stackrel{\text{for } E_j = E_k}{=} \langle E_j | \bar{\varrho} | E_k \rangle. \quad (E24)$$

This is generally not true for Eq. (E23), while it is guaranteed for the method introduced here (27).

Appendix F: Time averaged density matrix as matrix product operator

In appendix E, we explained an algorithm for finding the time averaged density matrix (TADM) $\bar{\varrho}$. But so far, this algorithm does not solve the main numerical problem which usually hinders us to calculate $\bar{\varrho}$: The exponential scaling of the Hilbert space with the number of the constituents and the associated demand for computational resources. In this section, we address this problem and present a monotone converging optimization algorithm based on a matrix product operator (MPO) approximation, which allows the handling of the exponential scaling (see overview articles [22–25]).

1. Short introduction to MPO

Any matrix operator M acting on a system consisting of n sites s_j can be written as

$$M = \sum_{s_1 \dots s_n; s'_1 \dots s'_n} \mathfrak{M}_{s_1 \dots s_n}^{s'_1 \dots s'_n} |s_1\rangle\langle s'_1| \otimes \dots \otimes |s_n\rangle\langle s'_n|, \quad (F1)$$

with a high-dimensional tensor $\mathfrak{M}_{s_1 \dots s_n}^{s'_1 \dots s'_n}$. The idea of a MPO is to express this high-dimensional tensor $\mathfrak{M}_{s_1 \dots s_n}^{s'_1 \dots s'_n}$

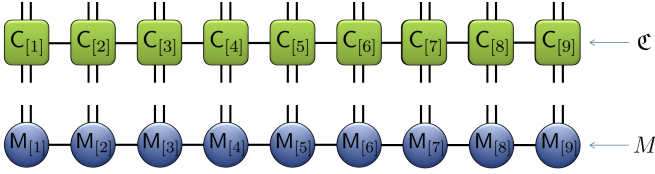


Figure 12: Graphical representation of the MPO for the commutator operator \mathfrak{C} (17) and the matrix M . Each MPO tensor is symbolized by a shape. Auxiliary indices are depicted by horizontal lines, while open vertical indices represent physical indices.

as a product of n low-dimensional tensors $M_{[j]}$.

$$\mathfrak{M}_{s_1 \dots s_n}^{s'_1 \dots s'_n} = \sum_{\alpha_1 \dots \alpha_n} M_{[1]s_1 s'_1}^{\alpha_n \alpha_1} \cdot M_{[2]s_2 s'_2}^{\alpha_1 \alpha_2} \cdots \cdots \cdots M_{[n-1]s_{n-1} s'_{n-1}}^{\alpha_{n-2} \alpha_{n-1}} \cdot M_{[n]s_n s'_n}^{\alpha_{n-1} \alpha_n}, \quad (\text{F2})$$

where s_j and s'_j represent the physical indices, while the α_j are auxiliary indices which are summed over. In case of closed boundary conditions (which we use here), the dimension of the outer index α_n is set to one (i.e., we can ignore this index).

Since Eq. (F2) is not really a well-readable expression (and it becomes even worse if we consider e.g. products of operators), one often resorts to graphical representations, as in Fig. 12. Here, we also use the (non-standard) symbolic shorthand notation

$$M = \prod_j M_{[j]}, \quad (\text{F3})$$

which represents the joint information of Eq. (F1) and Eq. (F2). In the same way, we write $\mathfrak{C} = \prod_j C_{[j]}$ for the commutator operator, where each tensor $C_{[j]}^{\alpha_{j-1} \alpha_j}_{s_j s'_j \bar{s}_j \bar{s}'_j}$ carries the four physical indices $s_j, s'_j, \bar{s}_j, \bar{s}'_j$. For the construction of the MPO tensors of \mathfrak{C} , see also appendix L. To calculate an expression like $\mathfrak{C}M = \prod_j C_{[j]} \cdot M_{[j]}$, we need to sum over the common physical indices

$$C_{[j]} M_{[j]} = \sum_{\bar{s}_j, \bar{s}'_j} C_{[j]s_j s'_j \bar{s}_j \bar{s}'_j}^{\alpha_{j-1} \alpha_j} M_{[j]\bar{s}_j \bar{s}'_j}^{\beta_{j-1} \beta_j} \quad (\text{F4})$$

and the auxiliary indices. To shorten the notation, in the following we will often use the multi-index $\sigma_j = (s_j, s'_j)$ for the two physical indices s_j, s'_j of a MPO tensor.

Many operators which are relevant for practical calculations allow an exact MPO representation based on tensors $M_{[j]}$ (F3) which are of relatively small and constant size, independent of the total number of the constituents. Here, we assume that this is also true for the initial density matrix $\varrho_0 = \prod_j P_{[j]}$ and the Hamiltonian $H = \prod_j H_{[j]}$. If it is true for the Hamiltonian, it is also true for the commutator operator $\mathfrak{C} = \prod_j C_{[j]}$ (17).

Unfortunately, this is not true for all operators. For a general operator \hat{O} , an exact MPO representation

$\hat{O} = \prod_j O_{[j]}$ might demand tensors $O_{[j]}$ whose size scales exponentially with the number of constituents. In this case, one can still use tensors $\tilde{O}_{[j]}$ of limited size to obtain an approximation $\hat{O} \approx \prod_j \tilde{O}_{[j]}$.

Once we put restrictions to the size of the MPO tensors, MPO no longer build a vector space. That is, adding two MPO might create a sum MPO whose tensors exceed the preset size limit. The same is even more likely for the product of two MPO. Therefore, we cannot use a simple one-to-one mapping to cast the algorithm presented in appendix E or any other algorithm into MPO form.

2. MPO tensor optimization

Assume we have two MPO $M' = \prod_j M'_{[j]}$ and $M'' = \prod_j M''_{[j]}$ differing only by one tensor $M'_{[k]} \neq M''_{[k]}$ (which still have the same dimensions), while all other tensors are identical $M'_{[j \neq k]} = M''_{[j \neq k]} = M_{[j \neq k]}$. Symbolically, we write these MPO as

$$\begin{aligned} M' &= M'_{[k]} \prod_{j \neq k} M_{[j]} \\ M'' &= M''_{[k]} \prod_{j \neq k} M_{[j]}. \end{aligned} \quad (\text{F5})$$

For $\alpha, \beta \in \mathbb{C}$, we find

$$\alpha M' + \beta M'' = (\alpha M'_{[k]} + \beta M''_{[k]}) \prod_{j \neq k} M_{[j]}. \quad (\text{F6})$$

The important observation is that the tensor $\alpha M'_{[k]} + \beta M''_{[k]}$ has the same dimensions as $M'_{[k]}$ and $M''_{[k]}$. That is, adding the MPO M' and M'' does not conflict with any preset limits for the size of the MPO tensors. Hence, MPO of the type M' and M'' which differ only by a single tensor still build a vector space. For this reason, these MPO are much more suitable to realize an adaptation of the algorithm explained in appendix E.

We express the TADM as $\bar{\varrho} = \varrho_0 - c \mathfrak{C}M$ (27), where $c \in \mathbb{C}$ and

$$M = \prod_j M_{[j]} \quad (\text{F7})$$

is the MPO we have to find. Our task is to design an algorithm which optimizes a single tensor $M_{[k]}$ while all other tensors $M_{[j \neq k]}$ are kept constant. Once we have this algorithm, we can apply it in repeated sweeps of the index k to all tensors $M_{[k]}$ in the MPO.

In appendix E, we introduced a general algorithm, which expresses M as a sum $M = \sum_l \alpha_l \mathcal{M}_l$ (E2). Here, we adopt this idea but extend it by the demand that the \mathcal{M}_l are all MPO with the same tensors $M_{[j \neq k]}$

$$\mathcal{M}_l = M_{[k]}^{(l)} \prod_{j \neq k} M_{[j]}. \quad (\text{F8})$$

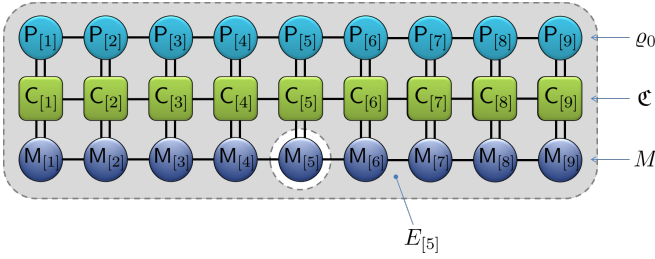


Figure 13: Graphical representation of the MPO overlap $\langle \varrho_0 | \mathfrak{C} | M \rangle$. The area $E_{[5]} = \varrho_0 \mathfrak{C} \prod_{j \neq 5} M_{[j]}$ defines the tensor environment of the tensor $M_{[5]}$. This corresponds to the situation in Eq. (F11), with $\tilde{M}_{[5]}^{(1)} = E_{[5]}^\dagger$.

The MPO \mathcal{M}_l differ only by the tensor $M_{[k]}^{(l)}$. Due to the linearity described by Eq. (F6), the summation of the MPO $M = \sum_l \alpha_l \mathcal{M}_l$ (E2) is equivalent to the summation of the tensors $M_{[k]}^{(l)}$

$$M_{[k]}^{\text{optimized}} = \sum_l \alpha_l M_{[k]}^{(l)}, \quad (\text{F9})$$

resulting in the locally optimized tensor $M_{[k]}^{\text{optimized}}$.

If we follow the ideas outlined in appendix E1 to obtain suitable MPO \mathcal{M}_l , we need to generate linear combinations of $\mathfrak{C}^p \varrho_0$ (E13), where p denotes an exponent. How can we calculate $\mathfrak{C}^p \varrho_0$ while we are at the same time forced to keep all MPO tensors $M_{[j \neq k]}$ unchanged? Here, we have to remind ourselves that the original intention in appendix E1 was to maximize the overlap $\langle \varrho_0 | \mathfrak{C} | M \rangle = \langle \varrho_0 | \mathfrak{C} | M \rangle$ (E8). Inserting Eq. (F8) in $\langle \varrho_0 | \mathfrak{C} | \mathcal{M}_1 \rangle$, we obtain

$$\begin{aligned} \langle \varrho_0 | \mathfrak{C} | \mathcal{M}_1 \rangle &\stackrel{(\text{F8})}{=} \langle \varrho_0 | \mathfrak{C} | M_{[k]}^{(1)} \prod_{j \neq k} M_{[j]} \rangle \\ &= \text{tr} \left(\left(\varrho_0 \mathfrak{C} \prod_{j \neq k} M_{[j]} \right) M_{[k]}^{(1)} \right). \end{aligned} \quad (\text{F10})$$

This is maximized for

$$\tilde{M}_{[k]}^{(1)} = \left(\varrho_0 \mathfrak{C} \prod_{j \neq k} M_{[j]} \right)^\dagger = \left(\prod_{j \neq k} M_{[j]} \right)^\dagger \mathfrak{C} \varrho_0, \quad (\text{F11})$$

see also Fig. 13. In the same fashion, we can generate the tensors $\tilde{M}_{[k]}^{(l)}$ analog to Eq. (E10)

$$\tilde{M}_{[k]}^{(l)} = \left(\prod_{j \neq k} M_{[j]} \right)^\dagger \left(\mathfrak{C} \varrho_0 - \sum_{p=1}^{l-1} \alpha_p \mathfrak{C}^2 \mathcal{M}_p \right), \quad (\text{F12})$$

with $\mathcal{M}_p = M_{[k]}^{(p)} \prod_{j \neq k} M_{[j]}$ (F8). As in Eq. (E10), we used a tilde to mark that $\tilde{M}_{[k]}^{(l)}$ has still to be orthonormalized (E3) against the other tensors. Due to the linearity expressed by Eq. (F6), orthonormalizing the tensor $\tilde{M}_{[k]}^{(l)}$ or the associated MPO $\tilde{\mathcal{M}}_l = \tilde{M}_{[k]}^{(l)} \prod_{j \neq k} M_{[j]}$

is basically the same procedure. In the orthonormalization, as well as in Eq. (F12), we encounter the term $\left(\prod_{j \neq k} M_{[j]} \right)^\dagger \mathfrak{C}^2 \prod_{j \neq k} M_{[j]}$, which is also depicted in Fig. 15 (appendix H).

3. Advisable modification of the algorithm

So far, we have presented a direct adaptation of the ideas presented in appendix E1 to obtain the locally optimized MPO tensors $M_{[k]}^{\text{optimized}}$ (F9). But this adaptation is far from being optimal and does not result in a monotone converging algorithm. This will be mended in this subsection.

To see the problem, imagine that for some reason, we have already found a perfect MPO M , where all MPO tensors $M_{[j]}$ are optimal. Now, let us denote

$$M_{[k]}^{\text{old}} = M_{[k]} \quad (\text{F13})$$

and apply the optimization procedure presented in the last subsection F2 to find a new tensor $M_{[k]}^{\text{optimized}}$. Since $M_{[k]}^{\text{old}}$ is already optimal according to our assumption, the optimization $M_{[k]}^{\text{optimized}} = \sum_l \alpha_l M_{[k]}^{(l)}$ (F9) should reproduce the tensor $M_{[k]}^{\text{old}}$. This is for sure true, if we sum up sufficiently many tensors $M_{[k]}^{(l)}$. But in practical applications, one would usually just calculate a handful of these tensors $M_{[k]}^{(l)}$, resulting in an $M_{[k]}^{\text{optimized}}$ which is supposedly worse than the tensor $M_{[k]}^{\text{old}}$ we started with.

For readers who are familiar with the Krylov subspace based MPO optimization for ground states $|E_0\rangle$

$$|E_0\rangle = \arg \min_{\langle \Psi | \Psi \rangle = 1} \langle \Psi | H | \Psi \rangle, \quad (\text{F14})$$

we mention that here, the main difference is that the Krylov subspace for the ground state search is based on [29]

$$\mathcal{K}_n = \text{span} \{ \Psi, H\Psi, H^2\Psi, \dots, H^{n-1}\Psi \}, \quad (\text{F15})$$

while the algorithm for the TADM is based on

$$\mathcal{K}_n = \text{span} \{ \mathfrak{C} \varrho_0, \mathfrak{C}^3 \varrho_0, \mathfrak{C}^5 \varrho_0, \dots, \mathfrak{C}^{2n-1} \varrho_0 \}, \quad (\text{F16})$$

according to Eq. (E13). If we start the ground state optimization with an optimal MPO $|\Psi\rangle = |E_0\rangle$, this optimal $|\Psi\rangle$ is part of the Krylov subspace used for the optimization. Therefore, the optimal solution is already obtained in the first step. Contrary to the ground state optimization, the algorithm for the TADM starts with $\mathfrak{C} \varrho_0$, which does not convey any previously gained information about the optimal solution.

Of course, starting the optimization with an already perfect solution is just an extreme example to illustrate the problem: The algorithm, as it is so far, does not learn from previous optimization steps. This is actually easy

to fix. We just include the old MPO tensor $M_{[k]}^{\text{old}}$ into the subspace basis we use for finding the optimal tensor $M_{[k]}^{\text{optimized}}$. The subspace we obtain in this fashion is no longer a pure Krylov subspace, but this is actually of no real importance.

So, we still use Eq. (F9)

$$M_{[k]}^{\text{optimized}} = \sum_l \alpha_l M_{[k]}^{(l)}, \quad (\text{F17})$$

but for the first basis tensor $M_{[k]}^{(1)}$, we now take the normalized (E3) old tensor

$$M_{[k]}^{(1)} = \frac{1}{\|\mathfrak{C}M\|} M^{\text{old}}_{[k]}. \quad (\text{F18})$$

For the second basis tensor $M_{[k]}^{(2)}$, we could use the formerly first tensor $\tilde{M}_{[k]}^{(2)} \stackrel{?}{=} (\prod_{j \neq k} M_{[j]})^\dagger \mathfrak{C} \varrho_0$ (F11). But following the same line of argumentation which led to Eq. (E10), we find it actually more advisable to use directly Eq. (F12) (the analog tensor equation of Eq. (E10))

$$\tilde{M}_{[k]}^{(>1)} = \left(\prod_{j \neq k} M_{[j]} \right)^\dagger \left(\mathfrak{C} \varrho_0 - \sum_{p=1}^{l-1} \alpha_p \mathfrak{C}^2 \mathcal{M}_p \right). \quad (\text{F19})$$

a. Further modifications

The algorithm has still room for further improvements, which are explained in detail in the following appendices. Here, we just outline what can still be done:

- Tensor networks exhibit a versatile gauge freedom. Choosing an optimal gauge is an essential ingredient for a successful tensor optimization. It is advisable to use a non-standard gauge, which is tailored for the weighted norm (E3) used in the algorithm. This is explained in appendix H.
- The tensor optimization is done in many successive sweeps. With a small alteration, we can take advantage of previous optimization sweeps to speed up the convergence. This is a special feature of the TADM algorithm, which we dubbed overarching orthonormalization. For more details, see appendix I
- Density matrices are always Hermitian matrices. This implies a symmetry which can be exploited and allows to map complex valued MPO onto real valued MPO with the same bond dimension. While most symmetries are connected to some special properties of the physical system in question, the Hermitian symmetry is common to all physical systems. For more, see appendix J.

Appendix G: Orthogonality proofs

Here, we provide some orthogonality proofs. First, we start with the matrices $\tilde{\mathcal{M}}_n$ (E10) respectively $\hat{\mathcal{M}}_n$ (E11) introduced in appendix E and after that, we look at their tensor network version $\tilde{M}_{[k]}^{(l)}$ (F18) and (F19). That is, we first show for the general method of appendix (E)

$$\langle \mathfrak{C} \mathcal{M}_{j < n-2} | \mathfrak{C} \hat{\mathcal{M}}_n \rangle = 0 \quad (\text{G1})$$

$$\langle \mathfrak{C} \mathcal{M}_{j < n-1} | \mathfrak{C} \tilde{\mathcal{M}}_n \rangle = 0, \quad (\text{G2})$$

which expresses the demanded orthogonality according to Eq. (E3).

We start with the proof of Eq. (G1), which is a standard proof for Krylov subspaces

$$\begin{aligned} \langle \mathfrak{C} \mathcal{M}_j | \mathfrak{C} \hat{\mathcal{M}}_n \rangle &\stackrel{(\text{E11})}{=} \langle \mathfrak{C} \mathcal{M}_j | \mathfrak{C} (\mathfrak{C}^2 \mathcal{M}_{n-1}) \rangle \\ &\stackrel{(18)}{=} \langle \mathfrak{C} (\mathfrak{C}^2 \mathcal{M}_j) | \mathfrak{C} \mathcal{M}_{n-1} \rangle \\ &\stackrel{(\text{E11})}{=} \langle \mathfrak{C} \hat{\mathcal{M}}_{j+1} | \mathfrak{C} \mathcal{M}_{n-1} \rangle \end{aligned} \quad (\text{G3})$$

The matrix $\hat{\mathcal{M}}_{j+1}$ lies in the subspace span $\{\mathcal{M}_1, \mathcal{M}_2, \dots, \mathcal{M}_{j+1}\}$, which is orthogonal to \mathcal{M}_{n-1} (according to the definition (E3)) for $j+1 < n-1$. Hence, for $j < n-2$, the overlap $\langle \mathfrak{C} \mathcal{M}_j | \mathfrak{C} \hat{\mathcal{M}}_n \rangle$ is zero such that $\hat{\mathcal{M}}_n$ needs only to be orthonormalized against \mathcal{M}_{n-2} and \mathcal{M}_{n-1} , as claimed before.

While the proof of Eq. (G1) only uses typical features of Krylov subspaces, the proof of Eq. (G2) takes in addition advantage of Eq. (E10), which is specific to the problem at hand. We start by rewriting $\tilde{\mathcal{M}}_n$ as

$$\begin{aligned} \tilde{\mathcal{M}}_n &\stackrel{(\text{E10})}{=} \mathfrak{C} \varrho_0 - \sum_{j=1}^{n-1} \alpha_j \mathfrak{C}^2 \mathcal{M}_j \\ &= \mathfrak{C} \left(\varrho_0 - \sum_{j=1}^{n-1} \alpha_j \mathfrak{C} \mathcal{M}_j \right) \\ &= \mathfrak{C} \mathcal{M}_\perp, \end{aligned} \quad (\text{G4})$$

with

$$\mathcal{M}_\perp := \varrho_0 - \sum_{j=1}^{n-1} \alpha_j \mathfrak{C} \mathcal{M}_j. \quad (\text{G5})$$

In this equation, the $\alpha_j = \langle \mathfrak{C} \mathcal{M}_j | \varrho_0 \rangle$ (E6) are chosen such that the $\alpha_j \mathfrak{C} \mathcal{M}_j$ annihilate the $\mathfrak{C} \mathcal{M}_j$ components in ϱ_0 . Hence, we find

$$\langle \mathfrak{C} \mathcal{M}_{j < n} | \mathcal{M}_\perp \rangle = 0. \quad (\text{G6})$$

With this result, we can prove Eq. (G2)

$$\begin{aligned} \langle \mathfrak{C} \mathcal{M}_j | \mathfrak{C} \tilde{\mathcal{M}}_n \rangle &\stackrel{(\text{G4})}{=} \langle \mathfrak{C} \mathcal{M}_j | \mathfrak{C}^2 \mathcal{M}_\perp \rangle \\ &\stackrel{(18)}{=} \langle \mathfrak{C}^3 \mathcal{M}_j | \mathcal{M}_\perp \rangle \\ &\stackrel{(\text{E11})}{=} \langle \mathfrak{C} \hat{\mathcal{M}}_{j+1} | \mathcal{M}_\perp \rangle. \end{aligned} \quad (\text{G7})$$

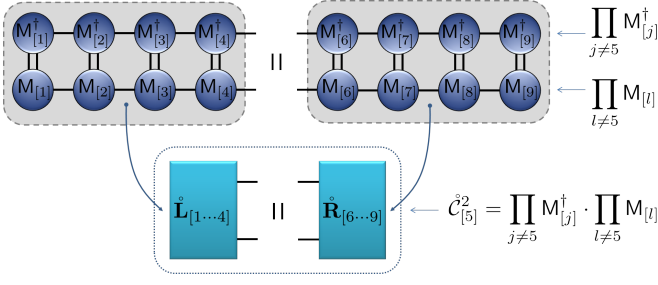


Figure 14: The MPO norm $\langle \prod_j M_{[j]} | \prod_l M_{[l]} \rangle$ (H4) can be expressed as weighted tensor norm $\langle M_{[k]} | \mathcal{C}_{[k]}^2 | M_{[k]} \rangle$. The MPO tensors can be gauged such that $\tilde{\mathbf{L}}_{[1 \dots k-1]} = \mathbb{1}$ and $\tilde{\mathbf{R}}_{[k+1 \dots n]} = \mathbb{1}$. This situation should be compared with the situation in Fig. 15, where such a gauge is generally not possible.

The matrix $\hat{\mathcal{M}}_{j+1}$ lies in the subspace span $\{\mathcal{M}_1, \mathcal{M}_2, \dots, \mathcal{M}_{j+1}\}$. Hence, according to Eq. (G6), we find $\langle \mathcal{E} \hat{\mathcal{M}}_{j+1} | \mathcal{M}_\perp \rangle = 0$ for $j+1 < n$ and with that $\langle \mathcal{E} \mathcal{M}_{j < n-1} | \mathcal{E} \mathcal{M}_n \rangle = 0$ (G7), as claimed in Eq. (G2).

1. Tensor network method

Finally, we have a look at the tensor network based method, as it was explained in appendix F3 for MPO. Here, we face two main differences compared to the general case: As a first difference, we only alter one MPO tensor $M_{[k]}$ at a time, which implies that we keep all other MPO tensors $M_{[j \neq k]}$ constant. This is e.g. the reason for the appearance of the term $(\prod_{j \neq k} M_{[j]})^\dagger$ in Eq. (F19). But with due diligence, one finds that this does not alter the line of argumentation used above. As a second difference, we no longer deal with a pure Krylov subspace, because of the extra role of the MPO tensor $M_{[k]}^{(1)} = M^{\text{old}}_{[k]}$ (F18). That is, the MPO $\mathcal{M}_1 = M_{[k]}^{(1)} \prod_{j \neq k} M_{[j]}$ (F8) is generally not orthogonal to $\tilde{\mathcal{M}}_n = \tilde{M}_{[k]}^{(n)} \prod_{j \neq k} M_{[j]}$

$$\langle \mathcal{E} \mathcal{M}_1 | \mathcal{E} \tilde{\mathcal{M}}_n \rangle \neq 0, \quad (\text{G8})$$

while for all other MPO $\mathcal{M}_l = M_{[k]}^{(l)} \prod_{j \neq k} M_{[j]}$ (F8), the line of argumentation used above still holds, i.e.

$$\langle \mathcal{E} \mathcal{M}_{1 < l < n-1} | \mathcal{E} \tilde{\mathcal{M}}_n \rangle = 0. \quad (\text{G9})$$

In other words, each new tensor $\tilde{M}_{[k]}^{(n)}$ needs to be orthonormalized against $M_{[k]}^{(1)}$ and $M_{[k]}^{(n-1)}$. This result will be of great importance for the speed up explained in appendix I.

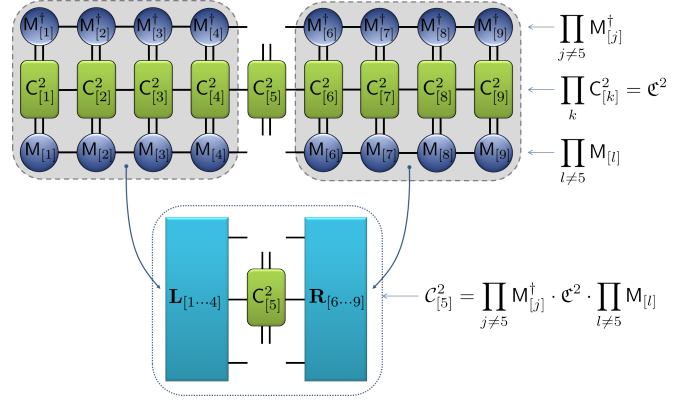


Figure 15: With the help of the effective tensor operator $\mathcal{C}_{[k]}^2$, the weighted MPO norm $\langle \prod_j M_{[j]} | \mathcal{C}_{[k]}^2 | \prod_l M_{[l]} \rangle$ (H4) can be expressed as weighted tensor norm $\langle M_{[k]} | \mathcal{C}_{[k]}^2 | M_{[k]} \rangle$.

Appendix H: Gauging the MPO

MPS and MPO contain a gauge freedom, which can be exploited to improve the performance of the algorithm. In our case, the optimal gauge is not given by the standard canonical forms, which are used in most other algorithms [23].

The gauge freedom of the MPS/MPO stems from the simple fact that one can always insert a matrix $a_{[j]}$ and its inverse $a_{[j]}^{-1}$ between two MPS tensors $M_{[j]}$ and $M_{[j+1]}$

$$M_{[j]\sigma_j}^{\alpha\beta} M_{[j+1]\sigma_{j+1}}^{\beta\gamma} = \underbrace{M_{[j]\sigma_j}^{\alpha\beta} a_{[j]}^{\beta\mu}}_{\tilde{M}_{[j]}} \underbrace{a_{[j]}^{-1\mu\nu} M_{[j+1]\sigma_{j+1}}^{\nu\gamma}}_{\tilde{M}_{[j+1]}} \quad (\text{H1})$$

and replace them by $M_{[j]} \rightarrow M_{[j]} a_{[j]}$ and $M_{[j+1]} \rightarrow a_{[j]}^{-1} M_{[j+1]}$. The aim of this section is to describe a method for finding beneficial matrices $a_{[j]}$.

For many application, it is advisable gauging a MPS M

$$M = M_{[k]} \prod_{j \neq k} M_{[j]} \quad (\text{H2})$$

in such a fashion that the norm of the entire MPS M reduces to the norm of the single MPS tensor $M_{[k]}$

$$\forall M_{[k]} : \quad \|M\| \stackrel{(\text{H2})}{=} \|M_{[k]} \prod_{j \neq k} M_{[j]}\| \stackrel{\text{special gauge}}{=} \|M_{[k]}\|. \quad (\text{H3})$$

This can be achieved by the canonical form described e.g. in Sec. 4.4 of Ref. [23]. Since the norm of the single tensor $M_{[k]}$ is easily controlled, this canonical form is extremely helpful for MPS based algorithm which have to fulfill the common side condition $\|M\| = 1$.

In our case, we have to deal with the weighted norm $\langle M | \mathcal{C}^2 | M \rangle = 1$ (24) as side condition, which favors a different kind of gauge. If this side condition could be simplified in the same way as Eq. (H3), i.e., $\langle M | \mathcal{C}^2 | M \rangle \stackrel{?}{=} 1$

$\|M_{[k]}\|$ for arbitrary $M_{[k]}$, the remaining overlap optimization (F10) would be trivially solved by Eq. (F11) without the necessity to approximate the optimal MPO tensor $M_{[k]}^{\text{optimal}}$ as a sum of many tensors $M_{[k]}^{(l)}$ as in Eq. (F9).

Unfortunately, a general $\langle M|\mathfrak{C}^2|M\rangle \stackrel{?}{=} \|M_{[k]}\|$ cannot be achieved by simply gauging the MPO. Still, we should attempt to get as close as possible to this relation to improve the performance of the entire algorithm. So, let us have a closer look at the weighted norm

$$\begin{aligned} \langle M|\mathfrak{C}^2|M\rangle &\stackrel{\text{(H2)}}{=} \langle M_{[k]} \prod_{j \neq k} M_{[j]} | \mathfrak{C}^2 | M_{[k]} \prod_{l \neq k} M_{[l]} \rangle \\ &= \langle M_{[k]} | \underbrace{\prod_{j \neq k} M_{[j]}^\dagger \mathfrak{C}^2 \prod_{l \neq k} M_{[l]}}_{\mathcal{C}_{[k]}^2} | M_{[k]} \rangle \\ &= \langle M_{[k]} | \mathcal{C}_{[k]}^2 | M_{[k]} \rangle, \end{aligned} \quad (\text{H4})$$

where we have introduced the effective tensor operator $\mathcal{C}_{[k]}^2$, see Fig 15. To have $\langle M|\mathfrak{C}^2|M\rangle \approx \|M_{[k]}\|$ for all $M_{[k]}$, we need $\mathcal{C}_{[k]}^2 \approx \mathbb{1}$.

We remark that we actually never calculate $\mathcal{C}_{[k]}^2$ explicitly, since the effort to do so scales with the fourth power of the bond dimensions of the MPO M , while the scaling of all operations presented so far does not exceed the third power. Therefore, we only calculate with the components of $\mathcal{C}_{[k]}^2$, which are $\mathbf{L}_{[1\dots k-1]}$, $\mathbf{C}_{[k]}^2$ and $\mathbf{R}_{[k+1\dots n]}$,

$$\mathcal{C}_{[k]}^2 \begin{matrix} \bar{\mu}_{k-1} \mu_{k-1} \bar{\mu}_k \mu_k \\ [\bar{\sigma}_k \sigma_k] \end{matrix} = \mathbf{L}_{[1\dots k-1]}^{\bar{\mu}_{k-1} \gamma_{k-1} \mu_{k-1}} \mathbf{C}_{[k]}^2 \begin{matrix} \gamma_{k-1} \gamma_k \\ [\bar{\sigma}_k \sigma_k] \end{matrix} \mathbf{R}_{[k+1\dots n]}^{\bar{\mu}_k \gamma_k \mu_k}, \quad (\text{H5})$$

as shown in Fig. 15. Hereby, $\mathbf{C}_{[j]}^2$ are the tensors of the MPO representing the squared commutator operator \mathfrak{C}^2 (17) (where the square in $\mathbf{C}_{[j]}^2$ is just symbolical, as in $\mathcal{C}_{[k]}^2$). The left $\mathbf{L}_{[1\dots k-1]}$ and right $\mathbf{R}_{[k+1\dots n]}$ can be calculated iteratively as

$$\begin{aligned} \mathbf{L}_{[1\dots j]}^{\bar{\mu}_j \gamma_j \mu_j} &= \mathbf{L}_{[1\dots j-1]}^{\bar{\mu}_{j-1} \gamma_{j-1} \mu_{j-1}} \\ &\quad \cdot \left(\mathbf{M}_{[j]}^* \right)_{\bar{\sigma}_j}^{\bar{\mu}_{j-1} \bar{\mu}_j} \left(\mathbf{C}_{[j]}^2 \right)_{\bar{\sigma}_j \sigma_j}^{\gamma_{j-1} \gamma_j} \mathbf{M}_{[j]}^{\mu_{j-1} \mu_j} \\ \mathbf{R}_{[j\dots n]}^{\bar{\mu}_{j-1} \gamma_{j-1} \mu_{j-1}} &= \left(\mathbf{M}_{[j]}^* \right)_{\bar{\sigma}_j}^{\bar{\mu}_{j-1} \bar{\mu}_j} \left(\mathbf{C}_{[j]}^2 \right)_{\bar{\sigma}_j \sigma_j}^{\gamma_{j-1} \gamma_j} \mathbf{M}_{[j]}^{\mu_{j-1} \mu_j} \\ &\quad \cdot \mathbf{R}_{[j+1\dots n]}^{\bar{\mu}_j \gamma_j \mu_j}. \end{aligned} \quad (\text{H6})$$

If we perform a gauge transformation as in Eq. (H1), we obtain

$$\begin{aligned} \mathbf{L}_{[1\dots k-1]}^{\bar{\mu} \gamma \mu} &\rightarrow \mathbf{L}_{[1\dots j]}^{\bar{\mu} \gamma \mu} \left(a_{[k-1]}^* \right)^{\bar{\mu} \bar{\nu}} a_{[k-1]}^{\mu \nu} \\ \mathbf{R}_{[k+1\dots n]}^{\bar{\mu} \gamma \mu} &\rightarrow \mathbf{R}_{[k+1\dots n]}^{\bar{\mu} \gamma \mu} \left(a_{[k]}^{-1} \right)^{\bar{\mu} \bar{\nu}} \left(a_{[k]}^{-1} \right)^{\mu \nu}. \end{aligned} \quad (\text{H7})$$

Now, we need to find beneficial gauge matrices $a_{[j]}$. To understand the procedure, it is helpful to look at the standard norm $\langle M|M\rangle$ without the commutator operator \mathfrak{C}^2 (Fig. 14). Here, the γ -index in $\mathbf{L}_{[1\dots k-1]}^{\bar{\mu} \gamma \mu}$ and $\mathbf{R}_{[k+1\dots n]}^{\bar{\mu} \gamma \mu}$

(H7) is absent and the remaining $\mathring{\mathbf{L}}_{[1\dots k-1]}^{\bar{\mu} \mu}$ and $\mathring{\mathbf{R}}_{[k+1\dots n]}^{\bar{\mu} \mu}$ can be treated as matrices. Using the trivial fact that $\mathring{\mathbf{L}} = \sqrt{\mathring{\mathbf{L}} \mathbb{1}} \sqrt{\mathring{\mathbf{L}}}^\dagger$ with $\sqrt{\mathring{\mathbf{L}}} = \sqrt{\mathring{\mathbf{L}}}$ and similar for $\mathring{\mathbf{R}}$, we choose the gauge matrices to be

$$a_{[k-1]} = \sqrt{\mathring{\mathbf{L}}_{[1\dots k-1]}^{-1}} \quad \text{and} \quad a_{[k]}^{-1} = \sqrt{\mathring{\mathbf{R}}_{[k+1\dots n]}^{-1}} \quad (\text{H8})$$

and the gauge transformation (H7) result in

$$\begin{aligned} \mathring{\mathbf{L}}_{[1\dots k-1]} &\xrightarrow{\text{(H7)}} a_{[k-1]} \mathring{\mathbf{L}}_{[1\dots k-1]} a_{[k-1]} \stackrel{\text{(H8)}}{=} \mathbb{1} \\ \mathring{\mathbf{R}}_{[k+1\dots n]} &\xrightarrow{\text{(H7)}} a_{[k]}^{-1} \mathring{\mathbf{R}}_{[k+1\dots n]} a_{[k]}^{-1} \stackrel{\text{(H8)}}{=} \mathbb{1}. \end{aligned} \quad (\text{H9})$$

With these identities, the MPO norm $\langle M|M\rangle$ reduces to the tensor norm $\langle M_{[k]}|M_{[k]}\rangle$, as for the canonical form.

Now, we come back to the weighted MPO norm $\langle M|\mathfrak{C}^2|M\rangle$, where $\mathbf{L}_{[1\dots k-1]}^{\bar{\mu} \gamma \mu}$ and $\mathbf{R}_{[k+1\dots n]}^{\bar{\mu} \gamma \mu}$ carry a γ -index and are given by Eq. (H6). In this case, the gauge matrices $a_{[k-1]}$ and $a_{[k]}$ do no longer have the same dimensions as $\mathbf{L}_{[1\dots k-1]}^{\bar{\mu} \gamma \mu}$ and $\mathbf{R}_{[k+1\dots n]}^{\bar{\mu} \gamma \mu}$ and hence, Eq. (H8) can not be used to obtain the gauge matrices. With the help of the multi-index $\xi = (\bar{\mu}, \gamma)$, $\mathbf{L}_{[1\dots k-1]}^{\xi \mu}$ and $\mathbf{R}_{[k+1\dots n]}^{\xi \mu}$ can still be written as matrices and be decomposed by a singular value decomposition

$$\begin{aligned} \mathbf{L}_{[1\dots k-1]}^{\xi \mu} &= U_{[L, k-1]}^{\xi \nu} D_{[L, k-1]}^{\nu \nu} V_{[L, k-1]}^{\nu \mu} \\ \mathbf{R}_{[k+1\dots n]}^{\xi \mu} &= U_{[R, k+1]}^{\xi \nu} D_{[R, k+1]}^{\nu \nu} V_{[R, k+1]}^{\nu \mu}. \end{aligned} \quad (\text{H10})$$

To mimic the effect of the inverse square root in Eq. (H8), we define the gauge matrices as

$$\begin{aligned} a_{[k-1]} &= V_{[L, k-1]}^\dagger D_{[L, k-1]}^{-\frac{1}{2}} V_{[L, k-1]} \\ a_{[k]}^{-1} &= V_{[R, k+1]}^\dagger D_{[R, k+1]}^{-\frac{1}{2}} V_{[R, k+1]}. \end{aligned} \quad (\text{H11})$$

Inserting these gauge matrices into Eq. (H7), does not turn $\mathbf{L}_{[1\dots k-1]}^{\bar{\mu} \gamma \mu}$ and $\mathbf{R}_{[k+1\dots n]}^{\bar{\mu} \gamma \mu}$ into identities as it was possible for $\mathring{\mathbf{L}}_{[1\dots k-1]}^{\bar{\mu} \mu}$ and $\mathring{\mathbf{R}}_{[k+1\dots n]}^{\bar{\mu} \mu}$ (H9), but at least $\mathbf{L}_{[1\dots k-1]}^{\bar{\mu} \gamma \mu}$ and $\mathbf{R}_{[k+1\dots n]}^{\bar{\mu} \gamma \mu}$ get closer to the identity.

We remark that this procedure is not optimal and could still be improved by more complicated methods. For example, if we use the gauge matrices (H11) to transform $\mathbf{L}_{[1\dots k-1]}^{\bar{\mu} \gamma \mu}$ and $\mathbf{R}_{[k+1\dots n]}^{\bar{\mu} \gamma \mu}$ according to Eq. (H7), we could iterate the procedure and use the transformed $\mathbf{L}_{[1\dots k-1]}$ and $\mathbf{R}_{[k+1\dots n]}$ to obtain further gauge matrices. However, in our applications, a single gauge transformation turned out to be quite profitable, while further iterations had no great impact.

1. Decomposing $\mathcal{C}_{[k]}^2$

So far, we just considered the left and right $\mathbf{L}_{[1\dots k-1]}^{\bar{\mu} \gamma \mu}$ and $\mathbf{R}_{[k+1\dots n]}^{\bar{\mu} \gamma \mu}$ separately to obtain the gauge matrices. In case of the standard MPO norm $\langle M|M\rangle$, this separated

treatment is perfectly justified (see Fig. 14), while for the weighted norm $\langle M|\mathcal{C}^2|M\rangle$, $\mathbf{L}_{[1\dots k-1]}^{\mu\gamma\mu}$ and $\mathbf{R}_{[k+1\dots n]}^{\mu\gamma\mu}$ are connected by the squared commutator operator \mathcal{C}^2 (Fig. 15). Therefore, the natural object to consider is the effective tensor operator $\mathcal{C}_{[k]}^2$. As already mentioned, calculating the effective tensor operator is $\mathcal{C}_{[k]}^2$ is numerically expensive. Fortunately, it will turn out that we do not require calculating $\mathcal{C}_{[k]}^2$ explicitly, but for the moment, let us pretend we have done so. We start by replacing the singular value decompositions in Eq. (H10) by the more suited decomposition

$$\begin{aligned} \left(\mathcal{C}_{[k]}^2\right)^{\xi_L\mu_{k-1}} &= \tilde{U}_{[L,k-1]}^{\xi_L\nu} \tilde{D}_{[L,k-1]}^{\nu\nu} \tilde{V}_{[L,k-1]}^{\nu\mu_{k-1}} \\ \left(\mathcal{C}_{[k]}^2\right)^{\xi_R\mu_k} &= \tilde{U}_{[R,k+1]}^{\xi_R\nu} \tilde{D}_{[R,k+1]}^{\nu\nu} \tilde{V}_{[R,k+1]}^{\nu\mu_k}, \end{aligned} \quad (\text{H12})$$

with the multi-indices $\xi_L = (\bar{\mu}_{k-1}, \bar{\mu}_k, \mu_k, \bar{\sigma}_k, \sigma_k)$ and $\xi_R = (\bar{\mu}_{k-1}, \mu_{k-1}, \bar{\mu}_k, \bar{\sigma}_k, \sigma_k)$. These new matrices can now be used in Eq. (H11) to obtain better gauge matrices $a_{[k-1]} = \tilde{V}_{[L,k-1]}^\dagger \tilde{D}_{[L,k-1]}^{-0.5} \tilde{V}_{[L,k-1]}$ and $a_{[k]}^{-1} = \tilde{V}_{[R,k+1]}^\dagger \tilde{D}_{[R,k+1]}^{-0.5} \tilde{V}_{[R,k+1]}$, which take the full operator $\mathcal{C}_{[k]}^2$ into account.

a. Successive decomposition of $\mathcal{C}_{[k]}^2$

Now, we show that we do not require calculating $\mathcal{C}_{[k]}^2$ explicitly. The needed matrices \tilde{D} and \tilde{V} of Eq. (H12) can be obtained relatively cheap by successively decomposing the components $\mathbf{L}_{[1\dots k-1]}$, $\mathcal{C}_{[k]}^2$ and $\mathbf{R}_{[k+1\dots n]}$ along the indices which connect the components. To demonstrate this procedure, we assume that we like to calculate the gauge matrix $a_{[k]}^{-1} = \tilde{V}_{[R,k+1]}^\dagger \tilde{D}_{[R,k+1]}^{-0.5} \tilde{V}_{[R,k+1]}$. We start by rewriting $\mathbf{L}_{[1\dots k-1]}^{\bar{\mu}_{k-1}\gamma_{k-1}\mu_{k-1}}$ as matrix $\mathbf{L}_{[1\dots k-1]}^{\zeta\gamma_{k-1}}$ with the multi-index $\zeta = (\bar{\mu}_{k-1}, \mu_{k-1})$ and apply a QR-decomposition

$$\mathbf{L}_{[1\dots k-1]}^{\zeta\gamma_{k-1}} = q_{[L,k-1]}^{\zeta\eta} r_{[L,k-1]}^{\eta\gamma_{k-1}}. \quad (\text{H13})$$

Next, the freshly obtained matrix $r_{[L,k-1]}^{\eta\gamma_{k-1}}$ is multiplied into the MPO tensor $\left(\mathcal{C}_{[k]}^2\right)_{\bar{\sigma}_k\sigma_k}^{\gamma_{k-1}\gamma_k}$

$$r_{[L,k-1]}^{\eta\gamma_{k-1}} \left(\mathcal{C}_{[k]}^2\right)_{\bar{\sigma}_k\sigma_k}^{\gamma_{k-1}\gamma_k} =: \left(\tilde{\mathcal{C}}_{[k]}^2\right)_{\bar{\sigma}_k\sigma_k}^{\eta\gamma_k}. \quad (\text{H14})$$

Now, we repeat this procedure and rewrite the modified tensor $\tilde{\mathcal{C}}_{[k]}^2$ as matrix $\left(\tilde{\mathcal{C}}_{[k]}^2\right)^{\kappa\gamma_k}$ with $\kappa = (\bar{\sigma}_k, \sigma_k, \eta)$ and perform another QR-decomposition

$$\left(\tilde{\mathcal{C}}_{[k]}^2\right)^{\kappa\gamma_k} = q_{[C,k]}^{\kappa\eta} r_{[C,k]}^{\eta\gamma_k}. \quad (\text{H15})$$

Finally, we multiply this $r_{[C,k]}^{\eta\gamma_k}$ into $\mathbf{R}_{[k+1\dots n]}^{\bar{\mu}_k\gamma_k\mu_k}$

$$\tilde{\mathbf{R}}_{[k+1\dots n]}^{\bar{\mu}_k\eta\mu_k} = r_{[C,k]}^{\eta\gamma_k} \mathbf{R}_{[k+1\dots n]}^{\bar{\mu}_k\gamma_k\mu_k}. \quad (\text{H16})$$

This new tensor $\tilde{\mathbf{R}}_{[k+1\dots n]}$ should now be used in Eq. (H10) instead of $\mathbf{R}_{[k+1\dots n]}$, i.e.

$$\tilde{\mathbf{R}}_{[k+1\dots n]}^{\xi\mu_k} = \hat{U}_{[R,k+1]}^{\xi\nu} \tilde{D}_{[R,k+1]}^{\nu\nu} \tilde{V}_{[R,k+1]}^{\nu\mu_k}, \quad (\text{H17})$$

with $\xi = (\bar{\mu}_k, \eta)$. Putting these three decompositions (H13), (H15), and (H17) together, we obtain

$$\begin{aligned} \mathcal{C}_{[k]}^2 &\stackrel{(\text{H5})}{=} \mathbf{L}_{[1\dots k-1]} \mathcal{C}_{[k]}^2 \mathbf{R}_{[k+1\dots n]} \\ &= q_{[L,k-1]} q_{[C,k]} \hat{U}_{[R,k+1]} \tilde{D}_{[R,k+1]} \tilde{V}_{[R,k+1]}. \end{aligned} \quad (\text{H18})$$

Since $\left(q_{[L,k-1]} q_{[C,k]} \hat{U}_{[R,k+1]}\right)^\dagger q_{[L,k-1]} q_{[C,k]} \hat{U}_{[R,k+1]} = \mathbb{1}$ has the same isometric property as $\tilde{U}_{[R,k]}$ in Eq. (H12), we find that Eq. (H18) is a correct singular value decompositions of $\mathcal{C}_{[k]}^2$. Hence, we can use $\tilde{D}_{[R,k+1]}$ and $\tilde{V}_{[R,k+1]}$ of Eq. (H17) for the gauge matrix $a_{[k]}^{-1} = \tilde{V}_{[R,k+1]}^\dagger \tilde{D}_{[R,k+1]}^{-0.5} \tilde{V}_{[R,k+1]}$ (H11). In order to calculate the gauge matrix $a_{[k-1]}$, we proceed in the same spirit, only in the opposite direction (first decomposing $\mathbf{R}_{[k+1\dots n]}$ then the modified $\mathcal{C}_{[k]}^2$ and finally the modified $\mathbf{L}_{[1\dots k-1]}$).

We like to remark that in our algorithm, we optimize the MPO tensors $\mathbf{M}_{[k]}$ in ascending, as well as in descending sweeps of the index k . In each of these alternating sweep directions, only one of the two gauge matrices $a_{[k-1]}$, $a_{[k]}^{-1}$ is calculated while for the other, we assume that the result obtained in the last sweep in opposite direction is a sufficiently good approximation (although one could also consider calculating both gauge matrices anew each sweep). That is, if the next MPO tensor we are going to optimize is $\mathbf{M}_{[k]}$, the last tensor that has been optimized should either be $\mathbf{M}_{[k-1]}$ or $\mathbf{M}_{[k+1]}$. In case $\mathbf{M}_{[k-1]}$ has been optimized last, we use the gauge matrix $a_{[k-1]}$ to obtain $\mathbf{M}_{[k-1]} \rightarrow \mathbf{M}_{[k-1]} a_{[k-1]}$ and $\mathbf{M}_{[k]} \rightarrow a_{[k-1]}^{-1} \mathbf{M}_{[k]}$, while after the optimization of $\mathbf{M}_{[k+1]}$, we need the gauge matrix $a_{[k]}^{-1}$ for the transformation $\mathbf{M}_{[k]} \rightarrow \mathbf{M}_{[k]} a_{[k]}$ and $\mathbf{M}_{[k+1]} \rightarrow a_{[k]}^{-1} \mathbf{M}_{[k+1]}$.

For the gauging of the MPO tensors, we need to invert matrices respectively their singular values. Numerically, this procedure might be troublesome. Therefore, one should regularize the gauge matrices. Further, it might be helpful to bring the MPO in their canonical form [23] before re-gauging them, since the canonical form is already a good approximation, which can be obtained without the need of inverting matrices

2. Physical gauge

The effective tensor operator $\left(\mathcal{C}_{[k]}^2\right)_{\bar{\sigma}_k\sigma_k}^{\bar{\mu}_{k-1}\mu_{k-1}\bar{\mu}_k\mu_k}$ (H5) carries four tensor indices $\bar{\mu}_{k-1}, \mu_{k-1}, \bar{\mu}_k, \mu_k$ corresponding to the auxiliary bonds and two (multi-)indices $\bar{\sigma}_k, \sigma_k$ corresponding to the physical dimensions. Of these six

indices, only the four auxiliary indices are effected by the MPO tensor gauge. To obtain an effective $\mathcal{C}_{[k]}^2$, as close to the identity as possible, we can also introduce a ‘‘gauge’’ for the physical indices, although this resembles more a transformation than a gauge. We remark that in our applications, the benefits of this transformation were far less pronounced than the benefits of the gauging applied to the auxiliary indices.

The idea is to place a matrix $b_{[k]}$ and its inverse $b_{[k]}^{-1}$ between the physical bonds of the MPO tensor $\mathbf{M}_{[k]}$ and the tensor $\mathcal{C}_{[k]}^2$ respectively $\mathcal{C}_{[k]}^2$ (H5)

$$\begin{aligned} \mathbf{M}_{[k]\sigma_k}^{\mu_{k-1}\mu_k} &\rightarrow \mathbf{M}_{[k]\sigma'_k}^{\mu_{k-1}\mu_k} b_{[k]\sigma'_k\sigma_k}^{-1} \\ \mathcal{C}_{[k]\bar{\sigma}_k\sigma_k}^2 &\rightarrow \mathcal{C}_{[k]\bar{\sigma}'_k\sigma'_k}^2 b_{[k]\bar{\sigma}'_k\bar{\sigma}_k}^* b_{[k]\sigma'_k\sigma_k}. \end{aligned} \quad (\text{H19})$$

Obviously, this transformations keeps the weighted norm $\langle \mathbf{M}_{[k]} | \mathcal{C}_{[k]}^2 | \mathbf{M}_{[k]} \rangle$ unchanged. But we also have to consider that the overlap $\langle \varrho_0 | \mathcal{C} | M \rangle$ (Fig. (13)) is effected by this transformation of the physical indices with $b_{[k]}$ and has to be transformed accordingly.

The procedure to obtain the optimal gauge $b_{[k]}$ for the physical indices is similar to the procedure used for finding the optimal gauge $a_{[k]}$ for the auxiliary indices.

We start by writing $\mathcal{C}_{[k]}^2$ as matrix $\left(\mathcal{C}_{[k]}^2\right)^{\xi\sigma_k}$ with the multi-index $\xi = (\bar{\mu}_{k-1}, \mu_{k-1}, \bar{\mu}_k, \mu_k, \bar{\sigma}_k)$ and the remaining physical index σ_k and perform a singular value decomposition

$$\left(\mathcal{C}_{[k]}^2\right)^{\xi\sigma_k} = U_{[k]} D_{[k]} V_{[k]}. \quad (\text{H20})$$

The transformation matrix $b_{[k]}$ is now obtained as

$$b_{[k]} = V_{[k]}^\dagger D_{[k]}^{-\frac{1}{2}} V_{[k]}. \quad (\text{H21})$$

As before, the singular value decomposition of $\mathcal{C}_{[k]}^2$ can be obtained by decompositions of its components $\mathbf{L}_{[1\dots k-1]}$, $\mathcal{C}_{[k]}^2$ and $\mathbf{R}_{[k+1\dots n]}$ (H5) along their connecting indices. That is, we write $\mathbf{L}_{[1\dots k-1]}^{\bar{\mu}\gamma\mu}$ and $\mathbf{R}_{[k+1\dots n]}^{\bar{\mu}\gamma\mu}$ as matrices with the multi-index $\kappa = (\bar{\mu}, \mu)$ and perform QR-decompositions

$$\begin{aligned} \mathbf{L}_{[1\dots k-1]}^{\kappa\gamma} &\rightarrow q_{[L,k-1]} r_{[L,k-1]} \\ \mathbf{R}_{[k+1\dots n]}^{\kappa\gamma} &\rightarrow q_{[R,k+1]} r_{[R,k+1]}. \end{aligned} \quad (\text{H22})$$

Then, the two r matrices are multiplied into $\mathcal{C}_{[k]}^2$

$$\left(\tilde{\mathcal{C}}_{[k]}^2\right)_{\bar{\sigma}_k\sigma_k}^{\alpha\beta} := r_{[L,k-1]}^{\alpha\gamma k-1} \left(\mathcal{C}_{[k]}^2\right)_{\bar{\sigma}_k\sigma_k}^{\gamma k-1 \gamma k} r_{[R,k+1]}^{\beta\gamma k} \quad (\text{H23})$$

Finally, we write $\tilde{\mathcal{C}}_{[k]}^2$ as matrix $\left(\tilde{\mathcal{C}}_{[k]}^2\right)^{\eta\sigma_k}$ with $\eta = (\alpha, \beta, \bar{\sigma}_k)$ and perform a singular value decomposition

$$\tilde{\mathcal{C}}_{[k]}^2 = \hat{U}_{[k]} D_{[k]} V_{[k]}, \quad (\text{H24})$$

which delivers the matrices $D_{[k]}$ and $V_{[k]}$ needed for the transformation matrix $b_{[k]} = V_{[k]}^\dagger D_{[k]}^{-\frac{1}{2}} V_{[k]}$ (H21).

Appendix I: Speeding up convergence by overarching orthonormalization

In this section, we introduce a method which allows for speeding up the convergence of the algorithm presented in appendix F 3. The key to this method is the insight that essential information gained in previous optimization sweeps can be passed on to later optimizations to obtain a faster convergence.

To understand this new method, we start by reviewing the general MPO optimization procedure. So far, we mainly discussed how a single MPO tensor $\mathbf{M}_{[k]}$ (F17) is optimized. During the optimization of the tensor $\mathbf{M}_{[k]}$, all other tensors $\mathbf{M}_{[j \neq k]}$ are kept constant. Since these tensors $\mathbf{M}_{[j \neq k]}$ are most likely suboptimal, the optimization of a single tensor $\mathbf{M}_{[k]}$ will generally not allow us to obtain the globally optimal MPO. According to Eq. (F17), $\mathbf{M}_{[k]} = \sum_l \alpha_l \cdot \mathbf{M}_{[k]}^{(l)}$ is optimized by summing up several weighted basis tensors $\mathbf{M}_{[k]}^{(l)}$. On the one hand, the more $\mathbf{M}_{[k]}^{(l)}$ we sum up, the better the result for the tensor $\mathbf{M}_{[k]}$. On the other hand, an exhaustive optimization of a single tensor $\mathbf{M}_{[k]}$ is a waste of computation time if the remaining tensors $\mathbf{M}_{[j \neq k]}$ are still far from optimal. Therefore, in practical applications, one will usually just sum up a few $\mathbf{M}_{[k]}^{(l)}$ and instead perform many repeated sweeps of the index k (which means we optimize the first to the last tensor and then start over again and again). During these sweeping cycles, the same tensor $\mathbf{M}_{[k]}$ is optimized many times, each time with different environmental tensors $\mathbf{M}_{[j \neq k]}$, which also have been optimized in between.

As a result of the first optimization sweeps, the tensors $\mathbf{M}_{[j]}$ are likely to change substantially. But with each completed sweeping cycle, the modifications of the tensors $\mathbf{M}_{[j]}$ should subside, since the $\mathbf{M}_{[j]}$ are converging towards their optimal value. When the changes have become sufficiently small, the environmental tensors $\mathbf{M}_{[j \neq k]}$ can be considered to be approximately constant between two optimization cycles of $\mathbf{M}_{[k]}$. This puts us into the position to reuse information won in previous optimizations of $\mathbf{M}_{[k]}$. To see this, we assume for a moment that the environmental tensors $\mathbf{M}_{[j \neq k]}$ do not change at all, and compare the situation where we perform many short optimizations of the MPO tensor $\mathbf{M}_{[k]}$ with the situation where we do one long optimization. Here, by short optimization, we mean that we sum up just a few basis tensors $\mathbf{M}_{[k]}^{(l)}$ to obtain the new MPO tensor $\mathbf{M}_{[k]}^{(l)}$, which corresponds to the situation in the algorithm.

In order to have a fair comparison, we assume that in total, the many short optimizations generate the same amount of linearly independent tensors $\mathbf{M}_{[k]}^{(l)}$ (F17) as the one long optimization. The crucial difference is that for the one long optimization, the tensors $\mathbf{M}_{[k]}^{(l)}$ are not only linearly independent, but also orthonormal (E3). Solely for orthonormal $\mathbf{M}_{[k]}^{(l)}$, Eq. (E6) provides the optimal overlap α_l for Eq. (F17). In other words: one long optimiza-

tion is superior to many short optimization.

What we intend to achieve is that the many short optimizations we use in the algorithm act the same way as one long optimization. That is, we have to find a way to maintain the orthonormalization of the basis tensors $M_{[k]}^{(l)}$ over many optimization cycles. In this context, the observation made in appendix G 1 is of special relevance that any newly generated basis tensor $\tilde{M}_{[k]}^{(n)}$ (F19) is already orthonormal to *all* basis tensors $M_{[k]}^{(l < n)}$ after it has been orthonormalized against the two basis tensors $M_{[k]}^{(1)}$ and $M_{[k]}^{(n-1)}$. This limits the amount of information we have to transmit from one optimization cycle to the next to ensure that all basis tensors $M_{[k]}^{(l)}$ generated in consecutive optimizations cycles are orthonormal.

The basis tensor $M_{[k]}^{(1)}$ is always given by the result of the optimization round before (F18). Since we assume that all tensors $M_{[j]}$ change only slightly from one short optimization to the next, the first basis tensor $M_{[k]}^{(1)}$ is roughly the same for the different optimization rounds. Hence, the orthonormalization against the slightly different $M_{[k]}^{(1)}$ in the many short optimizations should approximately have the same effect as the corresponding orthonormalization against $M_{[k]}^{(1)}$ in the one long optimization, which we like to mimic. Therefore, the only extra piece of information we have to transmit from one short optimization to the next is the lastly generated basis tensor $M_{[k]}^{(n)}$, which we denote as $M_{[k]}^{(\text{last})}$.

With that, we suggest the following improved rules to generate the tensors $M_{[k]}^{(l)}$

$$\begin{aligned} \tilde{M}_{[k]}^{(1)} &\stackrel{\text{(F18)}}{=} M_{[k]}^{\text{old}} \\ \tilde{M}_{[k]}^{(2)} &\stackrel{\text{new}}{=} M_{[k]}^{(\text{last})} \\ \tilde{M}_{[k]}^{(l > 2)} &\stackrel{\text{(F19)}}{=} \left(\prod_{j \neq k} M_{[j]} \right)^\dagger \left(\mathcal{C}_{\varrho 0} - \sum_{p=1}^{l-1} \alpha_p \mathcal{E}^2 \mathcal{M}_p \right). \quad (\text{I1}) \end{aligned}$$

In comparison to the one long optimization, the concatenated short optimizations need to do a few extra calculations to patch the different optimizations together. But the more important comparison is not the short optimization versus the long one, but the new method presented in this section versus the old method presented in appendix F 3.

In the worse case scenario, the basis tensor $\tilde{M}_{[k]}^{(2)} = M_{[k]}^{(\text{last})}$ has an overlap $\alpha_2 = 0$ (E6), i.e., the basis tensor $\tilde{M}_{[k]}^{(2)}$ of the new method is completely useless. Under this condition, every further basis tensor $\tilde{M}_{[k]}^{(l > 2)}$ produced by the new method will be identical to the basis tensor $\tilde{M}_{[k]}^{(l-1 > 1)}$ in the old method. That is, the maximal “damage” in the worse case scenario is that we have effectively one basis tensor less.

We explained the advantages of the new method for the idealized scenario that the tensors $M_{[j]}$ do not change at all, but it should be clear that also for slightly varying $M_{[j]}$, a positive residual effect remains. The less the tensors $M_{[j]}$ change from one optimization cycle to the next, the better are the results we can expect. Therefore, we might use the old method described in appendix F 3 as long as we detect strong changes in the $M_{[j]}$. When these changes drop below a preset threshold value, we might change to the new method presented here.

So far, our main argument for the new iteration Eq. (I1) has been the overarching orthonormalization. A much more trivial point might also be that the old iteration schema without the new definition for $\tilde{M}_{[k]}^{(2)}$ (I1) runs a certain risk generating each optimization cycle some basis tensors $M_{[k]}^{(l)}$ which are very much alike the $M_{[k]}^{(l)}$ of the round before. This is likely to happen if the changes in the tensor $M_{[k]}$ per optimization cycle are only small compared to the changes which are necessary to reach the optimal tensor $M_{[k]}^{\text{optimal}}$. That is, especially when the basis tensors $M_{[k]}^{(l)}$ prove to be badly chosen, the probability is high that these bad basis tensors are reproduced to a great part in the next round. The new definition for $\tilde{M}_{[k]}^{(2)}$ breaks this vicious cycle.

We like to finish with a practical advice: The prerequisite for the overarching orthonormalization to work is that all tensors only change slightly from one optimization sweep to another. We also have to take care not to introduce any changes gauging the MPO, as described in appendix H. That is, we have to use the adequate gauge for $M_{[k]}^{(\text{last})}$, as well. Now, we find that after several optimization rounds the gauge becomes approximately statical, as well and only changes slightly from sweep to sweep. Therefore, one might also keep the old gauge for $M_{[k]}^{(\text{last})}$ – at least theoretically. Unfortunately, we learned that for the QR-decomposition, some software libraries take care that the diagonal elements of the upper triangle matrix R has only positive diagonal elements, while other libraries do not. In case of combined ascending and descending optimization sweeps, gauging with negative diagonal elements can induce alternating signs of some tensor elements, wrecking the entire procedure, if the gauge for $M_{[k]}^{(\text{last})}$ is not adapted.

1. Comparison with other problems

At the beginning of appendix F 3, we shortly compared the approach for the time averaged density matrices with the Krylov subspace based MPO optimization for ground states (F14). Here, we refer again to the example of the ground state search to obtain a better understanding of the ingredients which are necessary for a successful application of the overarching orthonormalization method.

Usually, the MPO ground state search consists of many optimization sweeps, where for each tensor optimization,

we build up a small Krylov subspace (F15), as well. Hence, we can also aim for an orthonormalization which overarches many optimization cycles. For the ground state search, this can be obtained with slight modifications, i.e., we need to transmit the last two Krylov subspace basis (see appendix E1a). But unfortunately, this will not help us to improve the algorithm.

The important difference between the optimization of the ground state and the TADM is founded in the way the equation $M_{[k]}^{\text{optimized}} = \sum_l \alpha_l M_{[k]}^{(l)}$ (F9) is executed. Except for the choice of the symbols and their interpretation, the ground state search uses the same type of equation to find the optimal solution. The crucial point is that for the ground state search, the calculation of the optimal coefficients α_l (E6) and the execution of the summation can only be done at the very end, when all $M_{[k]}^{(l)}$ are known. Another way to say this is to state that the optimal value of α_l might depend on some $M_{[k]}^{(p)}$ which are calculated much later. For the TADM on the other hand, the optimal α_l can be calculated directly after a new $M_{[k]}^{(l)}$ has been generated. This allows us to sum up the $\alpha_l M_{[k]}^{(l)}$ components to a partial sum, immediately after they have been computed. That is, soon after the $M_{[k]}^{(l)}$ have been generated, we can forget them completely.

Principally, it is a solvable problem to memorize all the $M_{[k]}^{(l)}$ for the ground state search. But then we also need a strategy which takes into account that the environmental tensors $M_{[j \neq k]}$ are not really constant. As a consequence, calculations done with the $M_{[k]}^{(l)}$ become increasingly imprecise when they get older. Without going into further details, we state that for the ground state search, these problems seem to eat up most of the advantages one could hope to gain.

In conclusion, we find that the overarching orthonormalization method appears to be quite specific for the problem at hand, i.e., a linear problem with a bilinear side condition (weighted norm (E3)).

Appendix J: Mapping Hermitian matrices onto real matrices in the MPO framework

Any density matrix is Hermitian, which entails a redundant encoding. In this section, we show how this redundancy can be exploited by mapping the complex density matrix onto a real matrix, which contains the same amount of information but without the Hermitian redundancy. We remark that this mapping is not suitable for the double MPS ansatz (appendix M), but in the MPO framework, this mapping can be performed efficiently and allows us to obtain an algorithm which is entirely based on real numbers and hence, runs faster.

Exploiting symmetries to obtain a faster algorithm is a quite common approach. Taking advantage of the Hermitian symmetry is nonetheless unusual, since most sym-

metries are based on special properties of the physical system, while the Hermitian symmetry is universal and based on the mathematical formalism of quantum mechanics. We are not aware if a similar approach for MPO has ever been presented in the literature. Since the symmetry is universal, the corresponding algorithm can be applied to *all* physical systems.

Hermitian matrices are ubiquitous in quantum mechanics and it might surprise that they are not exploited more often in numerical algorithms. One reason why it is difficult to take advantage of the Hermitian symmetry is that there are no universal matrices A, B which could turn each Hermitian matrix M with the correct dimensions reversible into a real matrix M_{real}

$$AMB \stackrel{?}{=} M_{\text{real}}. \quad (\text{J1})$$

For a matrix $M = \sum_{jk} m_{jk} |j\rangle\langle k|$, hermiticity $m_{jk} = m_{kj}^*$ is a combined property of the bra and ket vector $|j\rangle$ and $\langle k|$, while the matrices A, B each only “know” either of them, i.e. bra or ket. To turn a Hermitian matrix into a real matrix, we need a linear map \mathfrak{U} which receives the combined information of $|j\rangle\langle k|$ as input. In this context, it is helpful to vectorize all matrices

$$M = \sum_{jk} m_{jk} |j\rangle\langle k| \rightarrow \sum_{jk} m_{jk} |j, k\rangle, \quad (\text{J2})$$

which in turn allows to write any linear map in form of a matrix $\sum_{jklm} s_{(jk)(lm)} |j, k\rangle\langle l, m|$. Now, a suitable map \mathfrak{U} to turn a Hermitian matrix into a real matrix is given by

$$\begin{aligned} \mathfrak{U} = & \sum_j |j, j\rangle\langle j, j| \\ & + \frac{1}{\sqrt{2}} \sum_{j>k} \left[|j, k\rangle(\langle j, k| + \langle k, j|) \right. \\ & \left. + i|k, j\rangle(\langle j, k| - \langle k, j|) \right], \quad (\text{J3}) \end{aligned}$$

with $i = \sqrt{-1}$. The factor $\frac{1}{\sqrt{2}}$ was inserted to ensure

$$\mathfrak{U}^\dagger \mathfrak{U} = \mathbb{1} := \sum_{j,k} |j, k\rangle\langle j, k|, \quad (\text{J4})$$

where \mathfrak{U}^\dagger is given by $(u_{(jk)(lm)} |j, k\rangle\langle l, m|)^\dagger = u_{(jk)(lm)}^* |l, m\rangle\langle j, k|$, i.e., to obtain the Hermitian conjugate, \mathfrak{U} is treated as a matrix.

Up to now, we just remarked that any density matrix is Hermitian. Since we search for a M with $\bar{\rho} = \rho_0 - c\mathfrak{C}M$ (27), the term $c\mathfrak{C}M$ has to be Hermitian, as well. Any phase factor $e^{i\phi}$ in $c = |c|e^{i\phi}$ can be absorbed into M , which allows us to demand that $c \in \mathbb{R}$. With that, M has to be antihermitian $M = -M^\dagger$ to have a Hermitian $c\mathfrak{C}M = (c\mathfrak{C}M)^\dagger$. Since we prefer M to be Hermitian, we include an extra factor $i = \sqrt{-1}$ into Eq. (27), i.e., we now use the approach

$$\bar{\rho} = \rho_0 - ci\mathfrak{C}M. \quad (\text{J5})$$

Multiplying this equation from the left with \mathfrak{U} (J3) and inserting the identity $\mathfrak{U}^\dagger \mathfrak{U} = \mathbb{1}$ (J4), we obtain the real equation

$$\begin{aligned} \underbrace{\mathfrak{U}\bar{\rho}}_{\bar{\rho}^{\text{real}}} &= \underbrace{\mathfrak{U}\rho_0}_{\rho_0^{\text{real}}} - c \underbrace{\mathfrak{U}i\mathfrak{C}\mathfrak{U}^\dagger}_{\mathfrak{C}^{\text{real}}} \underbrace{\mathfrak{U}M}_{M^{\text{real}}} \\ \bar{\rho}^{\text{real}} &= \rho_0^{\text{real}} - c\mathfrak{C}^{\text{real}}M^{\text{real}}, \end{aligned} \quad (\text{J6})$$

with $c = \langle i\mathfrak{C}M | \rho_0 \rangle = \langle \mathfrak{C}^{\text{real}}M^{\text{real}} | \rho_0^{\text{real}} \rangle \in \mathbb{R}$ and the side condition

$$\langle \mathfrak{C}^{\text{real}}M^{\text{real}} | \mathfrak{C}^{\text{real}}M^{\text{real}} \rangle = 1. \quad (\text{J7})$$

Since $\langle \mathfrak{C}^{\text{real}}M^{\text{real}} | \mathfrak{C}^{\text{real}}M^{\text{real}} \rangle = \langle \mathfrak{C}M | \mathfrak{C}M \rangle$, this is exactly the same side condition we used all the time (24).

So far, we just denoted $\mathfrak{C}^{\text{real}}$ as a real-valued map, but have not proved it. The map \mathfrak{U} (J3) was constructed such that it maps Hermitian matrices onto real matrices, but it is not evident that this entails $\mathfrak{C}^{\text{real}} = \mathfrak{U}i\mathfrak{C}\mathfrak{U}^\dagger$ to be real, as well. One could confirm this either via a detailed component by component check or simply by noticing that $\mathfrak{C}^{\text{real}}$ maps *arbitrary* real matrices onto real matrices and hence cannot contain any imaginary elements. Still, we have to come back to this point in appendix J 1, when we look at the MPO structure of $\mathfrak{C}^{\text{real}}$.

Now, we like to have a look at what we have found. The main idea of the entire transformation was to have a faster algorithm. Any (linear) map acting on $n \times n$ -matrices corresponds to a $n \times n \times n \times n$ -tensor. If we were relying on standard matrix and tensor multiplication, using such a huge tensor would be highly questionable. For MPO calculations on the other hand, the physical dimensions are often of secondary importance. The decisive characteristic is the bond dimension. In this context, it is relevant to note that for maps \mathfrak{U}_i which map Hermitian matrices onto real matrices, the outer product

$$\mathfrak{U}_\otimes = \bigotimes_{i=1}^n \mathfrak{U}_i = \mathfrak{U}_1 \otimes \mathfrak{U}_2 \otimes \mathfrak{U}_3 \otimes \dots \otimes \mathfrak{U}_n \quad (\text{J8})$$

describes a mapping from Hermitian matrices to real matrices, as well, with $\mathfrak{U}_\otimes^\dagger \mathfrak{U}_\otimes = \mathbb{1}$ (J4). This is easily checked applying \mathfrak{U}_\otimes to a suitable base consisting of outer products $\bigotimes_i H_i$ of Hermitian matrices H_i . The structure of \mathfrak{U}_\otimes corresponds to a trivial MPO with the bond dimension being one.

Further, we need to provide a single MPO representing the commutator operator \mathfrak{C} to perform the mapping $\mathfrak{C}^{\text{real}} = \mathfrak{U}i\mathfrak{C}\mathfrak{U}^\dagger$. We cannot use the definition of the commutator operator $\mathfrak{C} = [H, \dots]$ (17), since the mapping cannot be decomposed accordingly. To see this, remember that for a mapping like $H_{\text{real}} = \mathfrak{U}H$, the matrix H has to be vectorized, i.e., \mathfrak{U} acts on the bra *and* ket side. Vectorized matrices $\mathfrak{U}H$ and $\mathfrak{U}M$ do not allow a standard matrix multiplication $\mathfrak{U}H\mathfrak{U}M$. If we rewrite $\mathfrak{U}H$ and $\mathfrak{U}M$ as matrices, the resulting matrix product is no longer the correct multiplication needed for $\mathfrak{U}^\dagger \mathfrak{U} = \mathbb{1}$ to hold.

Many frequently used Hamiltonians H possess relatively simple MPO descriptions, with bond dimensions

which are small compared to the bond dimensions needed to obtain suitable MPO descriptions for M (J5). In this case, it is reasonable to write \mathfrak{C} as a single MPO as described in appendix L instead of using the definition $\mathfrak{C}M = HM - MH$ (17). As a bonus, this enables us to use a MPO compression algorithm to pre-compute \mathfrak{C}^2 , which is needed to calculate $\langle \mathfrak{C}M_j | \mathfrak{C}M_k \rangle$ (E3). Compared to the explicit use of $\langle [H, \mathcal{M}_j] | [H, \mathcal{M}_k] \rangle$, this often entails a speed up.

Since the Hermitian to real mapping MPO \mathfrak{U}_\otimes (J8) has the trivial bond dimension one, the real-valued MPO $\rho_0^{\text{real}} = \mathfrak{U}_\otimes \rho_0$, $\mathfrak{C}^{\text{real}} = \mathfrak{U}_\otimes i\mathfrak{C}\mathfrak{U}_\otimes^\dagger$ and $M^{\text{real}} = \mathfrak{U}_\otimes M$ (J6) have the same bond dimensions as their Hermitian counterparts. Further, we remark that the mappings $\rho_0 \rightarrow \rho_0^{\text{real}}$ and $\mathfrak{C} \rightarrow \mathfrak{C}^{\text{real}}$ only have to be applied once, at the beginning. Afterwards, we can compute M^{real} with the same algorithm we would have used to obtain the Hermitian M . At the very end, when M^{real} is calculated, one final mapping gives us $M = \mathfrak{U}_\otimes^\dagger M^{\text{real}}$.

1. Real MPO with complex MPO tensors

When we stated that ρ_0^{real} and $\mathfrak{C}^{\text{real}}$ are real-valued objects, we indirectly included the assumption that they are described by a single matrix or tensor. If we represent ρ_0^{real} and $\mathfrak{C}^{\text{real}}$ as MPO, they are decomposed into a product of tensors. These MPO tensors no longer have to be real. Usually, the simple transformation $\mathfrak{C}^{\text{real}} = \mathfrak{U}_\otimes i\mathfrak{C}\mathfrak{U}_\otimes^\dagger$ (J6) produces complex-valued MPO tensors. In this subsection, we describe a procedure to turn the complex-valued MPO tensors of ρ_0^{real} and $\mathfrak{C}^{\text{real}}$ into real-valued tensors.

In the following, we assume that we deal with open boundary conditions for the MPO. For most physical systems of interest, it should be no problem to find MPO with open boundary conditions for ρ_0^{real} and $\mathfrak{C}^{\text{real}}$. Under certain circumstances, periodic boundary conditions might be advisable for the MPO M^{real} (J6). But M^{real} is generated by the algorithm and not the result of a transformation. Therefore, the MPO tensors of M^{real} are real by construction.

Let us look at an arbitrary real operator \hat{O} represented as MPO in its left-canonical form

$$\hat{O} = \sum_{\alpha_1 \dots \alpha_{n-1}} \mathbf{U}_{[1]\sigma_1}^{\alpha_1} \mathbf{U}_{[2]\sigma_2}^{\alpha_1 \alpha_2} \dots \mathbf{U}_{[n-1]\sigma_{n-1}}^{\alpha_{n-2} \alpha_{n-1}} \mathbf{R}_{\sigma_n}^{\alpha_{n-1}}. \quad (\text{J9})$$

Here, the σ_j are multi-indices comprising all physical indices of the MPO tensors (i.e., in case of the map $\mathfrak{C}^{\text{real}}$, the MPO tensors have four physical indices). For an MPO in a left-canonical form, all MPO tensors $\mathbf{U}_{[j]}$ are left-normalized except for the rightmost tensor \mathbf{R} , i.e.,

$$\sum_{\sigma_j, \alpha_{j-1}} (\mathbf{U}_{[j]\sigma_j}^{\alpha_{j-1} \alpha_j})^* \mathbf{U}_{[j]\sigma_j}^{\alpha_{j-1} \alpha_j'} = \mathbb{1}^{\alpha_j \alpha_j'}, \quad (\text{J10})$$

respectively $\sum_{\sigma_1} (\mathbf{U}_{[1]\sigma_1}^{\alpha_1})^* \mathbf{U}_{[1]\sigma_1}^{\alpha_1'} = \mathbb{1}^{\alpha_1 \alpha_1'}$. Any MPO can be brought into the left-canonical form via a repeated ap-

plication of a singular value or QR decomposition, starting with the leftmost tensor. For details, see e.g. Sec. 4.4 of Ref. [23].

Using unitary matrices $V_{[j]}$, we can construct new tensors $\mathcal{O}_{[j]}$

$$\mathcal{O}_{[j]\sigma_j}^{\alpha_{j-1}\alpha_j} = \sum_{\beta\gamma} \left(V_{[j-1]}^{\beta\alpha_{j-1}} \right)^* \mathcal{U}_{[j]\sigma_j}^{\beta\gamma} V_{[j]}^{\gamma\alpha_j}, \quad (\text{J11})$$

respectively $\mathcal{O}_{[1]\sigma_1}^{\alpha_1} = \sum_{\beta} \mathcal{U}_{[1]\sigma_1}^{\beta} V_{[1]}^{\beta\alpha_1}$ and $\mathcal{P}_{\sigma_n}^{\alpha_{n-1}} = \sum_{\beta} \left(V_{[n-1]}^{\beta\alpha_{n-1}} \right)^* \mathcal{R}_{\sigma_n}^{\beta}$. With these new tensors, an alternative MPO representation for the operator \hat{O} is given by

$$\hat{O} = \sum_{\alpha_1 \dots \alpha_{n-1}} \mathcal{O}_{[1]\sigma_1}^{\alpha_1} \mathcal{O}_{[2]\sigma_2}^{\alpha_1\alpha_2} \dots \mathcal{O}_{[n-1]\sigma_{n-1}}^{\alpha_{n-2}\alpha_{n-1}} \mathcal{P}_{\sigma_n}^{\alpha_{n-1}}. \quad (\text{J12})$$

In appendix K, we will prove the existence of unitary matrices $V_{[j]}$ such that all MPO tensors $\mathcal{O}_{[j]}$ and \mathcal{P} are real valued. Interestingly, we have to demand that the MPO representation (J9) is maximally compressed to ensure the existence of suitable $V_{[j]}$. That is, we do not allow MPO dimensions which belong to vanishing singular values.

a. Finding the gauge matrices $V_{[j]}$

Once the existence of the unitary matrices $V_{[j]}$ is guaranteed, calculating them is relatively easy. We start with $V_{[1]}$ and note that due to the unitarity of the matrices $V_{[j]}$, we have

$$\mathcal{O}_{[1]\sigma_1}^{\alpha_1} \stackrel{(\text{J11})}{=} \sum_{\beta} \mathcal{U}_{[1]\sigma_1}^{\beta} V_{[1]}^{\beta\alpha_1} \Leftrightarrow \mathcal{U}_{[1]\sigma_1}^{\alpha_1} = \sum_{\beta} \mathcal{O}_{[1]\sigma_1}^{\beta} V_{[1]}^{*\alpha_1\beta}. \quad (\text{J13})$$

With this, we find

$$\begin{aligned} \sum_{\alpha_1} \mathcal{U}_{[1]\sigma_1}^{\alpha_1} \mathcal{U}_{[1]\sigma'_1}^{*\alpha_1} &= \sum_{\alpha_1, \beta, \gamma} \mathcal{O}_{[1]\sigma_1}^{\beta} \underbrace{V_{[1]}^{*\alpha_1\beta} V_{[1]}^{\alpha_1\gamma}}_{\delta^{\beta\gamma}} \mathcal{O}_{[1]\sigma'_1}^{*\gamma} \\ &= \sum_{\beta} \mathcal{O}_{[1]\sigma_1}^{\beta} \mathcal{O}_{[1]\sigma'_1}^{*\beta} \\ &=: \mathcal{W}_{[1]\sigma_1\sigma'_1}. \end{aligned} \quad (\text{J14})$$

We remark that $\sum_{\sigma} \mathcal{O}_{[1]\sigma}^{\beta} \mathcal{O}_{[1]\sigma}^{*\gamma} = \mathbb{1}^{\beta\gamma}$, while $\mathcal{W}_{[1]\sigma\sigma'} = \sum_{\beta} \mathcal{O}_{[1]\sigma}^{\beta} \mathcal{O}_{[1]\sigma'}^{*\beta}$, only equals $\mathbb{1}_{\sigma\sigma'}$ iff $\dim(\sigma) = \dim(\beta)$. For real objects as ϱ_0^{real} and $\mathfrak{C}^{\text{real}}$, we know that a decomposition into real MPO tensors exists. In this case, $\mathcal{W}_{[1]\sigma\sigma'}$ has to be real, as well.

Remember that the tensor $\mathcal{O}_{[1]\sigma}^{\beta}$ is still unknown, while $\mathcal{W}_{[1]\sigma\sigma'} = \sum_{\alpha} \mathcal{U}_{[1]\sigma}^{\alpha} \mathcal{U}_{[1]\sigma'}^{*\alpha}$ can be calculated. Since $\mathcal{W}_{[1]}$ (J14) can be written as matrix equation

$$\mathcal{W}_{[1]} = \mathcal{O}_{[1]} \mathbb{1} \mathcal{O}_{[1]}^{\dagger}, \quad (\text{J15})$$

we can obtain $\mathcal{O}_{[1]}$ as the eigenvectors of $\mathcal{W}_{[1]}$ (with all eigenvalues being one) or alternatively, via a singular value decomposition. The matrix $\mathcal{O}_{[1]}$ is not unique, but the important part is that it is always real-valued, in case $\mathcal{W}_{[1]\sigma\sigma'}$ is real, as it is the case for ϱ_0^{real} and $\mathfrak{C}^{\text{real}}$.

Having $\mathcal{O}_{[1]}$, we can calculate the matrix $V_{[1]}$ via

$$\begin{aligned} \sum_s \mathcal{O}_{[1]\sigma}^{*\alpha} \mathcal{U}_{[1]\sigma}^{\beta} &\stackrel{(\text{J11})}{=} \sum_{\beta, s} \underbrace{\mathcal{O}_{[1]\sigma}^{*\alpha} \mathcal{O}_{[1]\sigma}^{\gamma}}_{\delta^{\alpha\gamma}} V_{[1]}^{*\beta\gamma} \\ &= V_{[1]}^{*\beta\alpha}. \end{aligned} \quad (\text{J16})$$

With some slight adjustments, we can use the same technique to calculate the matrix $V_{[2]}$ and successively all following matrices $V_{[j]}$. Instead of Eq. (J13), we now have

$$\sum_{\alpha} V_{[j-1]}^{*\alpha\beta} \mathcal{U}_{[j]\sigma}^{\alpha\gamma} \stackrel{(\text{J11})}{=} \sum_{\delta} \mathcal{O}_{[j]\sigma}^{\beta\delta} V_{[j]}^{*\gamma\delta}, \quad (\text{J17})$$

where we assume that $V_{[j-1]}$ is already known. To facilitate the notation, we introduce

$$\mathcal{Q}_{[j]\mathfrak{S}}^{\gamma} = \mathcal{Q}_{[j](\sigma, \beta)}^{\gamma} := \sum_{\alpha} V_{[j-1]}^{*\alpha\beta} \mathcal{U}_{[j]\sigma}^{\alpha\gamma}, \quad (\text{J18})$$

with the multi-index $\mathfrak{S} = (\sigma, \beta)$. Replacing $\mathcal{U}_{[j]\sigma}^{\gamma}$ by $\mathcal{Q}_{[j]\mathfrak{S}}^{\gamma}$, we can repeat all the steps above to obtain $V_{[j]}$. In short, we calculate $\mathcal{W}_{[j]\mathfrak{S}\mathfrak{S}'} = \sum_{\gamma} \mathcal{Q}_{[j]\mathfrak{S}}^{\gamma} \mathcal{Q}_{[j]\mathfrak{S}'}^{*\gamma}$ (J14) and via a singular value decomposition of $\mathcal{W}_{[j]\mathfrak{S}\mathfrak{S}'}$, we obtain $\mathcal{O}_{[j]\mathfrak{S}}^{\alpha}$ (J15), which leads to $V_{[j]}^{*\beta\alpha} = \sum_{\mathfrak{S}} \mathcal{O}_{[j]\mathfrak{S}}^{*\alpha} \mathcal{Q}_{[j]\mathfrak{S}}^{\beta}$ (J16).

Appendix K: Existence of the gauge matrices $V_{[j]}$

In this section, we prove the existence of the unitary matrices $V_{[j]}$, which we used in the last section (appendix J1a) to transform the complex-valued tensors $\mathcal{U}_{[j]}$ into real-valued tensors $\mathcal{O}_{[j]}$ (J17). This proof is added for formal reasons only and is of no importance for the practical application of the algorithm.

MPO tensors are not uniquely defined. We look at the case where we have two different MPO which represent the same object \hat{O} .

$$\begin{aligned} \hat{O} &= \sum_{\alpha_1 \dots \alpha_{n-1}} \mathcal{U}_{[1]\sigma_1}^{\alpha_1} \dots \mathcal{U}_{[n-1]\sigma_{n-1}}^{\alpha_{n-2}\alpha_{n-1}} \mathcal{R}_{\sigma_n}^{\alpha_{n-1}} \\ &= \sum_{\alpha_1 \dots \alpha_{n-1}} \mathcal{O}_{[1]\sigma_1}^{\alpha_1} \dots \mathcal{O}_{[n-1]\sigma_{n-1}}^{\alpha_{n-2}\alpha_{n-1}} \mathcal{P}_{\sigma_n}^{\alpha_{n-1}}. \end{aligned} \quad (\text{K1})$$

Both MPO are supposed to be maximally compressed and in the left-canonical form (J10). We like to show that for these two MPO, all tensors $\mathcal{U}_{[j]}$ and $\mathcal{O}_{[j]}$ (respectively \mathcal{R} and \mathcal{P}) can always be related by unitary matrices $V_{[k]}$, as in Eq. (J11).

For the upcoming proof, we need to shorten the notation. To this end, we use the Einstein summation convention, i.e., we imply summation over identical indices. Further, we introduce the two matrices $\mathcal{U}_{[j]}^{\mathfrak{S}_j \alpha_j}$ and $\mathcal{O}_{[j]}^{\mathfrak{S}_j \alpha_j}$,

given as tensor products of the first j MPO tensors $\mathbf{U}_{[k]}$ respectively $\mathbf{O}_{[k]}$

$$\begin{aligned} \mathbf{U}_{[j]}^{\mathfrak{S}_j \alpha_j} &= \mathbf{U}_{[j-1]}^{\mathfrak{S}_{j-1} \alpha_{j-1}} \mathbf{U}_{[j] \sigma_j}^{\alpha_{j-1} \alpha_j} \\ &= \mathbf{U}_{[1] \sigma_1}^{\alpha_1} \cdots \mathbf{U}_{[j] \sigma_j}^{\alpha_{j-1} \alpha_j} \end{aligned} \quad (\text{K2})$$

and

$$\begin{aligned} \mathbf{O}_{[j]}^{\mathfrak{S}_j \alpha_j} &= \mathbf{O}_{[j-1]}^{\mathfrak{S}_{j-1} \alpha_{j-1}} \mathbf{O}_{[j] \sigma_j}^{\alpha_{j-1} \alpha_j} \\ &= \mathbf{O}_{[1] \sigma_1}^{\alpha_1} \cdots \mathbf{O}_{[j] \sigma_j}^{\alpha_{j-1} \alpha_j}, \end{aligned} \quad (\text{K3})$$

with the physical multi-index $\mathfrak{S}_j = (\sigma_1 \dots \sigma_j)$. Since the two MPO (K1) are in left-canonical form (J10), we find

$$\mathbf{U}_{[j]}^\dagger \mathbf{U}_{[j]} = \mathbb{1} = \mathbf{O}_{[j]}^\dagger \mathbf{O}_{[j]}, \quad (\text{K4})$$

while generally $\mathbf{U}_{[j]} \mathbf{U}_{[j]}^\dagger \neq \mathbb{1} \neq \mathbf{O}_{[j]} \mathbf{O}_{[j]}^\dagger$. Still, $\mathbf{U}_{[j]} \mathbf{U}_{[j]}^\dagger$ acts like an identity, when applied to $\mathbf{U}_{[j]}$

$$\left(\mathbf{U}_{[j]} \mathbf{U}_{[j]}^\dagger \right) \mathbf{U}_{[j]} = \mathbf{U}_{[j]} \underbrace{\left(\mathbf{U}_{[j]}^\dagger \mathbf{U}_{[j]} \right)}_{\mathbb{1}} = \mathbf{U}_{[j]}. \quad (\text{K5})$$

With that, $\mathbf{U}_{[j]} \mathbf{U}_{[j]}^\dagger$ also acts like an identity when applied to the MPO $\hat{\mathcal{O}}$ (K1)

$$\mathbf{U}_{[j]} \mathbf{U}_{[j]}^\dagger \hat{\mathcal{O}} = \hat{\mathcal{O}}, \quad (\text{K6})$$

which is easily seen when we use the MPO representation of $\hat{\mathcal{O}}$ based on the tensors $\mathbf{U}_{[j]}$. On the other hand, when we apply $\mathbf{U}_{[j]} \mathbf{U}_{[j]}^\dagger$ to the MPO $\hat{\mathcal{O}}$ represented as

$$\hat{\mathcal{O}} \stackrel{(\text{K1}), (\text{K3})}{=} \underbrace{\mathbf{O}_{[j]}^{\mathfrak{S}_j \alpha_j}}_{(\text{K3})} \mathbf{O}_{[j+1] \sigma_{j+1}}^{\alpha_j \alpha_{j+1}} \cdots \mathbf{O}_{[n-1] \sigma_{n-1}}^{\alpha_{n-2} \alpha_{n-1}} \mathbf{P}_{\sigma_n}^{\alpha_{n-1}}, \quad (\text{K7})$$

we find

$$\begin{aligned} \hat{\mathcal{O}} &= \mathbf{U}_{[j]} \mathbf{U}_{[j]}^\dagger \hat{\mathcal{O}} \\ &\stackrel{(\text{K7})}{=} \mathbf{U}_{[j]}^{\mathfrak{S}'_j \gamma} \underbrace{\mathbf{U}_{[j]}^* \mathbf{U}_{[j]}^{\mathfrak{S}_j \alpha_j} \mathbf{O}_{[j]}^{\mathfrak{S}_j \alpha_j}}_{=: \mathbf{W}_{[j]}^{\gamma \alpha_j}} \mathbf{O}_{[j+1] \sigma_{j+1}}^{\alpha_j \alpha_{j+1}} \cdots \mathbf{P}_{\sigma_n}^{\alpha_{n-1}} \\ &= \mathbf{U}_{[j]}^{\mathfrak{S}'_j \gamma} \mathbf{W}_{[j]}^{\gamma \alpha_j} \mathbf{O}_{[j+1] \sigma_{j+1}}^{\alpha_j \alpha_{j+1}} \cdots \mathbf{O}_{[n-1] \sigma_{n-1}}^{\alpha_{n-2} \alpha_{n-1}} \mathbf{P}_{\sigma_n}^{\alpha_{n-1}}. \end{aligned} \quad (\text{K8})$$

We demanded that the MPO $\hat{\mathcal{O}}$ is maximally compressed, i.e., it contains no vanishing singular values. Hence, the expression $\mathcal{R} = \mathbf{O}_{[j+1] \sigma_{j+1}}^{\alpha_j \alpha_{j+1}} \cdots \mathbf{O}_{[n-1] \sigma_{n-1}}^{\alpha_{n-2} \alpha_{n-1}} \mathbf{P}_{\sigma_n}^{\alpha_{n-1}}$ built from the right-hand tensors of the MPO is invertible. Applying this inverse \mathcal{R}^{-1} to the MPO $\hat{\mathcal{O}}$ in the form of the last line of Eq. (K8) as well as to the representation in Eq. (K7), we find

$$\begin{aligned} \underbrace{\hat{\mathcal{O}}}_{(\text{K7})} \mathcal{R}^{-1} &= \underbrace{\hat{\mathcal{O}}}_{(\text{K8})} \mathcal{R}^{-1} \\ \mathbf{O}_{[j]} &= \mathbf{U}_{[j]} \mathbf{W}_{[j]} \end{aligned} \quad (\text{K9})$$

Multiplying this equation with $\mathbf{O}_{[j]}^\dagger$ we find

$$\begin{aligned} \underbrace{\mathbf{O}_{[j]}^\dagger \mathbf{O}_{[j]}}_{\mathbb{1} \text{ (K4)}} &= \underbrace{\mathbf{O}_{[j]}^\dagger \mathbf{U}_{[j]}}_{\mathbf{W}_{[j]}^\dagger \text{ (K8)}} \mathbf{W}_{[j]} \\ \mathbb{1} &= \mathbf{W}_{[j]}^\dagger \mathbf{W}_{[j]}. \end{aligned} \quad (\text{K10})$$

Repeating the some line of argumentation for $\mathbf{O}_{[j]} \mathbf{O}_{[j]}^\dagger \hat{\mathcal{O}}$ as we used for $\mathbf{U}_{[j]} \mathbf{U}_{[j]}^\dagger \hat{\mathcal{O}}$, we arrive at the conclusion that

$$\begin{aligned} \mathbf{U}_{[j]} &= \mathbf{O}_{[j]} \mathbf{W}_{[j]}^\dagger \\ \mathbf{W}_{[j]} \mathbf{W}_{[j]}^\dagger &= \mathbb{1}. \end{aligned} \quad (\text{K11})$$

Putting all together, we find

$$\begin{aligned} \mathbf{O}_{[j]}^{\mathfrak{S}_j \gamma} &\stackrel{(\text{K9})}{=} \mathbf{U}_{[j]}^{\mathfrak{S}_j \alpha_j} \mathbf{W}_{[j]}^{\alpha_j \gamma} \\ &\stackrel{(\text{K2})}{=} \mathbf{U}_{[j-1]}^{\mathfrak{S}_{j-1} \alpha_{j-1}} \mathbf{U}_{[j] \sigma_j}^{\alpha_{j-1} \alpha_j} \mathbf{W}_{[j]}^{\alpha_j \gamma} \\ &\stackrel{(\text{K11})}{=} \mathbf{O}_{[j-1]}^{\mathfrak{S}_{j-1} \beta} \mathbf{W}_{[j-1]}^* \mathbf{U}_{[j] \sigma_j}^{\alpha_{j-1} \alpha_j} \mathbf{W}_{[j]}^{\alpha_j \gamma}. \end{aligned} \quad (\text{K12})$$

Multiplying this equation with $\mathbf{O}_{[j-1]}^* \mathbf{O}_{[j-1]}^{\mathfrak{S}_{j-1} \beta}$ and using the identity (K4), we finally obtain

$$\begin{aligned} \mathbf{O}_{[j-1]}^* \mathbf{O}_{[j-1]}^{\mathfrak{S}_{j-1} \beta} \mathbf{O}_{[j]}^{\mathfrak{S}_j \gamma} &= \mathbf{W}_{[j-1]}^* \mathbf{U}_{[j] \sigma_j}^{\alpha_{j-1} \alpha_j} \mathbf{W}_{[j]}^{\alpha_j \gamma} \\ \mathbf{O}_{[j-1]}^* \mathbf{O}_{[j-1]}^{\mathfrak{S}_{j-1} \delta} \mathbf{O}_{[j] \sigma_j}^{\delta \gamma} &\stackrel{(\text{K3})}{=} \mathbf{W}_{[j-1]}^* \mathbf{U}_{[j] \sigma_j}^{\alpha_{j-1} \alpha_j} \mathbf{W}_{[j]}^{\alpha_j \gamma} \\ \mathbf{O}_{[j] \sigma_j}^{\beta \gamma} &\stackrel{(\text{K4})}{=} \mathbf{W}_{[j-1]}^* \mathbf{U}_{[j] \sigma_j}^{\alpha_{j-1} \alpha_j} \mathbf{W}_{[j]}^{\alpha_j \gamma}. \end{aligned} \quad (\text{K13})$$

In the same way, it is easily shown that

$$\begin{aligned} \mathbf{O}_{[1] \sigma_1}^\gamma &= \mathbf{U}_{[1] \sigma_1}^{\alpha_1} \mathbf{W}_{[1]}^{\alpha_1 \gamma} \\ \mathbf{P}_{\sigma_n}^\beta &= \mathbf{W}_{[n-1]}^* \mathbf{R}_{\sigma_n}^{\alpha_{n-1} \beta}. \end{aligned} \quad (\text{K14})$$

Since we can be sure that for a real-valued operator $\hat{\mathcal{O}}$ an MPO based on real-valued tensors $\mathbf{O}_{[j]}$ and \mathbf{P} exist, we can also deduce the existence of some gauge matrices $\mathbf{V}_{[j]} = \mathbf{W}_{[j]}$ with the help of Eq. (K13) and (K14).

Appendix L: Constructing a MPO for the commutator operator \mathfrak{C}

To construct a MPO representation for the commutator operator \mathfrak{C} , first, we need to construct a MPO representation of the Hamilton operator H . This is e.g. described in Ref. [36, 37].

The commutator operator \mathfrak{C} acts on the vector space of linear operators with $\mathfrak{C}A = HA - AH$. Evidently, this can also be written as

$$\mathfrak{C}A = HA\mathbb{1} - \mathbb{1}AH$$

Now, let us rewrite the commutator operator symbolically as

$$\mathfrak{C} = H \otimes \mathbb{1} - \mathbb{1} \otimes H, \quad (\text{L1})$$

which is to be understood as $(H \otimes \mathbb{1})A = HA\mathbb{1}$ and $(\mathbb{1} \otimes H)A = \mathbb{1}AH$. Knowing a MPO representation of the Hamiltonian $H = \prod_j H_{[j]}$, we immediately obtain

$$\begin{aligned} H \otimes \mathbb{1} &= \prod_j H_{[j]}^{\alpha_j-1\alpha_j} \otimes \mathbb{1}_{[j]s'_j s_j} \\ \mathbb{1} \otimes H &= \prod_j \mathbb{1}_{[j]s_j s_j} \otimes H_{[j]s'_j s'_j}^{\beta_j-1\beta_j}, \end{aligned} \quad (\text{L2})$$

where $|s_j\rangle$ and $\langle s'_j|$ are the ket and bra components of the operator A .

To take care of the minus sign in the commutator, we multiply the MPO tensor $\mathbb{1}_{[1]} \otimes H_{[1]}$ with -1 . Then, we simply have to add the two MPO $H \otimes \mathbb{1}$ and $-\mathbb{1} \otimes H$. Adding two MPO is a standard procedure, which is e.g. explained in Sec. 4.3 and 5.2 of Ref. [23].

Appendix M: Double MPS

So far, we presented a general computation method for the time averaged density matrix (TADM) and explained in detail, how this method can be adapted for matrix product operators (MPO). MPO are just one example for tensor networks. Here, we discuss another (non-standard) type of tensor networks, where the TADM is obtained as a double sized matrix product states (MPS), which we dubbed double MPS.

Formally, a double MPS is a MPS with twice as many sites as the physical system has components. Hereby, the first part of the double MPS represents the ket-states $|u_i\rangle$ of the TADM or any other matrix $M = \sum_{ij} \lambda_{ij} \cdot |u_i\rangle\langle v_j|$, while the second part of the double MPS represents the bra-states $\langle v_j|$. The matrix λ_{ij} is encoded into the MPS-bond which connects the two parts, see also Fig. 16. If the double MPS is brought into a suitable canonical form [23], the basis states $|u_i\rangle$ and $|v_i\rangle$ encoded in M are orthogonal (i.e., $\langle u_i|u_{j \neq i}\rangle = 0 = \langle v_i|v_{j \neq i}\rangle$) and we can extract the matrix λ_{ij} from the double MPS. This allows e.g. to check whether or not M is a positive matrix. Assuming that the double MPS represents a positive Hermitian matrix, its entanglement entropy of bipartition for the half chain corresponds to the entropy of the entire matrix M .

We emphasize that the need for doubling the number of tensors to accommodate bra- and ket-vectors in a double MPS arises from our special ansatz taking advantage of the commutator, which needs to operate on the bra- and ket-vectors at the same time. As a consequence of this doubling, the bra- and ket-part are treated independently in a numerical algorithm which optimizes tensor by tensor. Therefore, the resulting operator is not

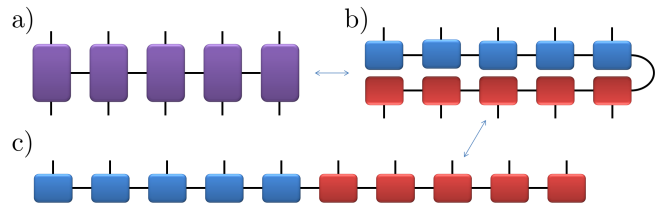


Figure 16: a) Graphical representation of a finite MPO with open boundary conditions. b) Any finite operator $\hat{O} = \sum_{ij} \lambda_{ij} |u_i\rangle\langle v_j|$ can be decomposed into two connected MPS, where the connecting bond between the MPS corresponds to λ_{ij} . Due to the connecting bond, the two MPS actually correspond to two collections of several MPS $|u_i\rangle$ and $\langle v_j|$. c) Formally, any finite MPO can be represented as MPS of twice the size.

forcedly Hermitian by construction

$$\sum_{ij} \lambda_{ij} |u_i\rangle\langle v_j| \stackrel{?}{=} \sum_{ij} (\lambda^\dagger)_{ji} |v_j\rangle\langle u_i|. \quad (\text{M1})$$

Still, since we intend to express the Hermitian TADM as double MPS, the optimization objective forces the algorithm to come up with a solution which is very close to Hermitian. At the end, for most applications, a lack of Hermiticity should not be more severe than any other numerical imprecision. If Hermiticity is of importance, we can still resort to $M' = \frac{1}{2}(M + M^\dagger)$.

Comparing Fig. 16 b) and c), we see that due to the unfolding process b) \rightarrow c), the order of sites in the second part of the double MPS is inverted. That is, in a double MPS, the tensors $M_{[1]} \cdots M_{[2n]}$ correspond to the physical sites $1, 2, \dots, n-1, n, n, n-1, \dots, 2, 1$. This ordering should be kept, since it is very convenient if we like to calculate expectation values, where we need to fold the double MPS as in Fig. 16 b).

1. Implementation

One of the great advantages of the double MPS is that with marginal adaptations, all algorithms we have developed so far for the MPO TADM can be reused, except the Hermite to real mapping explained in appendix J.

The MPO based algorithm is operating with three different MPO, representing the original density matrix ϱ_0 , the commutator operator \mathfrak{C} and the matrix M , which we optimize. All three have to be replaced by double MPS (where \mathfrak{C} actually corresponds to a double MPO). First, we observe that throughout the algorithm, a single multi-index $\sigma_j = (s_j, s'_j)$ is used for the two physical indices s_j and s'_j corresponding to the bra- and ket-index of the MPO tensors. Therefore, it is straight forward to replace the MPO structure in the algorithm by a (double) MPS structure. Of course, this is just a formal argument and we have to ensure the correct correspondence between MPO and double MPS.

The tensors $M_{[j]}$ of the double MPS which represents M are determined by the algorithm. For us, it remains to find the correct double MPS representation for ϱ_0 and \mathfrak{C} . For many interesting cases, the initial state is a pure state $\varrho_0 = |\Psi_0\rangle\langle\Psi_0|$. In this case, if $|\Psi_0\rangle$ can be represented as MPS, the construction of the double MPS is trivial. On the other hand, if we are not interested in the TADM $\bar{\varrho}$ but in the time average of an operator O_0 , a double MPS is generally not a suitable choice. For commonly used operators (as e.g. a Pauli matrix acting on the j th site $\alpha \cdot \sigma^{(j)} \equiv \mathbb{1}^{(1\dots j-1)} \otimes \alpha \cdot \sigma^{(j)} \otimes \mathbb{1}^{(j+1\dots n)}$), the needed bond dimension for a double MPS scales exponentially with the number of sites.

Finally, we need to construct the commutator operator \mathfrak{C} , which has formally the appearance of a double MPO, where each tensor carries two physical indices. In appendix L, we briefly outline the construction of \mathfrak{C} for the MPO based algorithm, where the commutator operator is symbolically written as

$$\mathfrak{C} = H \otimes \mathbb{1} - \mathbb{1} \otimes H, \quad (\text{M2})$$

see Eq. (L1). For the double MPS based algorithm, this symbolical form can be directly translated into a double MPO. That is, \mathfrak{C} is the difference of two double MPO, where one part of each double MPO represents the Hamiltonian and the other part the identity. It is easy to verify that for arbitrary double MPS A and B , this construction fulfills the property $\langle \mathfrak{C}A|B \rangle = \langle A|\mathfrak{C}B \rangle$, as it should (18).

Appendix N: Numerical aspects

In regard to numerical aspects, the result section focused strongly on the dependence of the results on the bond dimension. Here, we add a few comments concerning convergence properties and numerical precision.

1. Convergence

Tensor networks are usually optimized by successive local optimizations of one or two tensors at a time. Although it is well known that locally optimizing algorithms often run the risk of getting stuck in a local extremum, we find e.g. that matrix product state (MPS) based ground state search algorithms seem to be widely immune against this problem. They exhibit superb convergence properties for many physical systems of interest.

Can we hope that this is true for the optimization of the time averaged density matrix (TADM), as well?

An important difference between these two algorithms is that many commonly used Hamiltonians are sums of local operators only, while the squared commutator operator \mathfrak{C}^2 used in the TADM algorithm (26) is a highly non-local object. If we follow the alternative optimization strategy of appendix B, we even have to use the third and fourth power of \mathfrak{C} . In this case, we occasionally observed strong difficulties in finding the optimal solution if we started out with a randomized initial state. In case of the standard algorithm based on \mathfrak{C}^2 , we noticed convergence into local extrema, as well, but the observed deviations were only marginal.

2. Precision

A well known source for losses in the numerical precision are differences of big numbers which differ only by a very small number. To soften this effect for the commutator, we recommend to gauge the Hamiltonian such that $\text{tr}(H\varrho_0) = 0$, i.e

$$H \rightarrow H - \text{tr}(H\varrho_0). \quad (\text{N1})$$

Still, certain losses in the precision are inevitable. Especially the $T+$ method (46) discussed in appendix B is prone to numerical imprecision, since it employs the third and fourth power of \mathfrak{C} . In this algorithm, the value of $\varepsilon = \|\mathfrak{C}\bar{\varrho}_{\text{approx}}\|^2$ is minimized and should become zero for a perfect $\bar{\varrho}_{\text{approx}} = \bar{\varrho}$. Now, we have to see that the value of ε is not just limited by the achievable numerical precision, but during the optimization of ε , the average improvement per optimization step should also exceed the achievable numerical precision. Further, we are actually interested in the square root of ε respectively in the value $q = \frac{\|\mathfrak{C}\varrho_0\|}{\|\mathfrak{C}\bar{\varrho}_{\text{approx}}\|} \propto \sqrt{\varepsilon^{-1}}$ (45). Especially the combination double MPS (appendix M) and $T+$ method seems to be quite vulnerable. In some of our numerical simulations, the maximal reliable value of q was limited around $10^3 \dots 10^4$ due to numerical imprecision. An example for this effect can be seen in Fig. 1 b), where the precision of the double MPS $T+$ method saturates already for a bond dimension $D = 128$. Of course, we can always resort to a more precise floatingpoint operation, but this is usually not supported by the hardware and hence, needs a software emulation, which is significantly slower.